

INDUCTION MOTORS SIMULATION BY
FINITE ELEMENT METHOD
AND DIFFERENT POTENTIAL
FORMULATIONS WITH MOTION
VOLTAGE TERM

by

DÁNIEL MARCSA
B.Sc. student in Electrical Engineering

supervisor

DR. MIKLÓS KUCZMANN, PH.D.
Associate Professor

A thesis submitted to the
Széchenyi István University
for the degree of
BACHELOR OF SCIENCE
IN ELECTRICAL ENGINEERING

Department of Automation
Laboratory of Electromagnetic Fields
Széchenyi István University
Győr
2008

DIPLOMATERV FELADAT KIÍRÁS

MARCSA DÁNIEL

AUTOMATIZÁLÁSI SZAKIRÁNYOS HALLGATÓ RÉSZÉRE

A DIPLOMATERV CÍME:

INDUCTION MOTORS SIMULATION BY FINITE ELEMENT METHOD
AND DIFFERENT POTENTIAL FORMULATIONS
WITH MOTION VOLTAGE TERM

ASZINKRON MOTOROK SZIMULÁCIÓJA A VÉGESELEM-MÓDSZERREL ÉS KÜLÖNBÖZŐ
POTENCIÁLFORMALIZMUSOKKAL A ROTOR MOZGÁSÁNAK FIGYELEMBEVÉTELÉVEL

A diplomaterv feladat kiírása:

A végeelem-módszer alkalmazása a villamos forgógépek szimulációjában. Különböző potenciálformalizmusok használata, társítva a rotor forgásának modellezéséhez használt formulával. A nemzetközileg kiírt TEAM 30a feladatban megadott aszinkron motorok használata a szimulációhoz, az ott megadott paraméterekkel, anyagjellemzőkkel. A kapott eredményeken keresztül összehasonlítani az alkalmazott formalizmusokat.

2008. október 4.

Konzulens:

Dr. Kuczmann Miklós, Ph.D.
egyetemi docens
Távközlési Tanszék

Marcsa Dániel
B.Sc. hallgató

ANNOUNCEMENT OF THE B.Sc. THESIS

DÁNIEL MARCSA

STUDENT OF DEPARTMENT OF AUTOMATION

NAME OF THE B.Sc. THESIS:

INDUCTION MOTORS SIMULATION BY FINITE ELEMENT METHOD
AND DIFFERENT POTENTIAL FORMULATIONS
WITH MOTION VOLTAGE TERM

Announcement of the BSc Thesis:

The simulation of rotational machines by the finite element method. Different potential formulations used and coupled with the motion voltage term for this problem. The problem to be solved is the induction motors of problem 30a of TEAM workshops, with geometry and material parameters. Compare the different formulations by the solution of the problems.

4th of October 2008.

Supervisor:

Dr. Miklós Kuczmann, Ph.D.
Associate Professor
Department of Telecommunication

Dániel Marcsa
B.Sc. student

Contents

1	Introduction	2
1.1	The induction motor	2
1.2	The TEAM Problem No. 30a	3
1.2.1	The problem definition	4
1.3	Numerical methods	6
2	Equations of the Electromagnetic Field	8
2.1	The Maxwell's Equations	8
2.2	The constitutive relations	9
2.3	The regions and boundaries	10
3	Potential Formulations	12
3.1	Static Magnetic Fields	12
3.1.1	Formulation with magnetic vector potential, the \vec{A} - formulation	12
3.1.2	Formulation with reduced magnetic scalar potential, the Φ - formulation	14
3.2	Eddy Current Fields	16
3.2.1	The magnetic vector potential and the electric scalar potential, the \vec{A}, V - formulation	16
3.2.2	The current vector potential and the reduced magnetic scalar po- tential, the \vec{T}, Φ - formulation	18
3.3	Coupling static magnetic field and eddy current field formulations	19
3.3.1	The $\vec{A}, V - \vec{A}$ - formulation	20
3.3.2	The $\vec{T}, \Phi - \Phi$ - formulation	21
3.4	Coupled formulations with motion voltage term	22
3.4.1	Mathematical formulation of movement	22
3.4.2	The $\vec{A}, V - \vec{A}$ - formulation with the motion voltage term	24
3.4.3	The $\vec{T}, \Phi - \Phi$ - formulation with the motion voltage term	26
4	Weak formulation of eddy current problem	28
4.1	The weak formulation with Galerkin's method	28
4.1.1	The weak formulations of $\vec{A}, V - \vec{A}$ - formulation with motion voltage term	29
4.1.2	The weak formulations of $\vec{T}, \Phi - \Phi$ - formulation with motion voltage term	31

5	The finite element method	35
5.1	Fundamentals of finite element method	35
5.1.1	Preprocessing	35
	A. Model specification	35
	B. 2D finite element mesh	37
5.1.2	Shape functions	39
	A. Nodal shape functions	39
	B. Edge shape functions	43
5.1.3	Computation	47
	A. Solvers	48
5.1.4	Postprocessing	50
	A. Torque	50
	B. Induced voltage	51
	C. Losses	53
6	Solution of the Problem	55
6.1	Results of the single-phase induction motor	55
6.2	Results of the three-phase induction motor	63
7	Conclusions and future works	73
8	Acknowledgement	74
9	Bibliography	75

List of notation

\vec{A}	magnetic vector potential
\vec{B}	magnetic flux density [T]
B_r	radial component of magnetix flux density [T]
\vec{E}	electric field intensity [V/m]
\vec{F}	Maxwell's stress tensor
\vec{H}	magnetic field intensity [A/m]
H_Θ	azimuthal component of magnetic field intensity [A/m]
\vec{J}	eddy current density [A/m ²]
\vec{J}_0	source current density [A/m ²]
N	scalar weighting function
P_d	power dissipation [W/m]
\vec{T}_e	electromagnetic torque [Nm]
\vec{T}	current vector potential
\vec{T}_0	impressed current vector potential
V	electric scalar potential
V_i	induced voltage [V/m/turn]
\vec{W}	vector weighting function
Φ	reduced magnetic scalar potential
μ_0	permeability of vacuum [Vs/Am = H/m]
μ	permeability [Vs/Am = H/m]
ν	reluctivity [Am/Vs]
σ	conductivity [S/m]
ρ	resistivity [Ωm]
ω_s	synchronous speed [rad/s]
ω_r	angular velocity of the rotor [rad/s]

Abbreviations

BEM	Boundary Element Method
FDM	Finite Differential Method
FEM	Finite Element Method
FVM	Finite Volume Method
ICS	International Compumag Society
TEAM	Testing Electromagnetic Analysis Methods

Chapter 1

Introduction

1.1 The induction motor

Alternating current, or AC motors provide much of the motive force for industry. AC motors come in a variety of styles and power ratings. Alternating current motors are typically designed for use with specified input voltage signals. These motors may be classed as low, medium and high voltage. Low voltage motors typically consume between about 240V and 600V. Medium voltage motors consume voltages from about 400V up to about 15kV. High voltage motors consume voltage over 15kV [1, 2].

Alternating current motors used in industrial applications are typically synchronous motors having a starting winding and a running winding. The starting winding includes a starting capacitor or other capacitive component in series with the winding to shift the phase of the voltage and the current applied to the starting winding with respect to the voltage and the current applied to the running winding [1, 2].

AC motors are used in a variety of applications, including vehicle applications such as traction control. Traction motors are large electrical motors having the typical motor housing, stator and rotor assembly. Shaft is attached to the rotor, which extends through the housing. Fixed attached to a pinion end of the shaft is a motor pinion which in turn engages a bull or axle gear for rotating the axle. The motors used in vehicle applications are typically controlled such that the motor phase currents are sinusoidal. These motors are generally permanent magnet motors designed to have a sinusoidally-shaped back electromagnetic field waveform. An induction motor is used as a motor. The terminal voltage of the induction motor includes a transient voltage represented by the product of the differentiation term of a primary current and the leakage inductance of the induction motor [1, 2].

A wide variety of induction motors are available and are currently in use throughout a range of industrial applications. Induction motors typically include a rotor that rotates in response to a rotating magnetic flux generated by the alternating current in a stator associated with the rotor. A rotational speed differential between the rotor and the

rotating flux induces a current through a rotor cage. A rotor cage consists of a single aluminum casting having several conductive bars that run axially through the rotor and are joined at each end by two conductive end rings. Current induced in the bars generates a magnetic flux that opposes that of the stator, thus providing the rotor with rotational torque. The stator and the rotor may be mechanically and electrically configured in a variety of manners depending upon a number of factors, including: the application, the power available to drive the motor, and so forth [1, 2].

The induction motors are divided again into an inner rotor type induction motor and an outer rotor type induction motor in accordance with relative positions of rotors and stators. The inner rotor type induction motor is generally applied to a washing machine or something like that, and includes the rotor inside the stator. The ability to accurately determine the speed of a rotating rotor with respect to a stationary stator within an induction motor is vitally important to the every day operations of induction motors [1–3].

A flat induction motor is a motor which has a disk-shaped stator and rotor placed coaxially around a rotating shaft with their surfaces opposing each other. Normally, each the stator core and the rotor core have a spiral winding structure made of a magnetic steel strip. A plurality of open slots are formed in the winding structures from the outer edge toward the rotating shaft at equal intervals, leaving part of the magnetic steel strips. Single phase induction motors are normally provided with a cage type rotor and a coiled stator having two windings, one being for the running coil and the other for the starting coil [1–3].

Single phase induction motors are widely used, due to their simplicity, strength and high performance. They are used in household appliances, such as refrigerators, freezers, air conditioners, hermetic compressors, washing machines, pumps, fans, as well as in some industrial applications [1–3].

Linear induction motors are widely used in a number of industries and present certain advantages over rotary motors, particularly where propulsion along a predetermined path or guideway is required [1–3].

1.2 The TEAM Problem No. 30a

The TEAM (Testing Electromagnetic Analysis Methods) series of workshops originated in 1985 as a means of comparing eddy current codes, but it later expanded to include other aspects of computational electromagnetics including static and high frequency applications. The basic idea behind these workshops is a series of problems, each geared towards some aspect of computational electromagnetics. Although TEAM has a governing board, problem adoption is done in a forum open to all participants in TEAM activities. Once a problem is adopted, it is published and it is available to anyone in-

interested in using the problem, its results and any results that may be generated by participants. The problem definition contains comparison results, tables or plots that the user may compare to, and references to the sources of the problem and available published results. The benchmark problem of TEAM Workshops can be found the homepage of International Compumag Society (ICS) [4].

The one of purposes of the problems in TEAM is to test both formulations (that is, the mathematical models) used to build the program and the applications themselves. Although the stated goal is the testing of analysis methods through comparison of results, they also verify software correctness and, more importantly, program accuracy. The other purpose is to detect formulations and procedure characteristics, which must be modified and improved. Often these characteristics are not necessarily errors but have, perhaps, slow convergence, inefficient algorithms or methods of presentation, for example. The further purposes of the problems in TEAM to encourage unbiased testing with multiple formulations and multiple functions by as many different application as is practical, to share experience gained in solving various problems or in the development of programs, and to create a repository of solved problems, which can then be used by developers to verify new programs, and extensions and modifications of existing programs.

1.2.1 The problem definition

In this work the Problem No. 30a of TEAM Workshops (Induction motor analyses [4]) has been used. This problem consists of two induction motors, in which the eddy currents in the rotor are induced by the time harmonic current in the stator windings, and by the rotation of the rotor. Here, the problem is a linear eddy current field problem. The induction motors are invented motors, this problem has been used the comparison of the different numerical methods, the different formulations, and the originally presented analytically one.

The arrangement of the three-phase exposed winding induction motor problem is shown in Fig. 1.1. The phase groups of the three-phase exposed winding motors A, B, and C are lag each other in phase by 120° . The rotor angular velocity is ranging from 0 to 1200 rad/s. It is roughly three times faster than the angular velocity of the stator field is $\omega_s = 2\pi f = 377$ rad/s because the winding is excited at $f = 60$ Hz.

The arrangement of the single-phase induction motor problem is shown in Fig. 1.2. The range of computation of the single-phase induction motor for rotor angular velocities is from 0 to 358 rad/s (0.95% of the peak field speed) The synchronous speed of motor is $\omega_s = 2\pi f = 377$ rad/s, because the winding is excited at $f = 60$ Hz.

The windings of both motors are not embedded in slots. The source current density is maintained constant at 310 A/cm². In Fig. 1.1, and in Fig. 1.2 σ is the conductivity, μ_r is the relative permeability. Here, the relative permeability $\mu_r = 30$ has been used. The stator steel is laminated and its conductivity has been selected as $\sigma = 0$. The rotor

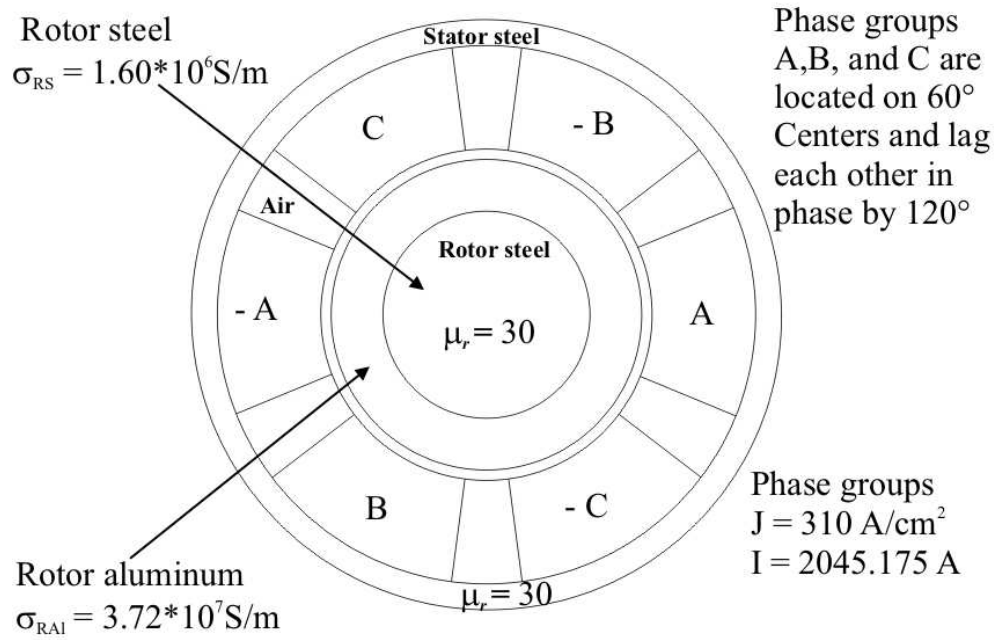


Fig. 1.1. The arrangement of the analyzed three-phase induction motor.

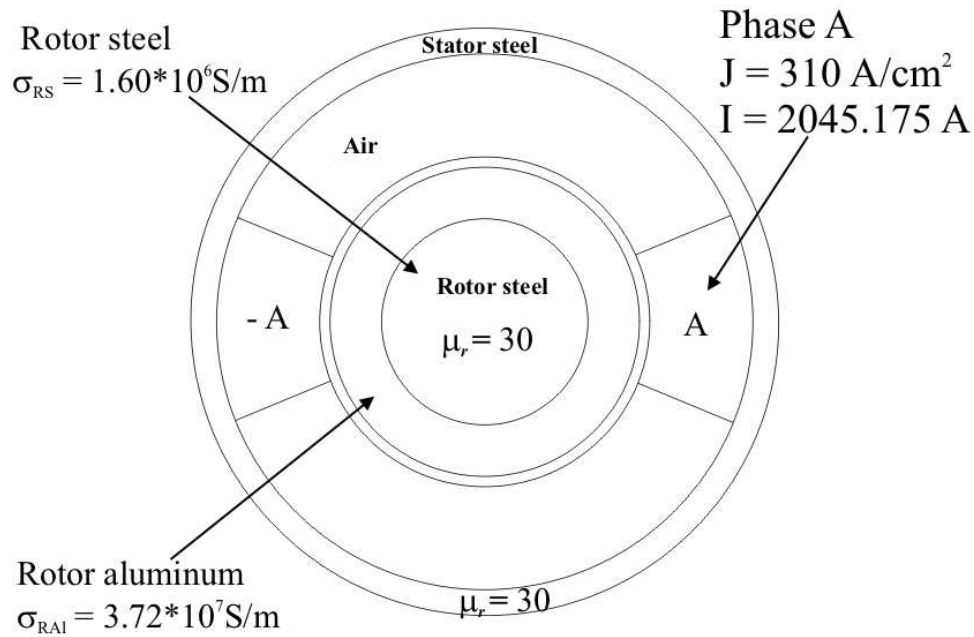


Fig. 1.2. The arrangement of the analyzed single-phase induction motor.

is made of rotor steel and rotor aluminum, i.e. the rotor steel is surrounded by the rotor aluminum. The conductivity of rotor steel is $\sigma_{RS} = 1.6 \cdot 10^6 \text{ S/m}$ and of the rotor aluminum is $\sigma_{RAI} = 3.72 \cdot 10^7 \text{ S/m}$. The rotation of rotor is counterclockwise.

The used methods are applied to compute the fundamental quantities both of the two induction motors. These are the electromagnetic torque, the induced voltage in the phase coil A, and it is computed as if the stator winding was comprised of a single turn,

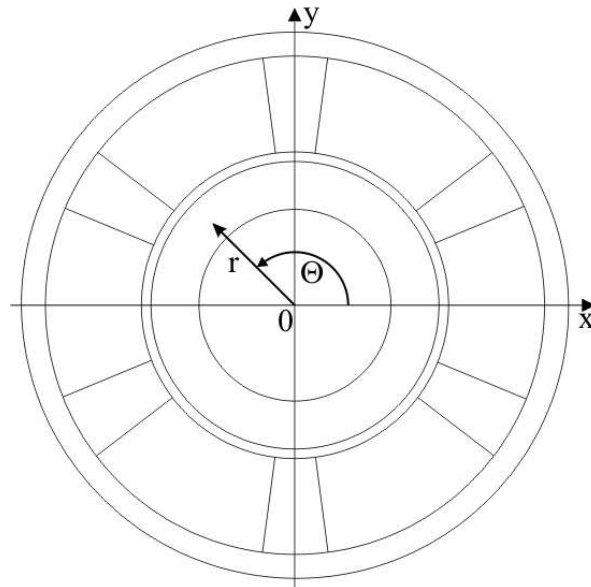


Fig. 1.3. The directions of polar coordinate system.

and average power dissipation, which due the eddy current loss in the whole rotor and in the rotor steel. The eddy current loss of rotor is computed as a sum of the eddy current loss of rotor steel and rotor aluminum. All quantities are computed on a per unit depth (1m) basis.

At the three-phase induction motor, the radial B field and the Θ -directed H field at $\omega_r = 200$ rad/s angular velocity have also been simulated. These quantities computed in the phase coil A along the x -axis in ten different point. In Fig. 1.3 shows the radial- and the Θ -direction. The polar coordinate r is the radial coordinate and Θ is the angular coordinate, it is often called the polar angle.

1.3 Numerical methods

In the design of engineering structures, numerical simulations play an increasingly important role. The differential equations that describe the physical phenomena can be solved analytically for a very limited class of problems only and even there only for simple geometries. More complex tasks require numerical approaches. Numerical analysis is also concerned with computing (in an approximate way) the solution of differential equations, both ordinary differential equations and partial differential equations. Partial differential equations are solved by discretizing the equation first, this means bringing it into a finite-dimensional subspace. This can be done by the finite difference method (FDM) [5, 6], the finite volume method (FVM) [7], the boundary element method (BEM) [8], or the finite element method (FEM) [5, 9–15]. The theoretical justification of these methods often involves theorems from functional analysis. These techniques reduces the problem to the solution of an algebraic equation.

In the finite difference method [5,6] the differential quotients have been approximated by difference quotients. So each derivative is approximated by a difference quotient. The differential equation will thus be transformed into a difference equation. The difference equations can then be written in matrix form. The matrix will be modified to suit some physical properties and in a last step the equations will be solved.

The finite volume method [7] is a numerical method for solving partial differential equations that calculates the values of the conserved variables averaged across a volume. One advantage of the finite volume method over the finite difference method is that it does not require a structured mesh, although a structured mesh can be used. The finite volume method can solve problems on irregular geometries too. Furthermore, one more advantage of the finite volume method over the finite element method is that it can conserve the variables on a coarse mesh easily. This is an important characteristic e.g. for fluid problems.

However, the influence of finite differetial method and finite volume method in solid physics is rather limited today, so that boundary element method mainly competes with finite element method in a common field, where both of these numerical methods have specific advantages.

The boundary element method [8] is a numerical computational method for solving linear partial differential equations which have been formulated as in boundary integral forms. In BEM only the boundary of the problem has been discretized. It can be applied in many areas of engineering and science including fluid mechanics, acoustics, electromagnetics.

The numerical analysis of electromagnetic field problems with the aid of the finite element method [5,9–15] has been one of the main directions of research in computational electromagnetics. This is the most widely used technique to approximate the solution of the partial differential equations. The basis of this extensively studied method is the weak formulation of partial differential equations.

In this work one of the above mentioned numerical methods, the finite element method (FEM) has been used. This numerical method, and the main steps of simulation with FEM have been presented particularly later.

Chapter 2

Equations of the Electromagnetic Field

2.1 The Maxwell's Equations

The Maxwell's equations of the eddy current field problems are presented in this chapter.

The induction motor is treated as an eddy current field problem. In eddy current field problems, the electric and the magnetic fields are coupled, because the field quantities are depending on the time variation (i.e. $\partial/\partial t \neq 0$), however the displacement current density can be neglected $|\mathbf{J}| \gg |\partial\mathbf{D}/\partial t|$, i.e. the differential equations of low frequency fields hold.

The studied eddy current field problem is separated into two parts; the conductor region (iron parts) Ω_c is surrounded by the nonmagnetic and non-conducting domain (e.g. air) Ω_n . The Maxwell's equations in the eddy current free region Ω_n model a static magnetic field, while in the eddy current region Ω_c , the magnetodynamic Maxwell's equations are valid. The scheme of the analyzed eddy current field problem can be seen in Fig. 2.1.

To the formulation of the problem, the differential equations are the following [9–20]:

$$\nabla \times \vec{H} = \vec{J}_0, \quad \text{in } \Omega_n, \quad (2.1)$$

$$\nabla \cdot \vec{B} = 0, \quad \text{in } \Omega_n, \quad (2.2)$$

$$\nabla \times \vec{H} = \vec{J}, \quad \text{in } \Omega_c, \quad (2.3)$$

$$\nabla \times \vec{E} = -\frac{\partial \vec{B}}{\partial t}, \quad \text{in } \Omega_c, \quad (2.4)$$

$$\nabla \cdot \vec{B} = 0, \quad \text{in } \Omega_c, \quad (2.5)$$

$$\nabla \cdot \vec{J} = 0, \quad \text{in } \Omega_c, \quad (2.6)$$

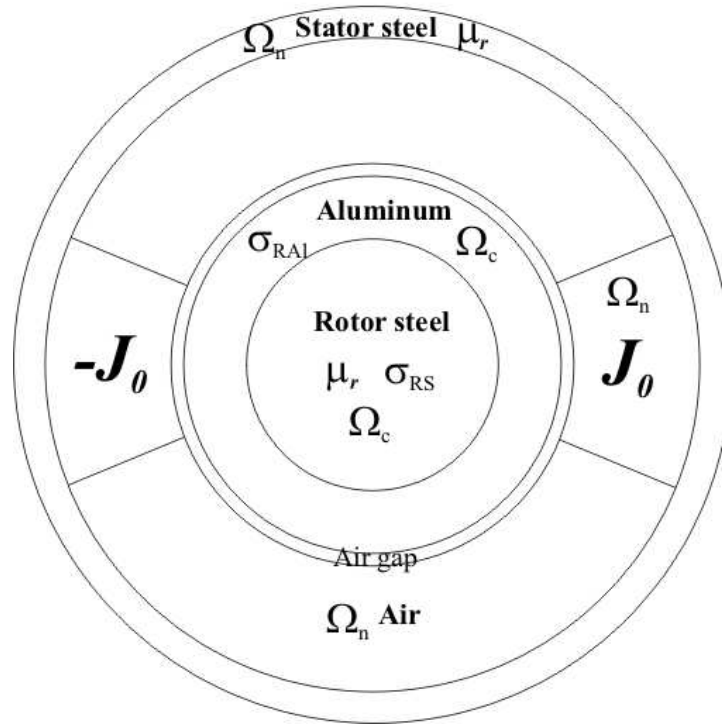


Fig. 2.1. The structure of the eddy current field problem.

where \vec{H} is the magnetic field intensity, \vec{B} is the magnetic flux density, \vec{E} is the electric field intensity, \vec{J} is the eddy current density, and \vec{J}_0 is the source current density.

2.2 The constitutive relations

The constitutive relations are as follows,

$$\vec{B} = \begin{cases} \mu_0 \vec{H}, & \text{in air, } \Omega_n, \\ \mu_0 \mu_r \vec{H}, & \text{in magnetically linear material, } \Omega_c, \end{cases} \quad (2.7)$$

and

$$\vec{J} = \sigma \vec{E}, \quad \text{in } \Omega_c. \quad (2.8)$$

The constitutive relationship (2.7) can be used in its inverse form as well i.e.,

$$\vec{H} = \begin{cases} \nu_0 \vec{B}, & \text{in air, } \Omega_n, \\ \nu_0 \nu_r \vec{B}, & \text{in magnetically linear material, } \Omega_c. \end{cases} \quad (2.9)$$

The inverse form of relation (2.8) is introduced as

$$\vec{E} = \rho \vec{J}, \quad \text{in } \Omega_c. \quad (2.10)$$

Here μ is the permeability, ν is the reluctivity, σ is the conductivity and ρ is the resistivity of the material, moreover $\nu = 1/\mu$ and $\rho = 1/\sigma$. The value of these data are given in the last chapter.

2.3 The regions and boundaries

The two regions Ω_c and Ω_n are coupled at the corresponding interface denoted by Γ_{nc} . The boundary of the eddy current free region is Γ_B , i.e. Γ_B denotes that the normal component of the magnetic flux density is vanishing, or it is assumed to be known by a term b .

Basically, Γ_E is the boundary of eddy current region where the tangential component of the electric field intensity is vanishing, but in this problem this boundary is not present, because the eddy current free region Ω_n is surrounding the eddy current region Ω_c . Furthermore, the boundary of eddy current region Γ_{Hc} and the boundary of eddy current free region Γ_{Hn} represent the symmetry plane, where the tangential component of the magnetic field intensity is zero. In this study, these (Γ_{Hc} , Γ_{Hn}) boundaries are not present, because this is only a 2D problem, and the number of unknowns is not too high.

Along the interface between the two disjunct regions Γ_{nc} , the tangential component of magnetic field intensity and the normal component of the magnetic flux density are continuous, moreover the normal component of the induced eddy currents is equal to zero.

These conditions can be formulated as

$$\vec{B} \cdot \vec{n} = -b \quad \text{or} \quad \vec{B} \cdot \vec{n} = 0, \quad \text{on } \Gamma_B, \quad (2.11)$$

where \vec{n} is the outer normal unit vector of the region, moreover

$$\vec{H}_c \times \vec{n}_c + \vec{H}_n \times \vec{n}_n = \vec{0}, \quad \text{on } \Gamma_{nc}, \quad (2.12)$$

and

$$\vec{B}_c \cdot \vec{n}_c + \vec{B}_n \cdot \vec{n}_n = 0, \quad \text{on } \Gamma_{nc}, \quad (2.13)$$

and

$$\vec{J} \cdot \vec{n}_c = 0, \quad \text{on } \Gamma_{nc}, \quad (2.14)$$

where \vec{n}_n , \vec{n}_c , \vec{H}_n , \vec{H}_c , \vec{B}_n and \vec{B}_c are the outer normal unit vector of the region filled with air and with conducting material, moreover the magnetic field intensity and the magnetic flux density vectors in the appropriate region on the boundary, respectively and it is evident that $\vec{n}_n = -\vec{n}_c$ along Γ_{nc} .

Here Γ_B is the boundary of the investigated region (here $b = 0$), and Γ_{nc} is the

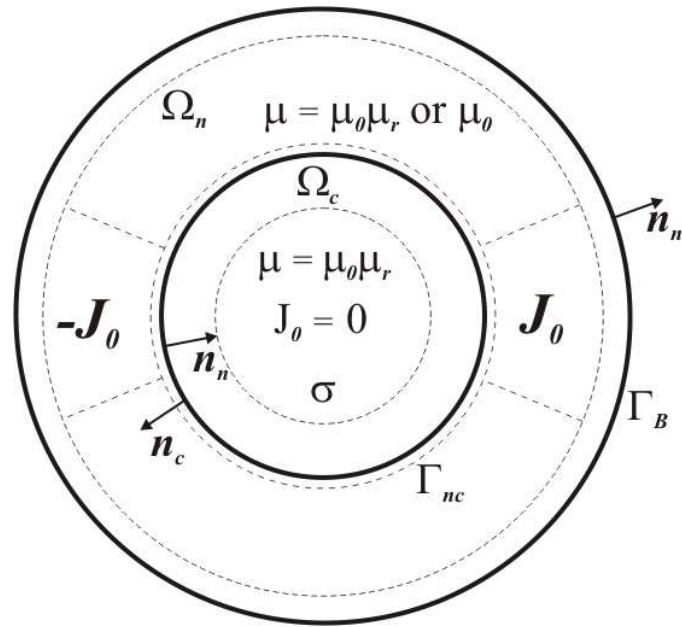


Fig. 2.2. The eddy current region is surrounded by nonconducting region.

interface between the conducting and the non-conducting region, as it is presented in Fig, 2.2.

Chapter 3

Potential Formulations

In the investigated eddy current field problem, the conductors, carrying the eddy currents are at least partially surrounded by a non-conducting medium, which is free of eddy currents.

The solutions of the Maxwell's equations are usually handled by potentials. Fundamentally, these are scalar and vector potentials [5, 6, 9–28].

3.1 Static Magnetic Fields

The TEAM 30a definition of static magnetic field can be found in section 2.1. The static magnetic field is defined by Maxwell's equations (2.1), (2.2), constitutive relations in (2.7), or in (2.9), moreover the boundary condition (2.11).

The static magnetic field can be described by the magnetic vector potential \vec{A} , and by the reduced magnetic scalar potential Φ [9–18, 23, 24, 28].

3.1.1 Formulation with magnetic vector potential, the \vec{A} - formulation

The magnetic vector potential is defined by [9–18, 20, 23]

$$\vec{B} = \nabla \times \vec{A}, \quad (3.1)$$

which satisfies (2.2) exactly, because of the identity $\nabla \cdot \nabla \times \vec{v} \equiv 0$ for any vector function $\vec{v} = \vec{v}(\vec{r})$. Substituting the definition (3.1) into the first Maxwell's equation (2.1) and using the constitutive relation from (2.9), it leads to the partial differential equation [9–15, 23]

$$\nabla \times (\nu \nabla \times \vec{A}) = \vec{J}_0, \quad \text{in } \Omega_n. \quad (3.2)$$

To ensure the uniqueness of the magnetic vector potential, the divergence of it can be selected according to Coulomb gauge [9, 11, 21, 23], i.e.

$$\nabla \cdot \vec{A} = 0. \quad (3.3)$$

Gauging is satisfied automatically in 2D, but unfortunately it is not true in 3D. The origin of numerical problems is the lack of uniqueness of the magnetic vector potential in three dimensional.

In 2D problems Coulomb gauge $\nabla \cdot \vec{A} = 0$ is satisfied automatically, if the source current density has only z component, the magnetic field intensity vector and the magnetic flux density vector have x and y components, i.e.

$$\vec{J}_0 = J_0(x, y)\vec{e}_z, \quad (3.4)$$

$$\vec{H} = H_x(x, y)\vec{e}_x + H_y(x, y)\vec{e}_y, \quad (3.5)$$

$$\vec{B} = B_x(x, y)\vec{e}_x + B_y(x, y)\vec{e}_y. \quad (3.6)$$

The magnetic vector potential has only z component,

$$\vec{A} = A_z(z)\vec{e}_z, \quad (3.7)$$

because ($A_x = 0$, $A_y = 0$ and $A_z = A_z(z)$)

$$\vec{B} = \nabla \times \vec{A} = \begin{vmatrix} \vec{e}_x & \vec{e}_y & \vec{e}_z \\ \frac{\partial}{\partial x} & \frac{\partial}{\partial y} & 0 \\ 0 & 0 & A_z \end{vmatrix} = \vec{e}_x \frac{\partial A_z}{\partial y} - \vec{e}_y \frac{\partial A_z}{\partial x}, \quad (3.8)$$

i.e. $B_x(x, y) = \partial A_z / \partial y$ and $B_y(x, y) = -\partial A_z / \partial x$. The divergence of this one component vector potential is equal to zero, because

$$\nabla \cdot \vec{A} = \frac{\partial A_z(x, y)}{\partial z} = 0. \quad (3.9)$$

The normal component of the magnetic flux density can be set as [9, 11, 21, 23]

$$\vec{B} \cdot \vec{n} = -b \Rightarrow (\nabla \times \vec{A}) \cdot \vec{n} = -b, \quad \text{on } \Gamma_B. \quad (3.10)$$

The left hand side of the last formulation can be rewritten as

$$(\nabla \times \vec{A}) \cdot \vec{n} = \nabla \cdot (\vec{A} \times \vec{n}) = -b, \quad (3.11)$$

finally

$$\nabla \cdot (\vec{n} \times \vec{A}) = b, \quad (3.12)$$

i.e.

$$\vec{n} \times \vec{A} = \vec{\alpha}, \quad \text{on } \Gamma_B, \quad (3.13)$$

where $\nabla \cdot \vec{\alpha} = b$. This is a Dirichlet type boundary condition. The selection of $\vec{\alpha}$ is not evident [9, 11], but in many practical cases $b=0$, so

$$\vec{n} \times \vec{A} = \vec{0}, \quad \text{on } \Gamma_B \quad (3.14)$$

can be selected.

Finally, the partial differential equation and the boundary condition of the presented two dimensional static magnetic field problem, which solution satisfies Coulomb gauge can be formulated as

$$\nabla \times (\nu \nabla \times \vec{A}) = \vec{J}_0, \quad \text{in } \Omega_n, \quad (3.15)$$

$$\vec{n} \times \vec{A} = 0, \quad \text{on } \Gamma_B. \quad (3.16)$$

3.1.2 Formulation with reduced magnetic scalar potential, the Φ - formulation

The magnetic field intensity vector in the eddy current free region Ω_n can be decomposed into two parts as [9, 11, 24, 28]

$$\vec{H} = \vec{T}_0 + \vec{H}_m. \quad (3.17)$$

The curl of the so called impressed current vector potential \vec{T}_0 is equal to the source current density \vec{J}_0 , and $\nabla \times \vec{H}_m$ is equal to zero, i.e. [9, 11, 24]

$$\nabla \times \vec{T}_0 = \vec{J}_0, \quad (3.18)$$

$$\nabla \times \vec{H}_m = 0. \quad (3.19)$$

The divergence of \vec{T}_0 can be selected according to Coulomb gauge [9], i.e.

$$\nabla \cdot \vec{T}_0 = 0, \quad (3.20)$$

which selection can be useful when creating the function \vec{T}_0 .

In a FEM procedure, \vec{T}_0 can be approximated by the vector finite elements, while Φ can be represented by nodal finite elements. There are many possibilities for the construction of the term \vec{T}_0 from the source current density \vec{J}_0 [9].

Here the minimizing a functional combined with an appropriate numerical technique is formulated, which has been used. In this technique, the source current density \vec{J}_0 has been represented by the curl of impressed current vector potential \vec{T}_0 , which satisfies (2.6) exactly, furthermore the divergence of \vec{T}_0 is selected to be equal zero. It must be noted that, \vec{T}_0 is calculated in free space, i.e. $\mu = \mu_0$ must be set everywhere in the

problem region. The partial differential equation defined in free space

$$\nabla \times \vec{T}_0 = \vec{J}_0, \quad \text{in } \Omega, \quad (3.21)$$

and the boundary conditions are

$$\vec{T}_0 \cdot \vec{n} = 0, \quad \text{on } \Gamma_B. \quad (3.22)$$

It can be solved by a numerical field calculation procedure, which is not sensitive to Coulomb gauge [9,11,21,23]. Finally \vec{T}_0 can be regarded as known, because this quantity is calculated before the numerical simulation.

The second step of Φ -formulation is the determination of the nonrotational part of the magnetic field intensity \vec{H}_m in (3.17). It can be given as the negative gradient of a reduced magnetic scalar potential Φ ,

$$\vec{H}_m = -\nabla\Phi, \quad (3.23)$$

because of the identity $\nabla \times (\nabla\varphi) \equiv \vec{0}$, for any scalar function $\varphi = \varphi(\vec{r})$. By this formulation the magnetic field intensity can be written as [9,11]

$$\vec{H} = \vec{T}_0 - \nabla\Phi, \quad (3.24)$$

which satisfies (2.1) in Ω_n . The magnetic scalar potential Φ is usually called the reduced magnetic scalar potential, because the source term is fundamentally hidden in \vec{T}_0 . Applying the constitutive relation in (2.7) results in the magnetic flux density

$$\vec{B} = \mu(\vec{T}_0 - \nabla\Phi). \quad (3.25)$$

The divergence of magnetic flux density is equal to zero according to (2.2). Finally the linear partial differential equation of the problem has the form

$$\nabla \cdot (\mu\nabla\Phi) = \nabla \cdot (\mu\vec{T}_0), \quad \text{in } \Omega_n, \quad (3.26)$$

which is a generalized Laplace-Poisson equation.

On the part Γ_B , setting the normal component of the magnetic flux density results in a Neumann type boundary condition,

$$\vec{B} \cdot \vec{n} = 0 \Rightarrow (\mu\vec{T}_0 - \mu\nabla\Phi) \cdot \vec{n} = 0, \quad \text{on } \Gamma_B, \quad (3.27)$$

since $\vec{B} = \mu(\vec{T}_0 - \nabla\Phi)$.

The partial differential equation and the boundary condition of a static magnetic

field problem can be obtained [9, 11, 28]

$$\nabla \cdot (\mu \nabla \Phi) = \nabla \cdot (\mu \vec{T}_0), \quad \text{in } \Omega_n, \quad (3.28)$$

$$\mu(\vec{T}_0 - \nabla \Phi) \cdot \vec{n} = 0, \quad \text{on } \Gamma_B, \quad (3.29)$$

where (3.29) formulates a homogeneous Neumann type boundary condition.

3.2 Eddy Current Fields

The TEAM 30a problem definition of the eddy current field can be found in section 2.1. The eddy current field is defined by Maxwell's equations (2.3), (2.4), (2.5), constitutive relations in (2.7) and (2.8), or the inverse relations in (2.9) and (2.10).

The eddy current field can be described by two potential functions, either a magnetic vector potential \vec{A} or a current vector potential \vec{T} . The magnetic vector potential \vec{A} can be coupled with an electric scalar potential, denoted by V . The current vector potential \vec{T} can be coupled with a reduced magnetic scalar potential Φ [6, 9–15, 21, 22, 25–38].

In the eddy current field, the field quantities are depending on the time variation ($\partial/\partial t \neq 0$). The eddy current field formulations are not only have used in the time domain, but these formulations are used in the frequency domain, too [6, 9, 10, 12–15, 21, 25, 29–31, 37, 38].

In frequency domain the derivation by time $\partial/\partial t$ is transformed to a multiplication by $j\omega$ [9, 10, 13, 16, 17, 19, 29, 37].

3.2.1 The magnetic vector potential and the electric scalar potential, the \vec{A} , V - formulation

The divergence-free magnetic flux density vector can be described by the curl of the magnetic vector potential \vec{A} , since $\nabla \cdot \nabla \times \vec{u} \equiv 0$, for any vector function $\vec{u} = \vec{u}(\vec{r})$, or $\vec{u} = \vec{u}(\vec{r}, t)$, i.e. [6, 9–15, 21, 22, 25, 29–33, 35, 37, 38]

$$\vec{B} = \nabla \times \vec{A}. \quad (3.30)$$

This automatically enforces the satisfaction of the magnetic Gauss' law (2.5). Substituting expression (3.30) into Faraday's law (2.4) results in

$$\nabla \times \vec{E} = -\frac{\partial}{\partial t} \nabla \times \vec{A} = -\nabla \times \frac{\partial \vec{A}}{\partial t} \Rightarrow \nabla \times \left(\vec{E} + \frac{\partial \vec{A}}{\partial t} \right) = \vec{0}, \quad (3.31)$$

because rotation (i.e. derivation by space) and derivation by time can be replaced. The curl-less vector field $\vec{E} + \partial\vec{A}/\partial t$ can be derived from the so-called electric scalar potential V ($\nabla \times \nabla\varphi \equiv \vec{0}$, for any scalar functions $\varphi = \varphi(\vec{r})$, or $\varphi = \varphi(\vec{r}, t)$) [6, 9, 11–15, 21, 22, 25],

$$\vec{E} + \frac{\partial\vec{A}}{\partial t} = -\nabla V, \quad (3.32)$$

and the electric field intensity vector can be described by two potentials as [6, 9, 11–15, 21, 22, 25]

$$\vec{E} = -\frac{\partial\vec{A}}{\partial t} - \nabla V. \quad (3.33)$$

Basically, the induction motor is a two-dimensional problem, and this results in the two dimensional case that the electric scalar potential can be selected as $V = 0$ in the \vec{A}, V - potential formulation [9, 11].

The electric field intensity in the two dimensional case is the following:

$$\vec{E} = -\frac{\partial\vec{A}}{\partial t}. \quad (3.34)$$

Substituting the relations (3.30) and (3.34) into (2.3), and using the constitutive relation in (2.8) and (2.9) leads to the partial differential equation

$$\nabla \times (\nu \nabla \times \vec{A}) + \sigma \frac{\partial\vec{A}}{\partial t} = \vec{0}, \quad \text{in } \Omega_c. \quad (3.35)$$

There is one unknown function (\vec{A}), that is why only one equations must be formulated.

Finally, here is the partial differential equation of the \vec{A}, V - formulation in two dimensional case [6, 9–15, 22, 29, 32, 33, 35, 37, 38],

$$\nabla \times (\nu \nabla \times \vec{A}) + \sigma \frac{\partial\vec{A}}{\partial t} = \vec{0}, \quad \text{in } \Omega_c. \quad (3.36)$$

The solution of the problem defined by the above equation is not unique in three dimensional case, because the divergence of the magnetic vector potential has not specified yet. The Coulomb gauge should be used in this formulation in three dimensios.

Fortunately, in two dimensional case the Coulomb gauge is satisfied automatically (see in Section 3.1.1).

In the frequency domain, the electric field intensity \vec{E} in two dimensional case is the following:

$$\vec{E} = -j\omega\vec{A}. \quad (3.37)$$

In the frequency domain only the second term of (3.36) has been changed. The partial

differential equation of two dimensional problem in the frequency domain are the following [6, 9, 10, 12–15, 21, 25, 29–31, 37, 38] :

$$\nabla \times (\nu \nabla \times \vec{A}) + \sigma j \omega \vec{A} = \vec{0}, \quad \text{in } \Omega_c. \quad (3.38)$$

3.2.2 The current vector potential and the reduced magnetic scalar potential, the \vec{T}, Φ - formulation

The solenoidal property of the induced eddy current density (2.6) results in the possibility of applying the current vector potential \vec{T} to represent the eddy current field in conducting materials,

$$\nabla \cdot \vec{J} = 0 \Rightarrow \vec{J} = \nabla \times \vec{T}, \quad (3.39)$$

because of the mathematical identity $\nabla \cdot \nabla \times \vec{v} \equiv 0$ for any vector function $\vec{v} = \vec{v}(\vec{r})$ or $\vec{v} = \vec{v}(\vec{r}, t)$ [9, 11, 21, 22, 26–28, 34, 36–38].

Substituting this relation back to the first Maxwells equation (2.3), i.e.

$$\nabla \times \vec{H} = \nabla \times \vec{T} \Rightarrow \nabla \times (\vec{H} - \vec{T}) = \vec{0}, \quad (3.40)$$

results in the reduced magnetic scalar potential Φ as

$$\vec{H} - \vec{T} = -\nabla \Phi \Rightarrow \vec{H} = \vec{T} - \nabla \Phi, \quad (3.41)$$

because $\nabla \times \nabla \varphi \equiv \vec{0}$ for any scalar function $\varphi = \varphi(\vec{r})$ or $\varphi = \varphi(\vec{r}, t)$ The first Maxwell's equation (2.3) has been satisfied exactly by this formulation.

Applying the impressed current vector potential \vec{T}_0 to represent the known source current density \vec{J}_0 placed in the eddy current free region takes it easier the coupling of the present formulation with the reduced magnetic scalar potential in the eddy current free region, i.e. appending \vec{T}_0 to (3.41) is advantageous [9, 11, 21, 22, 26–28, 34, 36–38],

$$\vec{H} = \vec{T}_0 + \vec{T} - \nabla \Phi, \quad (3.42)$$

because $\nabla \times \vec{T}_0 = \vec{0}$ in eddy current region Ω_c .

Substituting $\vec{J} = \nabla \times \vec{T}$ to (2.10), the electric field intensity can be expressed by the current vector potential as

$$\vec{E} = \rho \nabla \times \vec{T}. \quad (3.43)$$

Substituting this expression and the constitutive relation (2.7) into Faraday's law (2.4)

leads to the partial differential equation,

$$\nabla \times (\rho \nabla \times \vec{T}) + \mu \frac{\partial \vec{T}}{\partial t} - \mu \nabla \frac{\partial \Phi}{\partial t} = -\mu \frac{\partial \vec{T}_0}{\partial t}, \quad \text{in } \Omega_c. \quad (3.44)$$

The magnetic Gauss' law (2.2) can be rewritten in the form

$$\nabla \cdot (\mu \vec{T} - \mu \nabla \Phi) = -\nabla \cdot (\mu \vec{T}_0), \quad \text{in } \Omega_c. \quad (3.45)$$

The solution of these partial differential equations results in two unknowns (\vec{T} and Φ) of the \vec{T}, Φ - formulation.

Finally, here is the collection of partial differential equations of the \vec{T}, Φ - formulation [9, 11, 21, 22, 28, 36, 37]:

$$\nabla \times (\rho \nabla \times \vec{T}) + \mu \frac{\partial \vec{T}}{\partial t} - \mu \nabla \frac{\partial \Phi}{\partial t} = -\mu \frac{\partial \vec{T}_0}{\partial t}, \quad \text{in } \Omega_c, \quad (3.46)$$

$$\nabla \cdot (\mu \vec{T} - \mu \nabla \Phi) = -\nabla \cdot (\mu \vec{T}_0), \quad \text{in } \Omega_c. \quad (3.47)$$

In the frequency domain only the (3.46) has been modified.

The partial differential equations of two dimensional problem in the frequency domain are the following [9, 21, 22, 37, 38]

$$\nabla \times (\rho \nabla \times \vec{T}) + j\omega \mu \vec{T} - j\omega \mu \nabla \Phi = -j\omega \mu \vec{T}_0, \quad \text{in } \Omega_c, \quad (3.48)$$

$$\nabla \cdot (\mu \vec{T} - \mu \nabla \Phi) = -\nabla \cdot (\mu \vec{T}_0), \quad \text{in } \Omega_c. \quad (3.49)$$

3.3 Coupling static magnetic field and eddy current field formulations

In most eddy current field problems, the conductors carrying the eddy currents are at least partially surrounded by a nonconducting medium (e.g. air, laminated steel), where a static magnetic field is present (Fig. 2.1). The static magnetic field is induced both by the eddy currents and by the source current of coils. That is why the potential formulations of the static magnetic field and of the eddy current field must be coupled.

The static magnetic field in Ω_n can be described by a magnetic vector potential, or by a reduced magnetic scalar potential. In the first case, applying the magnetic vector potential \vec{A} is a more general way. Application of the reduced magnetic scalar potential Φ is simpler to use, however currents of coils must be represented by an impressed current vector potential \vec{T}_0 , which must be realized by vector finite element approximation.

The eddy current field in Ω_c can be represented by a vector potential coupled with a scalar potential. The magnetic vector potential \vec{A} can be coupled with the electric scalar

potential V and the current vector potential \vec{T} can be coupled with the reduced magnetic scalar potential Φ . However, the induction motor is a two-dimensional problem, and this results in the two dimensional case that the electric scalar potential can be selected as $V = 0$ in the $\vec{A}, V - \vec{A}$ - potential formulation.

3.3.1 The $\vec{A}, V - \vec{A}$ - formulation

The magnetic vector potential \vec{A} is used in this formulation throughout the region $\Omega_n \cup \Omega_c$ and the electric scalar potential V only in Ω_c . Here, the equations (3.15), (3.36) and boundary condition (3.16) have to be used to prepare the formulation, but the set of these equations have to be appended the interface Γ_{nc} between the two subregions Ω_n and Ω_c .

The magnetic vector potential is continuous, meaning that the tangential and the normal component of the magnetic vector potential are continuous on Γ_{nc} . The continuity of the tangential component of the magnetic vector potential immediately enforces the continuity of the normal component of the magnetic flux density from (2.13),

$$(\nabla \times \vec{A}) \cdot \vec{n}_c + (\nabla \times \vec{A}) \cdot \vec{n}_n = \nabla \cdot (\vec{A} \times \vec{n}_c) + \nabla \cdot (\vec{A} \times \vec{n}_n) = \nabla \cdot (\vec{A} \times \vec{n}_c + \vec{A} \times \vec{n}_n) = 0. \quad (3.50)$$

The continuity of the tangential component of the magnetic field intensity vector must be prescribed by an additional Neumann type interface condition on Γ_{nc} from (2.12),

$$(\nu \nabla \times \vec{A}) \times \vec{n}_c + (\nu \nabla \times \vec{A}) \times \vec{n}_n = \vec{0}. \quad (3.51)$$

It is obvious that the normal component of the eddy current density must vanish on Γ_{nc} .

The summarized partial differential equations and the boundary conditions are as follows [9, 11],

$$\nabla \times (\nu \nabla \times \vec{A}) + \sigma \frac{\partial \vec{A}}{\partial t} = \vec{0}, \quad \text{in } \Omega_c, \quad (3.52)$$

$$\nabla \times (\nu \nabla \times \vec{A}) = \vec{J}_0, \quad \text{in } \Omega_n, \quad (3.53)$$

$$\vec{n} \times \vec{A} = \vec{0}, \quad \text{on } \Gamma_B, \quad (3.54)$$

$$\vec{n}_c \times \vec{A} + \vec{n}_n \times \vec{A} = \vec{0}, \quad \text{on } \Gamma_{nc}, \quad (3.55)$$

$$(\nu \nabla \times \vec{A}) \times \vec{n}_c + (\nu \nabla \times \vec{A}) \times \vec{n}_n = \vec{0}, \quad \text{on } \Gamma_{nc}. \quad (3.56)$$

The equations of $\vec{A}, V - \vec{A}$ - formulation in the frequency domain are described by the same equations, only the equation (3.52) of conductive region has been changed.

The partial differential equations and boundary conditions of the $\vec{A}, V - \vec{A}$ - formulation in the frequency domain can be written as

$$\nabla \times (\nu \nabla \times \vec{A}) + j\omega\sigma\vec{A} = \vec{0}, \quad \text{in } \Omega_c, \quad (3.57)$$

$$\nabla \times (\nu \nabla \times \vec{A}) = \vec{J}_0, \quad \text{in } \Omega_n, \quad (3.58)$$

$$\vec{n} \times \vec{A} = \vec{0}, \quad \text{on } \Gamma_B, \quad (3.59)$$

$$\vec{n}_c \times \vec{A} + \vec{n}_n \times \vec{A} = \vec{0}, \quad \text{on } \Gamma_{nc}, \quad (3.60)$$

$$(\nu \nabla \times \vec{A}) \times \vec{n}_c + (\nu \nabla \times \vec{A}) \times \vec{n}_n = \vec{0}, \quad \text{on } \Gamma_{nc}. \quad (3.61)$$

3.3.2 The \vec{T} , Φ – Φ - formulation

The reduced magnetic scalar potential Φ is used in this formulation throughout the region $\Omega_n \cup \Omega_c$ and the current vector potential \vec{T} only in Ω_c . Here, the equations (3.28), (3.46) and (3.47), and boundary condition (3.29) have to be used to prepare the formulation, but the set of these equations have to be appended the interface Γ_{nc} between the two subregions Ω_n and Ω_c .

The magnetic field intensity vector is derived as $\vec{H} = \vec{T}_0 - \nabla\Phi$ in Ω_n and it is written as $\vec{H} = \vec{T}_0 + \vec{T} - \nabla\Phi$ in Ω_c . The tangential component of the magnetic field intensity can be set to be continuous on Γ_{nc} by a continuous magnetic scalar potential and by setting the tangential component of the current vector potential equal to zero by the boundary condition $\vec{T} \times \vec{n} = \vec{0}$ on Γ_{nc} , moreover the tangential component of the impressed current vector potential $\vec{T}_0 \times \vec{n}$ is continuous since it is represented by tangentially continuous vector shape functions. Vanishing the normal component of eddy current density on Γ_{nc} satisfies automatically,

$$\vec{J} = \nabla \times \vec{T} \Rightarrow \vec{J} \cdot \vec{n} = (\nabla \times \vec{T}) \cdot \vec{n} = \nabla \cdot (\vec{T} \times \vec{n}) = 0, \quad (3.62)$$

because $\vec{T} \times \vec{n} = \vec{0}$ on Γ_{nc} .

The continuity of the normal component of magnetic flux density must be specified a Neumann type interface condition (see (3.69)).

The summarized equations of this formulation are as follows [9, 11],

$$\nabla \times (\rho \nabla \times \vec{T}) + \mu \frac{\partial \vec{T}}{\partial t} - \mu \nabla \frac{\partial \Phi}{\partial t} = -\mu \frac{\partial \vec{T}_0}{\partial t}, \quad \text{in } \Omega_c, \quad (3.63)$$

$$\nabla \cdot (\mu \vec{T} - \mu \nabla \Phi) = -\nabla \cdot (\mu \vec{T}_0), \quad \text{in } \Omega_c, \quad (3.64)$$

$$-\nabla \cdot (\mu \nabla \Phi) = -\nabla \cdot (\mu \vec{T}_0), \quad \text{in } \Omega_n, \quad (3.65)$$

$$(\mu \vec{T}_0 - \nabla \Phi) \cdot \vec{n} = 0, \quad \text{on } \Gamma_B, \quad (3.66)$$

$$\Phi \text{ is continuous on } \Gamma_{nc}, \quad (3.67)$$

$$\vec{T} \times \vec{n}_c = \vec{0}, \quad \text{on } \Gamma_{nc}, \quad (3.68)$$

$$(\mu \vec{T}_0 + \mu \vec{T} - \mu \nabla \Phi) \cdot \vec{n}_c + (\mu \vec{T}_0 - \mu \nabla \Phi) \cdot \vec{n}_n = 0, \quad \text{on } \Gamma_{nc}. \quad (3.69)$$

The reduced magnetic scalar potential is a continuous scalar variable in the entire region $\Omega_c \cup \Omega_n$ and on the interface Γ_{nc} , and 3.67 is satisfied automatically.

The equations of the $\vec{T}, \Phi - \Phi$ - formulation in the frequency domain are described by the same equations, only one of the equation (3.63) of conductive region has been changed.

The partial differential equations and boundary conditions of the $\vec{T}, \Phi - \Phi$ - formulation in the frequency domain can be written as

$$\nabla \times (\rho \nabla \times \vec{T}) + j\omega \mu \vec{T} - j\omega \mu \nabla \Phi = -j\omega \mu \vec{T}_0, \quad \text{in } \Omega_c, \quad (3.70)$$

$$\nabla \cdot (\mu \vec{T} - \mu \nabla \Phi) = -\nabla \cdot (\mu \vec{T}_0), \quad \text{in } \Omega_c, \quad (3.71)$$

$$-\nabla \cdot (\mu \nabla \Phi) = -\nabla \cdot (\mu \vec{T}_0), \quad \text{in } \Omega_n, \quad (3.72)$$

$$(\mu \vec{T}_0 - \nabla \Phi) \cdot \vec{n} = 0, \quad \text{on } \Gamma_B, \quad (3.73)$$

$$\Phi \text{ is continuous on } \Gamma_{nc}, \quad (3.74)$$

$$\vec{T} \times \vec{n}_c = \vec{0}, \quad \text{on } \Gamma_{nc}, \quad (3.75)$$

$$(\mu \vec{T}_0 + \mu \vec{T} - \mu \nabla \Phi) \cdot \vec{n}_c + (\mu \vec{T}_0 - \mu \nabla \Phi) \cdot \vec{n}_n = 0, \quad \text{on } \Gamma_{nc}. \quad (3.76)$$

3.4 Coupled formulations with motion voltage term

Assuming that the analysed model has a moving part, it is necessary to take into account the movement. This can be performed by using the motion voltage term $\vec{v} \times \vec{B}$ [10, 13, 29–38], where \vec{v} is the angular velocity, and \vec{B} is the magnetic flux density. However, this method is suitable only when the moving part is invariable along the movement direction. In this case with the spatial discretization of the field equations, the matrices created by finite element method are unsymmetrical [10, 32, 35].

3.4.1 Mathematical formulation of movement

In some special case, it is possible to find a coordinate system in which the material properties are not directly affected by the motion of the moving parts. If there is such a coordinate system, this results in a false solution of field equations. Transformation of equations for the field quantities is needed [10, 29, 32, 33, 37, 38].

In induction machines consider a rotor moving in one direction with velocity \vec{v} relative to a reference frame $\vec{O}(x, y)$ and a local reference frame $\vec{O}'(x', y')$, which is moving with the rotor [29, 33].

The displacement currents are negligible, because of the low frequencies used in the electrical machines, and the Maxwell's equations can be written in the fixed reference frame as [29, 33, 37, 38]:

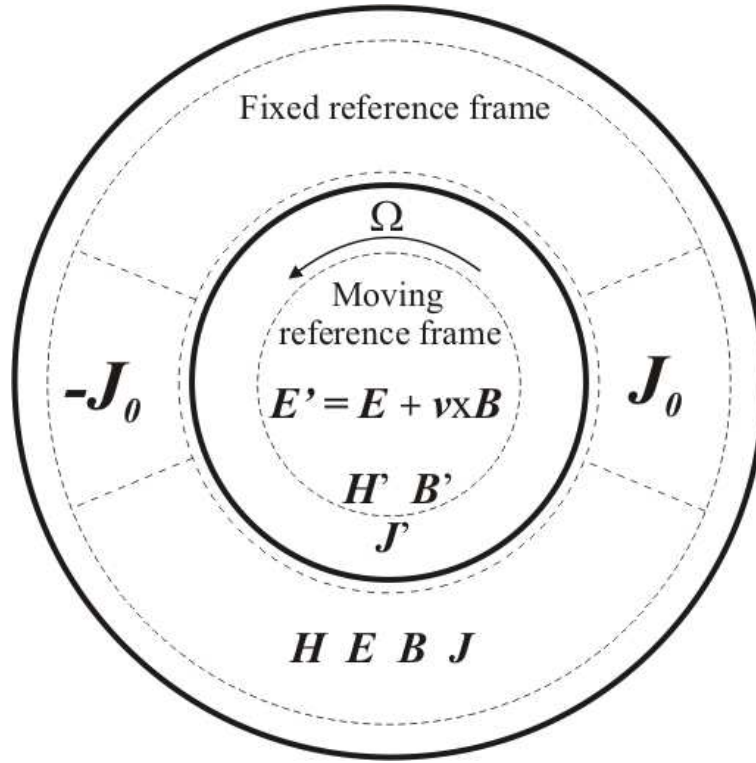


Fig. 3.1. The structure of the eddy current field problem with moving part.

$$\nabla \times \vec{H} = \vec{J}, \quad \text{in } \Omega_c \cup \Omega_n, \quad (3.77)$$

$$\nabla \times \vec{E} = -\frac{\partial \vec{B}}{\partial t}, \quad \text{in } \Omega_c, \quad (3.78)$$

$$\nabla \cdot \vec{B} = 0, \quad \text{in } \Omega_c \cup \Omega_n, \quad (3.79)$$

$$\vec{J} = \begin{cases} \vec{J}_0, & \text{in } \Omega_n, \\ \sigma \vec{E}, & \text{in } \Omega_c. \end{cases} \quad (3.80)$$

Electromagnetic phenomena are described by the same Maxwell's equations in the fixed, and in the moving reference frames. In the moving reference frame the vectors \vec{H}' , \vec{B}' and \vec{J}' are unchanged in the fixed and in the moving reference frames. Only the electric field intensity vector \vec{E} is modified, because of adding the motion voltage term $\vec{v} \times \vec{B}$ to \vec{E} [29, 33, 37, 38]. In the moving reference frame the vectors are

$$\vec{H}' = \vec{H}, \quad (3.81)$$

$$\vec{E}' = \vec{E} + \vec{v} \times \vec{B}, \quad (3.82)$$

$$\vec{B}' = \vec{B}, \quad (3.83)$$

$$\vec{J}' = \vec{J}, \quad (3.84)$$

where the quantities observed from the coordinate system $\vec{O}'(x', y')$ are marked by apostrophes.

Substituting the equation (3.82) into (3.80) gives the next relation in Ω_c :

$$\vec{J} = \sigma \vec{E}' = \sigma(\vec{E} + \vec{v} \times \vec{B}), \quad (3.85)$$

because the motion of the conductor region of the induced induction motor eddy currents, and the eddy currents are depending on the velocity. The (3.85) has been used the $\vec{A}, V - \vec{A}$ - formulation, and gives the well-known equation, which presents the next section.

At the $\vec{T}, \Phi - \Phi$ - potential formulation an other way gives the basic equation with motion voltage term [34,36–38]. In the moving reference frame the (3.78) is the following

$$\nabla \times \vec{E}' = -\frac{\partial \vec{B}'}{\partial t}, \quad (3.86)$$

and in this equation the magnetic flux \vec{B}' is unchanged (see in (3.83)), only the electric field intensity \vec{E}' is modified (see in (3.82)).

Substitute the equation (3.82) into (3.86) gives the next relation:

$$\nabla \times \vec{E}' = -\frac{\partial \vec{B}'}{\partial t} \Rightarrow \nabla \times (\vec{E} + \vec{v} \times \vec{B}) = -\frac{\partial \vec{B}}{\partial t}. \quad (3.87)$$

The (3.87) has been used the $\vec{T}, \Phi - \Phi$ - formulation, and gives the partial differential equation of this formulation with motion.

3.4.2 The $\vec{A}, V - \vec{A}$ - formulation with the motion voltage term

This potential formulation coupled with moving velocity \vec{v} seems to be the most widely used formulation of electrical machines analysis [10,29–33,35,37,38].

Substituting (3.34) into the (3.85) gives the next equation:

$$\vec{J} = \sigma\left(-\frac{\partial \vec{A}}{\partial t} + \vec{v} \times \vec{B}\right). \quad (3.88)$$

In two dimensional case using the $\vec{A}, V - \vec{A}$ - formulation, the motion voltage term is the following. The velocity has only x and y components, i.e.

$$\vec{v} = v(x, y, t), \quad (3.89)$$

and the magnetic flux density has the same components, and this results in that the

motion voltage term in two dimensional case has only z component, i.e.

$$\vec{v} \times \vec{B} = \begin{vmatrix} \vec{e}_x & \vec{e}_y & \vec{e}_z \\ v_x & v_y & 0 \\ B_x & B_y & 0 \end{vmatrix} = \vec{e}_z(v_x B_y - v_y B_x). \quad (3.90)$$

Combining (3.90) with (3.8) results in the motion voltage term is the following form:

$$\vec{v} \times \vec{B} = \vec{v} \times \nabla \times \vec{A} = \begin{vmatrix} \vec{e}_x & \vec{e}_y & \vec{e}_z \\ v_x & v_y & 0 \\ \frac{\partial A_z}{\partial y} & -\frac{\partial A_z}{\partial x} & 0 \end{vmatrix} = \vec{e}_z(-v_x \frac{\partial A_z}{\partial x} - v_y \frac{\partial A_z}{\partial y}). \quad (3.91)$$

Substituting equation (3.88) into (2.3) and using relation $\vec{B} = \nabla \times \vec{A}$ result in the $\vec{A}, V - \vec{A}$ -formulation with motion in the conductive region Ω_c in the time domain,

$$\nabla \times (\nu \nabla \times \vec{A}) + \sigma \left(\frac{\partial \vec{A}}{\partial t} - \vec{v} \times \nabla \times \vec{A} \right) = \vec{0}, \quad \text{in } \Omega_c, \quad (3.92)$$

The summarized equations are the following in time domain,

$$\nabla \times (\nu \nabla \times \vec{A}) + \sigma \left(\frac{\partial \vec{A}}{\partial t} - \vec{v} \times \nabla \times \vec{A} \right) = \vec{0}, \quad \text{in } \Omega_c, \quad (3.93)$$

$$\nabla \times (\nu \nabla \times \vec{A}) = \vec{J}_0, \quad \text{in } \Omega_n, \quad (3.94)$$

$$\vec{n} \times \vec{A} = \vec{0}, \quad \text{on } \Gamma_B, \quad (3.95)$$

$$\vec{n}_c \times \vec{A} + \vec{n}_n \times \vec{A} = \vec{0}, \quad \text{on } \Gamma_{nc}, \quad (3.96)$$

$$(\nu \nabla \times \vec{A}) \times \vec{n}_c + (\nu \nabla \times \vec{A}) \times \vec{n}_n = \vec{0}, \quad \text{on } \Gamma_{nc}. \quad (3.97)$$

The summarized equations of the $\vec{A}, V - \vec{A}$ -formulation using a moving velocity in the frequency domain is given by

$$\nabla \times (\nu \nabla \times \vec{A}) + \sigma(j\omega \vec{A} - \vec{v} \times \nabla \times \vec{A}) = \vec{0}, \quad \text{in } \Omega_c, \quad (3.98)$$

$$\nabla \times (\nu \nabla \times \vec{A}) = \vec{J}_0, \quad \text{in } \Omega_n, \quad (3.99)$$

$$\vec{n} \times \vec{A} = \vec{0}, \quad \text{on } \Gamma_B, \quad (3.100)$$

$$\vec{n}_c \times \vec{A} + \vec{n}_n \times \vec{A} = \vec{0}, \quad \text{on } \Gamma_{nc}, \quad (3.101)$$

$$(\nu \nabla \times \vec{A}) \times \vec{n}_c + (\nu \nabla \times \vec{A}) \times \vec{n}_n = \vec{0}, \quad \text{on } \Gamma_{nc}. \quad (3.102)$$

3.4.3 The $\vec{T}, \Phi - \Phi$ - formulation with the motion voltage term

Basically this potential formulation has not been used in the simulation of induction machines, but some papers in the literature can be found from the other part of FEM analysis [34, 36–38].

Substitute equation (3.86) into (3.78) gives the next relation:

$$\nabla \times (\vec{E} + \vec{v} \times \vec{B}) = -\frac{\partial \vec{B}}{\partial t}. \quad (3.103)$$

At this formulation in two dimensional case the motion voltage term is the following. The velocity has been two component in two dimensional case, see (3.89). Substituting the relations (3.42) into the motion voltage term $\vec{v} \times \vec{B}$ and using the constitutive relation in (2.7) gives the following

$$\vec{v} \times \vec{B} = \vec{v} \times \mu \vec{H} = \vec{v} \times \mu(\vec{T}_0 + \vec{T} - \nabla \Phi). \quad (3.104)$$

Substitute the relation (3.104) and (3.42) and the constitutive relation in (2.7) into the (3.103) results in the following partial differential equation,

$$\nabla \times (\rho \nabla \times \vec{T} + \vec{v} \times \mu(\vec{T}_0 + \vec{T} - \nabla \Phi)) = -\mu \frac{\partial \vec{T}_0}{\partial t} - \mu \frac{\partial \vec{T}}{\partial t} + \mu \frac{\partial \nabla \Phi}{\partial t}. \quad (3.105)$$

Summarized the equations of the $\vec{T}, \Phi - \Phi$ - formulation with motion voltage term in the time domain are the following:

$$\nabla \times (\rho \nabla \times \vec{T} + \vec{v} \times \mu(\vec{T}_0 + \vec{T} - \nabla \Phi)) + \mu \frac{\partial \vec{T}}{\partial t} - \mu \frac{\partial \nabla \Phi}{\partial t} = -\mu \frac{\partial \vec{T}_0}{\partial t}, \quad \text{in } \Omega_c, \quad (3.106)$$

$$\nabla \cdot (\mu \vec{T} - \mu \nabla \Phi) = -\nabla \cdot (\mu \vec{T}_0), \quad \text{in } \Omega_c, \quad (3.107)$$

$$-\nabla \cdot (\mu \nabla \Phi) = -\nabla \cdot (\mu \vec{T}_0), \quad \text{in } \Omega_n, \quad (3.108)$$

$$(\mu \vec{T}_0 - \nabla \Phi) \cdot \vec{n} = 0, \quad \text{on } \Gamma_B, \quad (3.109)$$

$$\Phi \text{ is continuous on } \Gamma_{nc}, \quad (3.110)$$

$$\vec{T} \times \vec{n}_c = \vec{0}, \quad \text{on } \Gamma_{nc}, \quad (3.111)$$

$$(\mu \vec{T}_0 + \mu \vec{T} - \mu \nabla \Phi) \cdot \vec{n}_c + (\mu \vec{T}_0 - \mu \nabla \Phi) \cdot \vec{n}_n = 0, \quad \text{on } \Gamma_{nc}. \quad (3.112)$$

The summarized equations of this formulations in the frequency domain are the following:

$$\nabla \times (\rho \nabla \times \vec{T} + \vec{v} \times \mu(\vec{T}_0 + \vec{T} - \nabla \Phi)) + j\omega \mu \vec{T} - j\omega \mu \nabla \Phi = -j\omega \mu \vec{T}_0, \quad \text{in } \Omega_c, \quad (3.113)$$

$$\nabla \cdot (\mu \vec{T} - \mu \nabla \Phi) = -\nabla \cdot (\mu \vec{T}_0), \quad \text{in } \Omega_c, \quad (3.114)$$

$$-\nabla \cdot (\mu \nabla \Phi) = -\nabla \cdot (\mu \vec{T}_0), \quad \text{in } \Omega_n, \quad (3.115)$$

$$(\mu \vec{T}_0 - \nabla \Phi) \cdot \vec{n} = 0, \quad \text{on } \Gamma_B, \quad (3.116)$$

$$\Phi \text{ is continuous on } \Gamma_{nc}, \quad (3.117)$$

$$\vec{T} \times \vec{n}_c = \vec{0}, \quad \text{on } \Gamma_{nc}, \quad (3.118)$$

$$(\mu \vec{T}_0 + \mu \vec{T} - \mu \nabla \Phi) \cdot \vec{n}_c + (\mu \vec{T}_0 - \mu \nabla \Phi) \cdot \vec{n}_n = 0, \quad \text{on } \Gamma_{nc}. \quad (3.119)$$

Chapter 4

Weak formulation of eddy current problem

The finite element method is associated with variational methods [25] or residual methods [5,6,9,11–17]. The residual methods are established directly from the physical equations. It is a respectable advantage comparing with the different methods since is relatively easier to understand and to apply. This is the main reason why nowadays most of the FEM analysis is performed by using the residual method. The Galerkin's method is a particular form of residual method and it is widely used in electromagnetism. The finite element method is based on the Galerkin's method of the weighted residual method [5,6,9,11–18,22,25].

The weighted residual method [6] can be applied to minimize the residual of a partial differential equation. The best approximation for the potentials can be obtained when the integral of the residual of the partial differential equation multiplied by a weighting function over the problem domain is equal to zero. The weighting function can be arbitrary, but in Galerkin's method, the weighting functions are selected to be the same as those used for expansion of the approximate solution. Furthermore, the weak formulation of eddy current field formulations is presented in this chapter.

4.1 The weak formulation with Galerkin's method

The weak formulation of the weighted residual method can be obtained when applying the rule of integration by parts to decrease the order of the differential operator in the inner product. The finite element method can be derived from this group of the weighted residual method. In the case of finite element method, the weighting function and the basis function of the approximating function are the same.

The finite element method use the the weak formulation with Galerkins method when the basis functions of the approximating function and the weighting function are the same. Here, the weak formulations of the potential formulations according to Galerkin's

method are presented, which are appropriate in the finite element method. In the following $\vec{W} = \vec{W}(\vec{r})$ denotes the vector weighting function as well as the basis functions of approximating function and $N = N(\vec{r})$ denotes the scalar weighting function as well as the basis functions of approximating function [5, 6, 9, 11–15, 22].

Scalar potentials $\Phi = \Phi(\vec{r})$, or $\Phi = \Phi(\vec{r}, t)$ are approximated by an expansion in terms of I elements of an entire function set N_i . Vector potentials $\vec{A} = \vec{A}(\vec{r})$, or $\vec{A} = \vec{A}(\vec{r}, t)$ are approximated by an expansion in terms of J elements of an entire function set \vec{W}_j . Shape functions N_i and \vec{W}_j are the elements of an entire function set, which can be defined in many ways. The definition of these elements are presented in chapter 5.

In the following \vec{A}^κ , \vec{T}_0^κ , \vec{T}^κ , Φ^κ will denote the approximated unknown potential functions.

4.1.1 The weak formulations of $\vec{A}, V - \vec{A}$ - formulation with motion voltage term

In three dimensional case, there are two unknown potentials in this formulation, the magnetic vector potential \vec{A} in the whole problem region $\Omega_c \cup \Omega_n$ and the electric scalar potential V defined only in the eddy current region Ω_c , consequently two partial differential equations are needed.

In two dimensional case, than this induction machine problems, it is only one unknown potential in this formulation, the magnetic vector potential \vec{A} in the whole problem region $\Omega_c \cup \Omega_n$, consequently only one equation is needed.

The weak formulation is based on the partial differential equations (3.93) and (3.94) and on the interface condition (3.97),

$$\begin{aligned}
& \int_{\Omega_c \cup \Omega_n} \vec{W}_k \cdot [\nabla \times (\nu \nabla \times \vec{A}^\kappa)] d\Omega \\
& + \int_{\Omega_c} \sigma \vec{W}_k \cdot \left(\frac{\partial \vec{A}^\kappa}{\partial t} - \vec{v} \times \nabla \times \vec{A}^\kappa \right) d\Omega \\
& + \int_{\Gamma_{nc}} \vec{W}_k \cdot [(\nu \nabla \times \vec{A}^\kappa) \times \vec{n}_c + (\nu \nabla \times \vec{A}^\kappa) \times \vec{n}_n] d\Gamma \\
& = \int_{\Omega_n} \vec{W}_k \cdot \vec{J}_0^\kappa d\Omega,
\end{aligned} \tag{4.1}$$

where $k = 1, \dots, I$.

The second order derivative in the first and in the third integrals can be reduced to first order one by using the mathematical identity

$$\nabla \cdot (\vec{a} \times \vec{b}) = \vec{b} \cdot \nabla \times \vec{a} - \vec{a} \cdot \nabla \times \vec{b}, \tag{4.2}$$

with the notation $\vec{a} = \nu \nabla \times \vec{A}^\kappa$ and $\vec{b} = \vec{W}_k$, finally

$$\begin{aligned}
& \int_{\Omega_c \cup \Omega_n} \nu (\nabla \times \vec{W}_k) \cdot (\nabla \times \vec{A}^\kappa) \, d\Omega \\
& + \int_{\Omega_c} \vec{W}_k \cdot \sigma \left(\frac{\partial \vec{A}^\kappa}{\partial t} - \vec{v} \times \nabla \times \vec{A}^\kappa \right) \, d\Omega \\
& + \int_{\Gamma_{nc}} [(\nu \nabla \times \vec{A}^\kappa \times \vec{W}_k)] \cdot \vec{n} \, d\Gamma + \int_{\Gamma_B \cup \Gamma_{nc}} [(\nu \nabla \times \vec{A}^\kappa \times \vec{W}_k)] \cdot \vec{n} \, d\Gamma \\
& + \int_{\Gamma_{nc}} \vec{W}_k \cdot [(\nu \nabla \times \vec{A}^\kappa) \times \vec{n}_c + (\nu \nabla \times \vec{A}^\kappa) \times \vec{n}_n] \, d\Gamma \\
& = \int_{\Omega_n} \vec{W}_k \cdot \vec{J}_0^\kappa \, d\Omega
\end{aligned} \tag{4.3}$$

can be obtain. The first and the second boundary integral terms are vanishing on the boundary part Γ_{nc} , respectively, because of the third integral term after using the identity

$$[(\nu \nabla \times \vec{A}^\kappa) \times \vec{W}_k] \cdot \vec{n} = [\vec{n} \times (\nu \nabla \times \vec{A}^\kappa)] \cdot \vec{W}_k = -\vec{W}_k \cdot [(\nu \nabla \times \vec{A}^\kappa) \times \vec{n}]. \tag{4.4}$$

The second boundary integral term is equal to zero on the rest part Γ_B , because of the Dirichlet type boundary condition (3.95), i.e. $\vec{W}_k \times \vec{n} = \vec{0}$ on this boundary.

Finally, in the two dimensional case the weak formulation of the \vec{A} - potential formulation with motion voltage term in the time domain is the following:

$$\begin{aligned}
& \int_{\Omega_c \cup \Omega_n} \nu (\nabla \times \vec{W}_k) \cdot (\nabla \times \vec{A}^\kappa) \, d\Omega \\
& + \int_{\Omega_c} \vec{W}_k \cdot \sigma \left(\frac{\partial \vec{A}^\kappa}{\partial t} - \vec{v} \times \nabla \times \vec{A}^\kappa \right) \, d\Omega \\
& = \int_{\Omega_n} \vec{W}_k \cdot \vec{J}_0^\kappa \, d\Omega.
\end{aligned} \tag{4.5}$$

The weak formulation of this potential formulation in the frequency domian is the following, which coming from the partial differential equations (3.98) and (3.99) and on the interface condition (3.102):

$$\begin{aligned}
& \int_{\Omega_c \cup \Omega_n} \nu (\nabla \times \vec{W}_k) \cdot (\nabla \times \vec{A}^\kappa) \, d\Omega \\
& + \int_{\Omega_c} \vec{W}_k \cdot \sigma (j\omega \vec{A}^\kappa - \vec{v} \times \nabla \times \vec{A}^\kappa) \, d\Omega \\
& = \int_{\Omega_n} \vec{W}_k \cdot \vec{J}_0^\kappa \, d\Omega,
\end{aligned} \tag{4.6}$$

where $k = 1, \dots, I$.

4.1.2 The weak formulations of \vec{T} , $\Phi - \Phi$ - formulation with motion voltage term

There are two unknown potentials in this formulation, too, the current vector potential \vec{T} in the eddy current region Ω_c and the reduced magnetic scalar potential Φ in the whole region $\Omega_c \cup \Omega_n$, that is two equations must be realized, coming from the partial differential equations (3.106)-(3.108) and the boundary and interface conditions (3.109)-(3.112).

The first weak formulation is based on the partial differential equation (3.106),

$$\begin{aligned} & \int_{\Omega_c} \vec{W}_k \cdot [\nabla \times (\rho \nabla \times \vec{T}^\kappa + \vec{v} \times \mu(\vec{T}_0^\kappa + \vec{T}^\kappa - \nabla \Phi^\kappa))] d\Omega \\ & + \int_{\Omega_c} \vec{W}_k \cdot \left[\mu \frac{\partial \vec{T}^\kappa}{\partial t} - \mu \nabla \frac{\partial \Phi^\kappa}{\partial t} \right] d\Omega \\ & = - \int_{\Omega_c} \mu \vec{W}_k \cdot \frac{\partial \vec{T}_0^\kappa}{\partial t} d\Omega, \end{aligned} \quad (4.7)$$

where $k = 1, \dots, J$.

The second order derivatives in the first integral can be reduced to first order one by using the identity

$$\nabla \cdot (\vec{a} \times \vec{b}) = \vec{b} \cdot \nabla \times \vec{a} - \vec{a} \cdot \nabla \times \vec{b}, \quad (4.8)$$

with the notation $\vec{a} = \rho \nabla \times \vec{T}^\kappa + \vec{v} \times \mu(\vec{T}_0^\kappa + \vec{T}^\kappa - \nabla \Phi^\kappa)$ and $\vec{b} = \vec{W}_k$,

$$\begin{aligned} & \int_{\Omega_c} [\rho (\nabla \times \vec{W}_k) \cdot (\nabla \times \vec{T}^\kappa + \vec{v} \times \mu(\vec{T}_0^\kappa + \vec{T}^\kappa - \nabla \Phi^\kappa))] d\Omega \\ & + \int_{\Omega_c} \left[\mu \vec{W}_k \cdot \frac{\partial \vec{T}^\kappa}{\partial t} - \mu \vec{W}_k \cdot \nabla \frac{\partial \Phi^\kappa}{\partial t} \right] d\Omega \\ & + \int_{\Gamma_{nc}} [(\rho \nabla \times \vec{T}^\kappa + \vec{v} \times \mu(\vec{T}_0^\kappa + \vec{T}^\kappa - \nabla \Phi^\kappa)) \times \vec{W}_k] \cdot \vec{n} d\Gamma \\ & = - \int_{\Omega_c} \mu \vec{W}_k \cdot \frac{\partial \vec{T}_0^\kappa}{\partial t} d\Omega. \end{aligned} \quad (4.9)$$

The first boundary integral term is equal to zero on the part Γ_{nc} , because of the Dirichlet type boundary and interface condition (3.111), i.e. $\vec{W}_k \times \vec{n} = 0$ on Γ_{nc} .

Finally, the first equation of the weak form is the following:

$$\begin{aligned}
& \int_{\Omega_c} [\rho(\nabla \times \vec{W}_k) \cdot (\nabla \times \vec{T}^\kappa + \vec{v} \times \mu(\vec{T}_0^\kappa + \vec{T}^\kappa - \nabla \Phi^\kappa))] \, d\Omega \\
& + \int_{\Omega_c} \left[\mu \vec{W}_k \cdot \frac{\partial \vec{T}^\kappa}{\partial t} - \mu \vec{W}_k \cdot \nabla \frac{\partial \Phi^\kappa}{\partial t} \right] \, d\Omega \\
& = - \int_{\Omega_c} \mu \vec{W}_k \cdot \frac{\partial \vec{T}_0^\kappa}{\partial t} \, d\Omega.
\end{aligned} \tag{4.10}$$

The partial differential equations (3.107) and (3.108), moreover the Neumann type boundary conditions (3.109), (3.112) can be summarized in the weak formulation presented next. The time derivative of these partial differential equations and the according Neumann type boundary conditions must be performed, anyway the resulting system of equations will not be symmetric. It is noted that, it is useful to multiply the partial differential equations (3.107) and (3.108) by -1. After taking the time derivative, the following form can be obtained:

$$\begin{aligned}
& - \int_{\Omega_c} N_k \nabla \cdot \left(\mu \frac{\partial \vec{T}^\kappa}{\partial t} - \mu \nabla \frac{\partial \Phi^\kappa}{\partial t} \right) \, d\Omega \\
& + \int_{\Omega_n} N_k \nabla \cdot \left(\mu \nabla \frac{\partial \Phi^\kappa}{\partial t} \right) \, d\Omega \\
& + \int_{\Gamma_B} N_k \left(\mu \frac{\partial \vec{T}^\kappa}{\partial t} \cdot \vec{n} - \mu \nabla \frac{\partial \Phi^\kappa}{\partial t} \cdot \vec{n} \right) \, d\Gamma \\
& + \int_{\Gamma_{nc}} N_k \left(\mu \frac{\partial \vec{T}_0^\kappa}{\partial t} + \mu \frac{\partial \vec{T}^\kappa}{\partial t} - \mu \nabla \frac{\partial \Phi^\kappa}{\partial t} \right) \cdot \vec{n}_c \, d\Gamma \\
& + \int_{\Gamma_{nc}} N_k \left(\mu \frac{\partial \vec{T}_0^\kappa}{\partial t} - \mu \nabla \frac{\partial \Phi^\kappa}{\partial t} \right) \cdot \vec{n}_n \, d\Gamma \\
& = \int_{\Omega_c} N_k \nabla \cdot \left(\mu \frac{\partial \vec{T}_0^\kappa}{\partial t} \right) \, d\Omega \\
& + \int_{\Omega_n} N_k \nabla \cdot \left(\mu \frac{\partial \vec{T}_0^\kappa}{\partial t} \right) \, d\Omega,
\end{aligned} \tag{4.11}$$

where $k = 1, \dots, I$.

The first, the second and the last three integral terms can be reformulated by the use of the identity

$$\nabla(\varphi \vec{a}) = \vec{a} \cdot \nabla \varphi + \varphi \nabla \cdot \vec{a} \tag{4.12}$$

with the notation $\varphi = N_k$ and $\vec{a} = \mu \partial \vec{T}^\kappa / \partial t$, or $\vec{a} = \mu \nabla \partial \Phi^\kappa / \partial t$, or $\vec{a} = \mu \partial \vec{T}_0^\kappa / \partial t$,

$$\begin{aligned}
& \int_{\Omega_c} \mu \nabla N_k \cdot \frac{\partial \vec{T}^\kappa}{\partial t} d\Omega - \int_{\Gamma_{nc}} N_k \mu \frac{\partial \vec{T}^\kappa}{\partial t} \cdot \vec{n} d\Gamma \\
& - \int_{\Omega_c} \mu \nabla N_k \cdot \frac{\partial \Phi^\kappa}{\partial t} d\Omega + \int_{\Gamma_{nc}} N_k \mu \frac{\partial \Phi^\kappa}{\partial t} \cdot \vec{n} d\Gamma \\
& - \int_{\Omega_n} \mu \nabla N_k \cdot \frac{\partial \Phi^\kappa}{\partial t} d\Omega + \int_{\Gamma_B \cup \Gamma_{nc}} N_k \mu \frac{\partial \Phi^\kappa}{\partial t} \cdot \vec{n} d\Gamma \\
& + \int_{\Gamma_B} N_k \left(\mu \frac{\partial \vec{T}_0^\kappa}{\partial t} \cdot \vec{n} - \mu \nabla \frac{\partial \Phi^\kappa}{\partial t} \cdot \vec{n} \right) d\Gamma \\
& + \int_{\Gamma_{nc}} N_k \left(\mu \frac{\partial \vec{T}_0^\kappa}{\partial t} + \mu \frac{\partial \vec{T}^\kappa}{\partial t} - \mu \nabla \frac{\partial \Phi^\kappa}{\partial t} \right) \cdot \vec{n}_c d\Gamma \\
& + \int_{\Gamma_{nc}} N_k \left(\mu \frac{\partial \vec{T}_0^\kappa}{\partial t} - \mu \nabla \frac{\partial \Phi^\kappa}{\partial t} \right) \cdot \vec{n}_n d\Gamma \\
& = - \int_{\Omega_c} \mu \nabla N_k \cdot \frac{\partial \vec{T}_0^\kappa}{\partial t} d\Omega + \int_{\Gamma_{nc}} N_k \mu \frac{\partial \vec{T}_0^\kappa}{\partial t} \cdot \vec{n} d\Gamma \\
& - \int_{\Omega_n} \mu \nabla N_k \cdot \frac{\partial \vec{T}_0^\kappa}{\partial t} d\Omega + \int_{\Gamma_B \cup \Gamma_{nc}} N_k \mu \frac{\partial \vec{T}_0^\kappa}{\partial t} \cdot \vec{n} d\Gamma.
\end{aligned} \tag{4.13}$$

The first, and the second, moreover the third and the last boundary terms defined on Γ_{nc} are vanishing, because of the same terms with opposite sign in the fifth and sixth boundary integral term. The fourth boundary integral, defined on Γ_B is vanishing according to the terms in the third and in the eighth boundary integrals.

Finally, the following weak formulation can be obtained:

$$\begin{aligned}
& \int_{\Omega_c} \mu \nabla N_k \cdot \frac{\partial \vec{T}^\kappa}{\partial t} d\Omega - \int_{\Omega_c \cup \Omega_n} \mu \nabla N_k \cdot \frac{\partial \Phi^\kappa}{\partial t} d\Omega \\
& = - \int_{\Omega_c \cup \Omega_n} \mu \nabla N_k \cdot \frac{\partial \vec{T}_0^\kappa}{\partial t} d\Omega.
\end{aligned} \tag{4.14}$$

Finally, the weak formulation of the \vec{T} , $\Phi - \Phi$ - formulation in the time domain is the following,

$$\begin{aligned}
& \int_{\Omega_c} [\rho (\nabla \times \vec{W}_k) \cdot (\nabla \times \vec{T}^\kappa + \vec{v} \times \mu (\vec{T}_0^\kappa + \vec{T}^\kappa - \nabla \Phi^\kappa))] d\Omega \\
& + \int_{\Omega_c} \left[\mu \vec{W}_k \cdot \frac{\partial \vec{T}^\kappa}{\partial t} - \mu \vec{W}_k \cdot \nabla \frac{\partial \Phi^\kappa}{\partial t} \right] d\Omega \\
& = - \int_{\Omega_c} \mu \vec{W}_k \cdot \frac{\partial \vec{T}_0^\kappa}{\partial t} d\Omega,
\end{aligned} \tag{4.15}$$

$$\begin{aligned}
& - \int_{\Omega_c} \mu \nabla N_k \cdot \frac{\partial \vec{T}^\kappa}{\partial t} d\Omega + \int_{\Omega_c \cup \Omega_n} \mu \nabla N_k \cdot \frac{\partial \Phi^\kappa}{\partial t} d\Omega \\
& = \int_{\Omega_c \cup \Omega_n} \mu \nabla N_k \cdot \frac{\partial \vec{T}_0^\kappa}{\partial t} d\Omega.
\end{aligned} \tag{4.16}$$

The weak formulation of this potential formulation in the frequency domain is the following, which coming from the partial differential equations (3.114) and (3.115) and on the Neumann type boundary conditions (3.116), (3.119),

$$\begin{aligned}
& \int_{\Omega_c} [\rho(\nabla \times \vec{W}_k) \cdot (\nabla \times \vec{T}^\kappa + \vec{v} \times \mu(\vec{T}_0^\kappa + \vec{T}^\kappa - \nabla \Phi^\kappa))] d\Omega \\
& + \int_{\Omega_c} \left[\mu \vec{W}_k \cdot \text{j}\omega \vec{T}^\kappa - \mu \vec{W}_k \cdot \nabla \text{j}\omega \Phi^\kappa \right] d\Omega \\
& = - \int_{\Omega_c} \mu \vec{W}_k \cdot \text{j}\omega \vec{T}_0^\kappa d\Omega,
\end{aligned} \tag{4.17}$$

where $k = 1, \dots, J$,

$$\begin{aligned}
& - \int_{\Omega_c} \mu \nabla N_k \cdot \text{j}\omega \vec{T}^\kappa d\Omega + \int_{\Omega_c} \mu \nabla N_k \cdot \text{j}\omega \Phi^\kappa d\Omega \\
& + \int_{\Omega_n} \mu \nabla N_k \cdot \text{j}\omega \Phi^\kappa d\Omega \\
& = \int_{\Omega_c} \mu \nabla N_k \cdot \text{j}\omega \vec{T}_0^\kappa d\Omega + \int_{\Omega_n} \mu \nabla N_k \cdot \text{j}\omega \vec{T}_0^\kappa d\Omega,
\end{aligned} \tag{4.18}$$

where $k = 1, \dots, I$.

Chapter 5

The finite element method

The basis of numerical techniques is to reduce the partial differential equations by using scalar and vector potentials to algebraic ones. These algebraic equations can be solved by numerical methods e.g. (4.6), (4.17) [5,6,9,11–14,16,17,22,25]. This reduction can be done by discretizing the partial differential equations in time if necessary and in space. The potential functions, the approximation method and the generated mesh distinguish the numerical field solvers.

The Finite Element Method (FEM) is the most popular and the most flexible numerical technique to determine the approximate solution of the partial differential equations in engineering. For example, commercially available FEM software package is COMSOL Multiphysics [39], which has been used in this work.

5.1 Fundamentals of finite element method

This section summarizes the finite element method as a computer aided design (CAD) technique in electrical engineering to obtain the electromagnetic field quantities in the case of eddy current field problems. Here, we show how to approximate potential functions with nodal and vector functions, and the main steps of simulation with FEM. This shown in Fig. 5.1.

5.1.1 Preprocessing

A. Model specification

Firstly, in the model specification phase, the model of the problem, which simulation require electromagnetic field calculations must be set up, i.e. we have to find out the partial differential equations, which must be solved with prescribed boundary and continuity conditions. We have to find out, whether it is a eddy current free reagon, where has been used the static magnetic field equations, and which one is an eddy current region

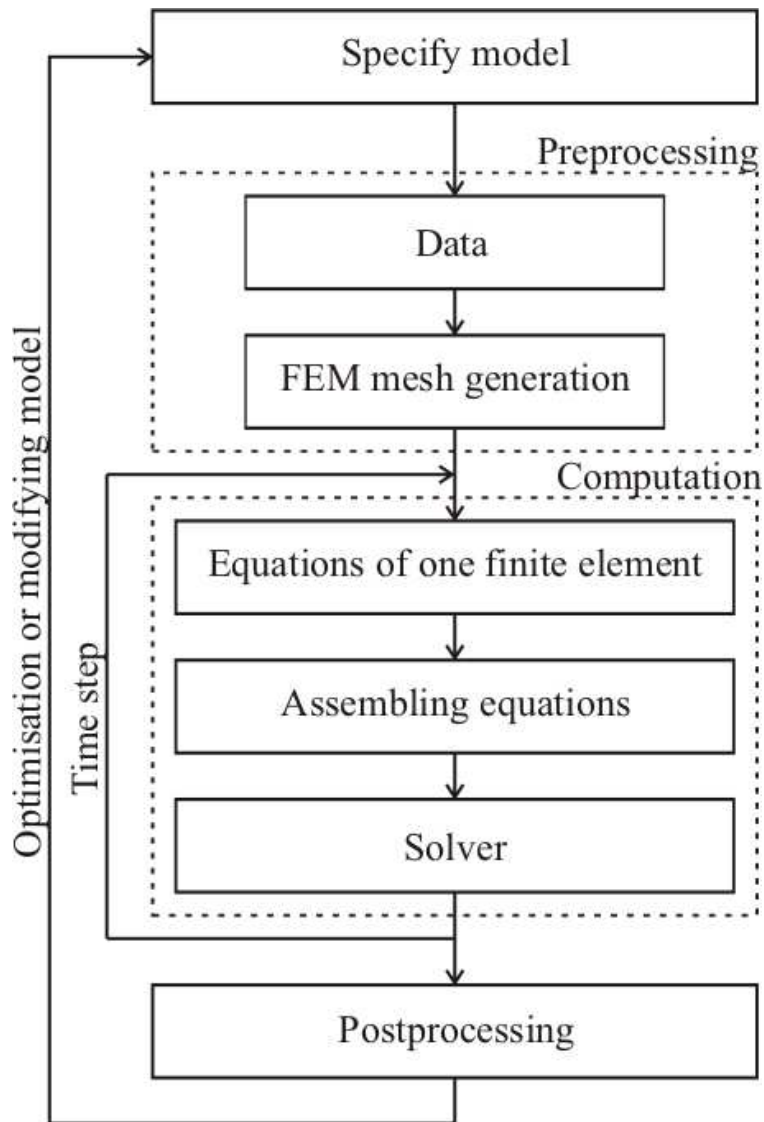


Fig. 5.1. Steps of simulation by finite element method.

where has been used the magnetodynamic Maxwell's equations, and how the characteristics of the materials look like. After selecting potentials, the weak formulation of these partial differential equations must be worked out as well. It is depending on the problem, of course, but the chosen mathematical model of the arrangement should be adequate to calculate electromagnetic field quantities in the given accuracy. The geometry of the problem must be defined by a CAD software tool.

The next step is the preprocessing task. Here we have to give the values of different parameters, such as the material properties, i.e. the relative permeability, the excitation signal, angular velocity and the others. The geometry can be simplified according to symmetries or axial symmetries.

This step is shown in Fig. 5.2. In this figure the geometry of the three-phase motor, the used constants, the different subdomain expressions e.g. constitutive relations, and the weak formulations of partial differential equations of subdomains can be seen.

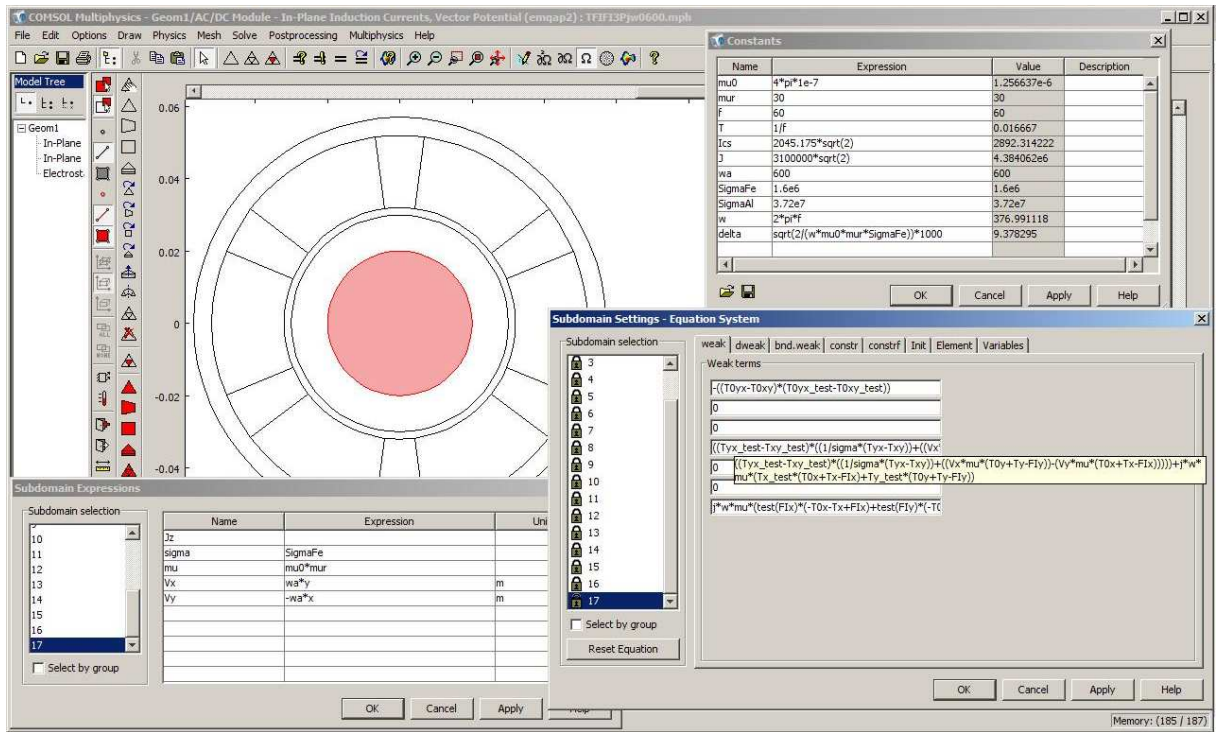


Fig. 5.2. The model specification in COMSOL Multiphysics.

B. 2D finite element mesh

In the preprocessing task the geometry of the problem must be discretized by a finite element mesh. The fundamental idea of FEM is to divide the problem region to be analyzed into smaller finite elements with given shape. A finite element can be triangles or quadrangles in two dimensions.

A triangle (Fig. 5.3(a)) has three vertices 1, 2 and 3, here numbered anticlockwise and has 3 edges. The quadrangle element (Fig. 5.3(b)) has 4 nodes and 4 edges.

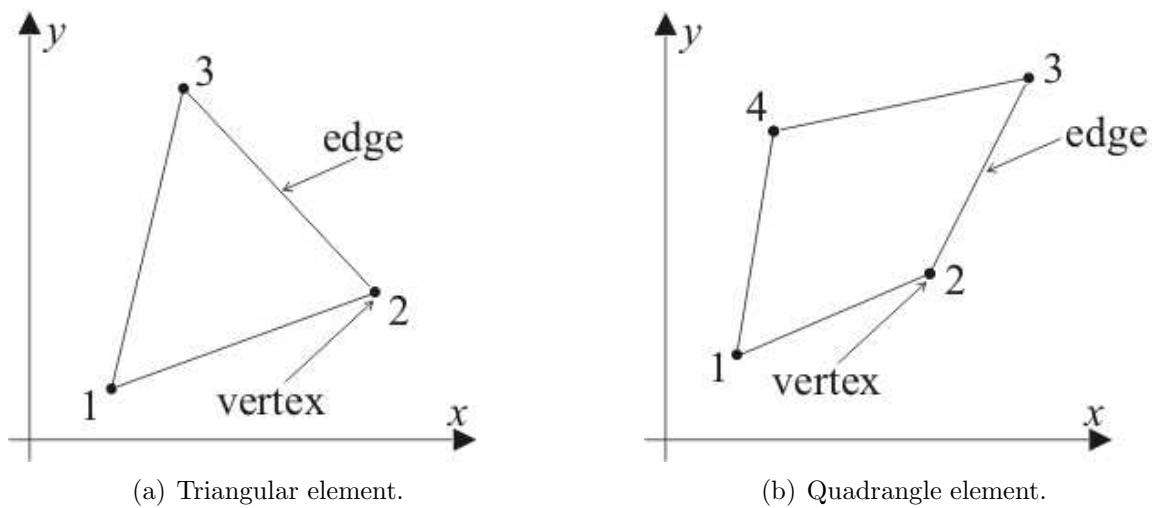


Fig. 5.3. Typical finite elements in the two dimensional $x - y$ plane.

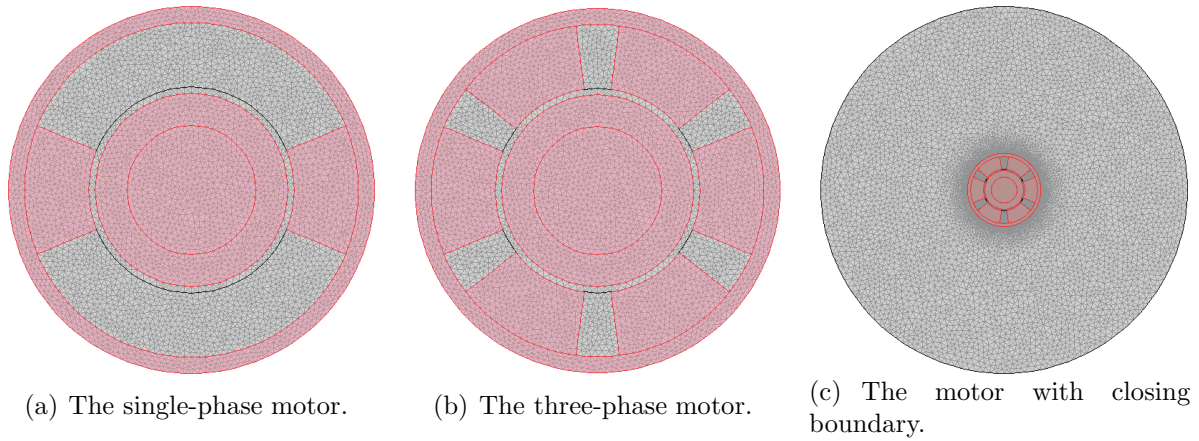


Fig. 5.4. The two induction motors is meshed by triangles.

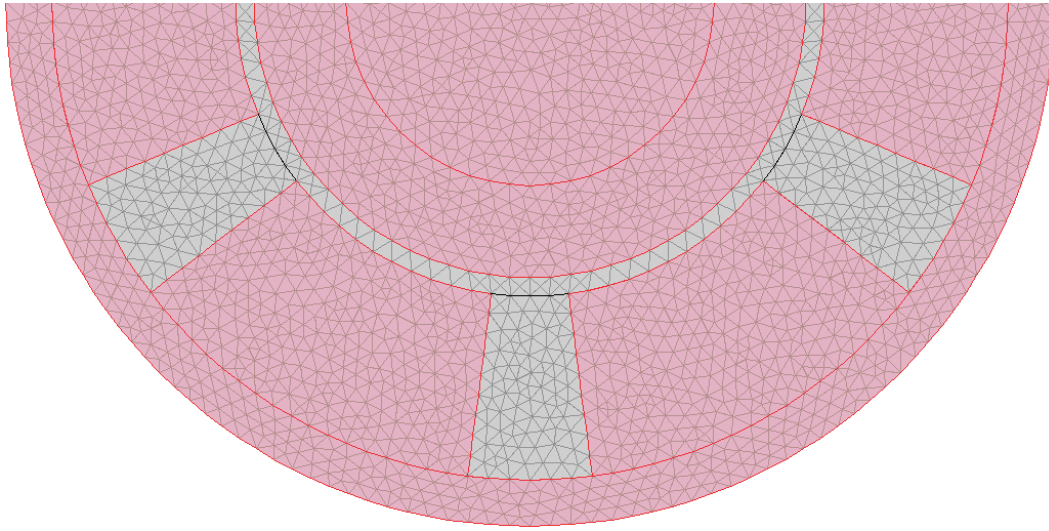


Fig. 5.5. The three-phase induction motor is meshed by triangles.

FEM mesh, as illustration, generated by COMSOL multiphysics can be seen in Fig. 5.4 and Fig. 5.5. The arrangement of single-phase (Fig. 5.4(a)), and of three-phase motor (Fig. 5.4(b)) have been discretized by a triangular mesh as it is shown at the Fig. 5.4. In Fig. 5.5, the enlarged region of the half of the three-phase motor is shown.

All the simulations have been studied using the same mesh, which consists of 43522 second-order triangular elements as it can be seen on the left hand side of Fig. 5.4. Fig. 5.4(c) shows the used mesh to calculate the impressed current vector potential \vec{T}_0 . \vec{T}_0 is calculated in free space, i.e. $\mu = \mu_0$ must be set everywhere in the problem region. The mesh of induction motor and the closing boundary consists of 223426 second-order triangular elements. The number of unknowns are different in the two potential formulations. Using the $\vec{A}, V - \vec{A}$ - formulation, the number of unknowns is 87405, and in case of the $\vec{T}, \Phi - \Phi$ - formulation the number of unknowns is 147107. In case of the $\vec{A}, V - \vec{A}$ - formulation, only the magnetic vector potential \vec{A} in all the problem region $\Omega_c \cup \Omega_n$ is present. In the $\vec{T}, \Phi - \Phi$ - formulation, current vector potential \vec{T} only in the

conductive region Ω_c , while the reduced magnetic scalar potential Φ in the conductive and non-conductive region $\Omega_c \cup \Omega_n$ must be used.

5.1.2 Shape functions

The presented potential functions can be scalar valued, e.g. the reduced magnetic scalar potential Φ , or vector valued, e.g. the magnetic vector potential \vec{A} , or the current vector potential \vec{T} and or the impressed current vector potential \vec{T}_0 .

The scalar potential functions can be approximated by the so-called nodal shape functions and the vector potential functions can be approximated by either nodal or so-called vector shape functions, also called edge shape functions.

Generally, a shape function is a simple continuous polynomial function defined in a finite element and it is depending on the type of the used finite element.

Each shape function is defined in the entire problem region, and a scalar shape function corresponds to just one nodal point and each vector shape function corresponds to just one edge. Each scalar shape function is nonzero over just those finite elements that contain its nodal point and equals to zero over all other elements and each vector shape function is nonzero over just those finite elements that contain its edge and equals to zero over all other elements. Furthermore, the scalar shape function has a value unity at its nodal point and zero at all the other nodal points, and the line integral of a vector shape function is equal to one along its edge and the line integral of it is equal to zero along the other edges. Moreover the shape functions are linearly independent, i.e. no shape function equals a linear combination of the other shape functions.

The accuracy of solution obtained by FEM can be increased in three ways. The first one is called h -FEM, it is increasing the number of finite elements, i.e. decreasing the element size. The second way is called p -FEM, it is to increase the degree of polynomials building up a shape function. The third way is called hp -FEM, it is the mixture of the previous methods.

A. Nodal shape functions

Scalar potential functions can be represented by a linear combination of shape functions associated with nodes of the finite element mesh. Within a finite element, a scalar potential function $\Phi = \Phi(\vec{r}, t)$ is approximated by [9, 12]

$$\Phi \simeq \sum_{i=1}^m N_i \Phi_i, \quad (5.1)$$

where $N_i = N_i(\vec{r})$ and $\Phi_i = \Phi_i(t)$ are the nodal shape functions and the value of potential function corresponding to the i^{th} node, respectively. The number of degrees of freedom is $m = 3$ in a 2D problem using triangular FEM mesh, and the shape functions are linear,

and the number of degree of freedom is $m=6$ the shape functions are second order. The nodal shape functions can be defined by the relation

$$N_i = \begin{cases} 1, & \text{at the node } i, \\ 0, & \text{at other nodes.} \end{cases} \quad (5.2)$$

2D linear shape functions can be built up as follows when using a finite element mesh with triangular finite elements. Linear basis functions can be introduced by using the so-called barycentric coordinate system in a triangle. The barycentric coordinate system is a coordinate system for an n -dimensional Euclidean space in which each point is represented by n constants whose sum is 1, and whose product with a given set of linearly independent points equals the point. The area of a triangle is denoted by Δ and it can be calculated as

$$\Delta = \frac{1}{2} \begin{vmatrix} 1 & x_1 & y_1 \\ 1 & x_2 & y_2 \\ 1 & x_3 & y_3 \end{vmatrix}, \quad (5.3)$$

where (x_1, y_1) , (x_2, y_2) and (x_3, y_3) are the coordinates of the three nodes of the triangle in the global coordinate system building an anticlockwise sequence. The area functions (see Fig. 5.6) of a given point inside the triangle with coordinates (x, y) can be calculated as

$$\Delta_1 = \frac{1}{2} \begin{vmatrix} 1 & x & y \\ 1 & x_2 & y_2 \\ 1 & x_3 & y_3 \end{vmatrix}, \quad \Delta_2 = \frac{1}{2} \begin{vmatrix} 1 & x_1 & y_1 \\ 1 & x & y \\ 1 & x_3 & y_3 \end{vmatrix}, \quad \Delta_3 = \frac{1}{2} \begin{vmatrix} 1 & x_1 & y_1 \\ 1 & x_2 & y_2 \\ 1 & x & y \end{vmatrix}, \quad (5.4)$$

i.e. $\Delta_1 = \Delta_1(x, y)$, $\Delta_2 = \Delta_2(x, y)$ and $\Delta_3 = \Delta_3(x, y)$ are depending on the coordinates x and y .

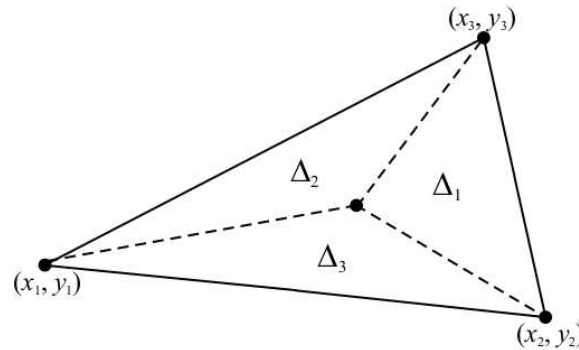


Fig. 5.6. The area of the triangle.

The barycentric coordinates are $L_i = L_i(x, y)$ can be defined by the above area functions as

$$L_i = \frac{\Delta_i}{\Delta}, \quad i = 1, 2, 3. \quad (5.5)$$

Three linear shape functions $N_i = N_i(x, y)$ can be described as

$$N_i = L_i, \quad i = 1, 2, 3. \quad (5.6)$$

The shape function N_i is equal to 1 at the i^{th} node of the triangle and it is equal to zero at the other two nodes, because Δ_i is equal to Δ at node i and it is equal to zero at the other two nodes. That is why the relation (5.2) is satisfied. It is obvious that the three shape functions are linearly independent.

If the potential at the nodes is known, then a linear approximation of the potential function can be represented by (5.1). The derivative of a first order approximation is zeroth order, i.e. constant. The magnetic field intensity \vec{H} , or the magnetic flux density \vec{B} are constant within a triangle, if these are obtained from a first order approximation by $\vec{H} = -\nabla\Phi$, or $\vec{B} = \nabla \times \vec{A}$. This may result in inaccurate solution. This is the reason why higher order approximations are studied.

Higher order shape functions can also be built up by using the barycentric coordinates L_1 , L_2 and L_3 introduced above in (5.5) [9, 12].

A polynomial of order n must contain all possible terms $x^p y^q$, $0 \leq p + q \leq n$, as it is presented by Pascal's triangle [9, 14, 15],

$$\begin{array}{cccc} 1 & & & \\ x & y & & \\ x^2 & xy & y^2 & \dots \end{array}$$

The first row contains the only one term of the zeroth order polynomials, the second and third rows contain the terms of the first and second order polynomials. Pascal's triangle can be used to generate the elements of a polynomial with given order. Such a polynomial contains

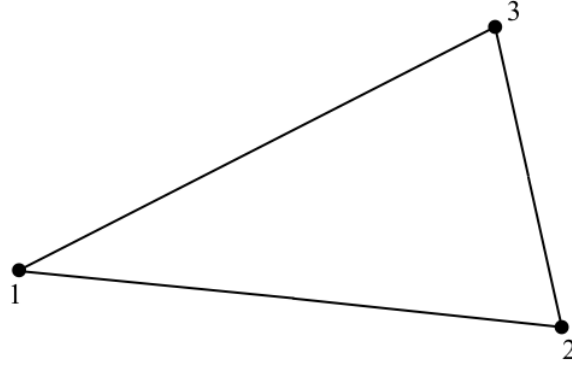
$$m = \frac{(n+1)(n+2)}{2} \quad (5.7)$$

elements altogether, i.e. $m = 1$ and $m = 3$ in the case of zeroth and the first and the second order polynomials. It means that m coefficients must be expressed, finally m points must be placed within a triangle. Pascal's triangle can be continued, of course.

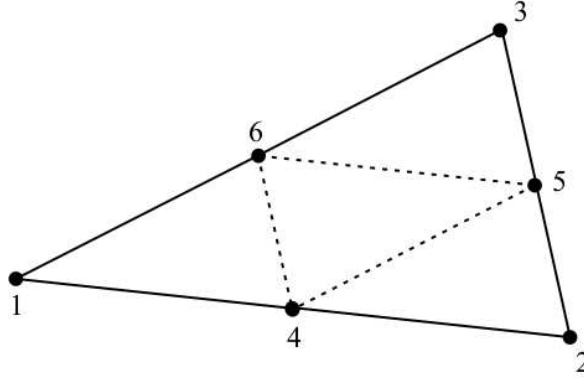
The interpolation function of order n can be constructed as

$$N_i = P_I^n(L_1)P_J^n(L_2)P_K^n(L_3), \quad \text{where } I + J + K = n, \quad (5.8)$$

and the integers I , J and K label the nodes within the triangle, resulting in a numbering scheme. Fig. 5.7 illustrated the numbering scheme of the first (Fig. 5.7(a)) and the second (Fig. 5.7(b)) order approximations.



(a) Linear element.



(b) Quadratic element.

Fig. 5.7. Numbering scheme for triangular elements.

The polynomials $P_I^n(L_1)$, $P_J^n(L_2)$ and $P_K^n(L_3)$ are defined as

$$P_I^n(L_1) = \prod_{p=0}^{I-1} \frac{nL_1 - p}{I - p} = \frac{1}{I!} \prod_{p=0}^{I-1} nL_1 - p, \quad \text{if } I > 0, \quad (5.9)$$

$$P_J^n(L_2) = \prod_{p=0}^{J-1} \frac{nL_2 - p}{J - p} = \frac{1}{J!} \prod_{p=0}^{J-1} nL_2 - p, \quad \text{if } J > 0, \quad (5.10)$$

$$P_K^n(L_3) = \prod_{p=0}^{K-1} \frac{nL_3 - p}{K - p} = \frac{1}{K!} \prod_{p=0}^{K-1} nL_3 - p, \quad \text{if } K > 0, \quad (5.11)$$

and as a definition

$$P_0^n = 1. \quad (5.12)$$

If $n=1$, then $m=3$, i.e. (see Fig. 5.7(a))

$$\begin{aligned} N_1 &= P_1^1(L_1)P_0^1(L_2)P_0^1(L_3) = L_1, \\ N_2 &= P_0^1(L_1)P_1^1(L_2)P_0^1(L_3) = L_2, \\ N_3 &= P_0^1(L_1)P_0^1(L_2)P_1^1(L_3) = L_3, \end{aligned} \quad (5.13)$$

since

$$P_1^1(L_i) = \prod_{p=0}^{1-1} \frac{1L_i - p}{1 - p} = L_i, \quad (5.14)$$

as it was mentioned (5.6).

If $n=2$, then $m=3$, i.e. (see Fig. 5.7(a))

$$\begin{aligned} N_1 &= P_2^2(L_1)P_0^2(L_2)P_0^2(L_3) = L_1(2L_1 - 1), \\ N_2 &= P_0^2(L_1)P_2^2(L_2)P_0^2(L_3) = L_2(2L_2 - 1), \\ N_3 &= P_0^2(L_1)P_0^2(L_2)P_2^2(L_3) = L_3(2L_3 - 1), \\ N_4 &= P_1^1(L_1)P_1^1(L_2)P_0^1(L_3) = 4L_1L_2, \\ N_5 &= P_0^1(L_1)P_1^1(L_2)P_1^1(L_3) = 4L_2L_3, \\ N_6 &= P_1^1(L_1)P_0^1(L_2)P_1^1(L_3) = 4L_1L_3, \end{aligned} \quad (5.15)$$

because

$$P_1^2(L_i) = \prod_{p=0}^{1-1} \frac{2L_i - p}{1 - p} = 2L_i, \quad (5.16)$$

and

$$P_2^2(L_i) = \prod_{p=0}^{2-1} \frac{2L_i - p}{2 - p} = L_i(2L_i - 1). \quad (5.17)$$

The scalar potential along any edge of a triangle is the linear combination of the values defined in the points of this edge (see Fig. 5.7), so that, if two triangles share the same vertice, the potential will be continuous across the interface element boundary. This means that the approximate solution is continuous everywhere, however its normal derivate is not.

The magnetic vector potential \vec{A} , and the magnetic scalar potential Φ have been approximated by second order nodal shape function in this study.

B. Edge shape functions

Vector potentials can be represented by either nodal shape functions or so-called edge shape functions. Edge shape functions are also called vector shape functions [9, 12].

The natural approach is to treat the vector field $\vec{T} = \vec{T}(\vec{r}, t)$ as two coupled scalar fields $T_x = T_x(\vec{r}, t)$, $T_y = T_y(\vec{r}, t)$, i.e.

$$\vec{T} = T_x \vec{e}_x + T_y \vec{e}_y \quad (5.18)$$

in 2D, respectively, \vec{e}_x , \vec{e}_y are the orthogonal unit vectors in the $x - y$ plane.

Nodal shape functions can be used in this case as well, as it was presented for scalar potentials in the previous section, however each node has two or three unknowns in 2D

or in 3D, respectively. Nodal shape functions can be applied to approximate the scalar components of the vector field \vec{T} . For example in 2D, \vec{T} can be approximated as

$$\vec{T} \simeq \sum_{i=1}^m N_i(T_{x,i}\vec{e}_x + T_{y,i}\vec{e}_y) = \vec{e}_x \sum_{i=1}^m N_i T_{x,i} + \vec{e}_y \sum_{i=1}^m N_i T_{y,i}. \quad (5.19)$$

Here $N_i = N_i(\vec{r})$ are the usual nodal shape functions defined by (5.2) and $T_{x,i} = T_{x,i}(t)$, $T_{y,i} = T_{y,i}(t)$, are the values of components of the approximated vector potential at node i . The number of degrees of freedom is $2m$ in a 2D problem using a triangular mesh.

Nodal shape functions are used to approximate gauged vector potentials. This approach was the first in the history of finite element method in electromagnetics. Unfortunately, there are some problems when the usual nodal based finite elements are used to interpolate vector potentials. The lack of gauging results in a system of algebraic equations, which has infinite number of solution and the application of iterative solvers sometimes fails. In this work the nodal shape function can be applied to approximate the magnetic vector potential \vec{A} , because this is a 2D problem, and the gauge is satisfied automatically.

The vector shape functions have been developed in the last decades, which application in static and eddy current field problems is more and more popular, because of their advantages. The use of edge shape functions solve the problems described above. Vector shape functions are usually called edge shape functions, because they are associated to the edges of the FEM mesh.

Instead of scalar shape functions, edge shape functions $\vec{W}_i = \vec{W}_i(\vec{r})$ can be applied to approximate a vector potential \vec{T} ,

$$\vec{T} \simeq \sum_{i=1}^K \vec{W}_i T_i, \quad (5.20)$$

where $T_i = T_i(t)$ is the line integral of the vector potential \vec{T} along the edge i . The approximation of the vector function T is known along the edges of the mesh, then (5.20) can be used to interpolate the function anywhere and in linear case $K = 3$. First order vector shape functions are defined by the line integral

$$\int_l \vec{W}_i \cdot d\vec{l} = \begin{cases} 1, & \text{along edge } i, \\ 0, & \text{at other edges,} \end{cases} \quad (5.21)$$

i.e. the line integral of the vector shape function \vec{W}_i along the i^{th} edge is equal to one. In other words, the vector shape function \vec{W}_i has tangential component only along the i^{th} edge and it has only normal component along the other edges, because $\vec{W}_i \cdot d\vec{l}$ is equal to zero only if the vectors \vec{W}_i and $d\vec{l}$ are perpendicular to each others.

If two triangles share the same vertices, the tangential component of the approxi-

mated vector potential will be continuous across the interface element boundary. This means that the tangential component of the approximate solution is continuous everywhere, however its normal component is not. In the words of equations, according to the definition (5.21), the line integral of the vector potential along the m^{th} edge is equal to T_m , i.e.

$$\int_{l_m} \vec{T} \cdot d\vec{l} = \int_{l_m} \left(\sum_{i=1}^K \vec{W}_i T_i \right) \cdot d\vec{l} = \sum_{i=1}^K \int_{l_m} (\vec{W}_i T_i) \cdot d\vec{l} = T_m \int_{l_m} \vec{W}_m \cdot d\vec{l} = T_m. \quad (5.22)$$

The vector function

$$\vec{w}_{ij} = L_i \nabla L_j - L_j \nabla L_i \quad (5.23)$$

will be applied to construct the edge shape functions, because it can be used in functions, which satisfies (5.21) and (5.22). According to the notations in (3.103), the edges of a finite element are pointing from node i to node j , as it can be seen in Fig. 5.8.

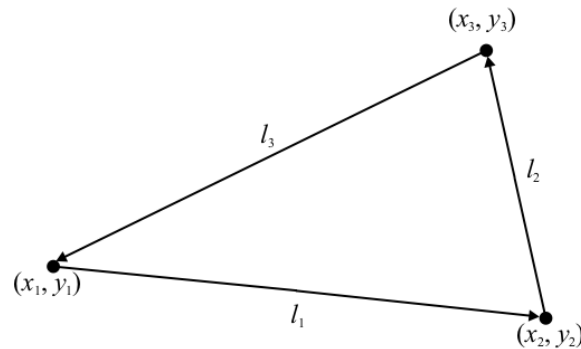


Fig. 5.8. The definition of edges with local directions of the triangular finite element.

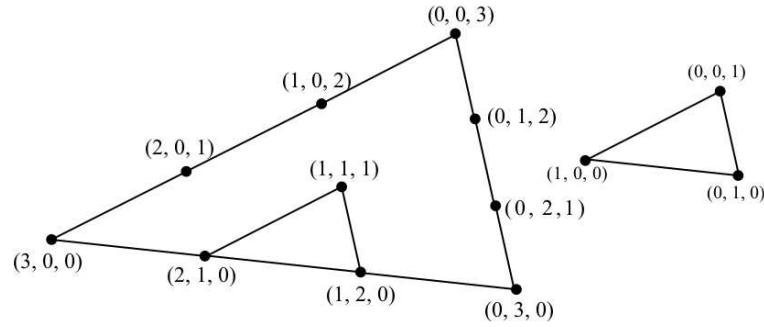
The edge shape functions defined on triangles based on (5.23) are collected. The basic 2D vector shape functions \vec{W}_i can be constructed by using the first order nodal shape functions,

$$\begin{aligned} \vec{W}_1 &= l_1(N_1 \nabla N_2 - N_2 \nabla N_1) \delta_1, \\ \vec{W}_2 &= l_2(N_2 \nabla N_3 - N_3 \nabla N_2) \delta_2, \\ \vec{W}_3 &= l_3(N_3 \nabla N_1 - N_1 \nabla N_3) \delta_3. \end{aligned} \quad (5.24)$$

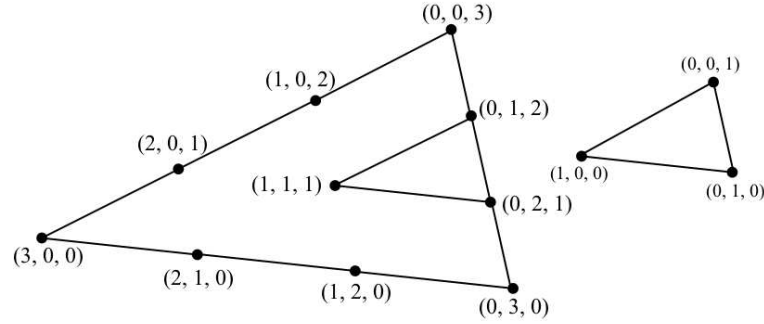
Here l_i (Fig. 5.8) denotes the length of the i^{th} edges of the triangle. The value of δ_i is equal to ± 1 , depending on whether the local direction of the edge is the same as the global direction or opposite (see Fig. 5.8 for local direction). This set of vector functions is called zeroth order vector shape functions.

If the approximation of the vector function \vec{T} is known along the edges of the mesh, then (5.20) can be used to interpolate the function anywhere and in linear case $m = 3$.

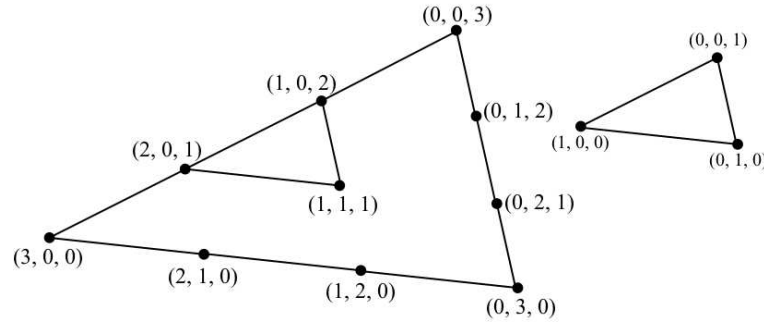
Higher order vector shape functions can be constructed by using the vector function



(a) Numbering scheme for the first order vector element associated with \vec{w}_{12} .



(b) Numbering scheme for the first order vector element associated with \vec{w}_{23} .



(c) Numbering scheme for the first order vector element associated with \vec{w}_{31} .

Fig. 5.9. Numbering scheme for the first order vector elements.

\vec{w}_{ij} defined by (5.23), too. This vector function must be multiplied by a complete interpolatory polynomial, which results in the higher order vector shape functions. First and second order polynomials will be used to build up first and second order vector shape functions. Here, we follow [9, 12], the method is as follows.

First of all, an indexing sequence must be set up, which is similar to the method used to build up the scalar shape functions, because the higher order vector shape functions are based on the Lagrange polynomials and (5.23). In the case of in first order approximation, the numbering scheme of the third order scalar interpolation can be used and the points are shown in Fig. 5.9 must be used to represent first order vector shape functions associated to the edge $\{1, 2\}$, $\{2, 3\}$ and $\{3, 1\}$, respectively. The interpolation points have been selected in this special way, because the interpolation of field vectors along

vertices have been avoided, i.e. the points have been shifted inside the triangle and the indexing scheme of order $n + 2$ is used to represent the vector interpolation of order n . This is called global numbering and denoted by (I, J, K) on the 'big' triangle, local numbering means the numbering scheme with the real order (i, j, k) defined over the 'small' triangle.

The COMSOL Multiphysics software uses this kind of vector shape functions, however $n = 0$, $n = 1$ and $n = 2$ are named as linear and quadratic vector shape functions.

In Fig. 5.10 the absolute value of magnetic flux density inside the rotor steel along the line $x = -20, \dots, 20\text{mm}$, $y = 0\text{mm}$ can be seen.

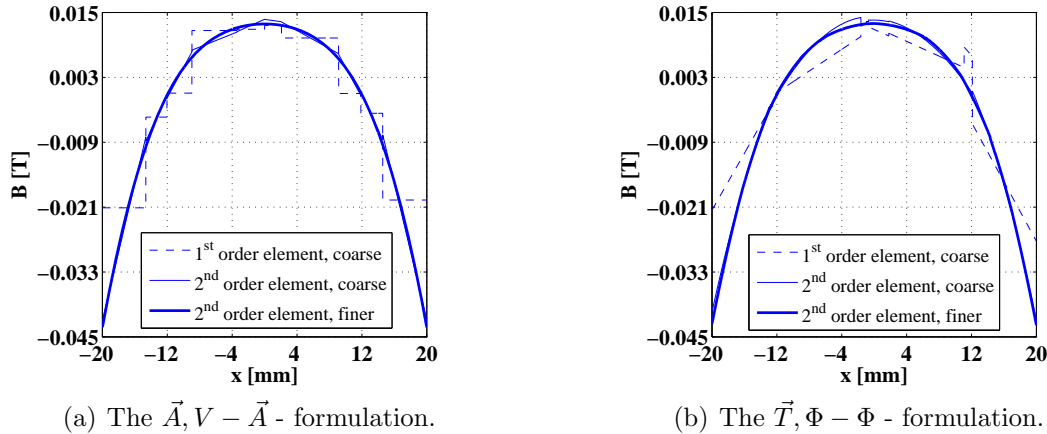


Fig. 5.10. Comparison between the different order element and different FEM mesh.

The accuracy of solution can not be increased very well by increasing the number of finite elements, however applying higher order approximation results in better distribution of the magnetic flux density. Here, the coarse mesh consists of 1335 triangles with 695 unknowns and the approximation is linear. The coarse mesh consist of 1335 trinagles with 2724 unknowns, the very fine mesh consists of 33568 triangles with 67453 unknowns when second order approximation is applied.

Fig. 5.11 shows the comparison between results simulated by the $\vec{A}, V - \vec{A}$ - formulation and by the $\vec{T}, \Phi - \Phi$ - formulation, both formulations with the second order approximation. The fine mesh with 8358 elements and 16877 unknowns has been used. The solutions of both potential formulations seem to be equal.

5.1.3 Computation

The next step in FEM simulations is solving the problem. The FEM equations, based on the weak formulations [5, 6, 9, 11–14, 16–18, 22, 25], must be set up in the level of one finite element, then these equations must be assembled through the FEM mesh. Assembling means that the global system of equations is built up, which solution is the approximation of the introduced potential. The obtained global system of algebraic

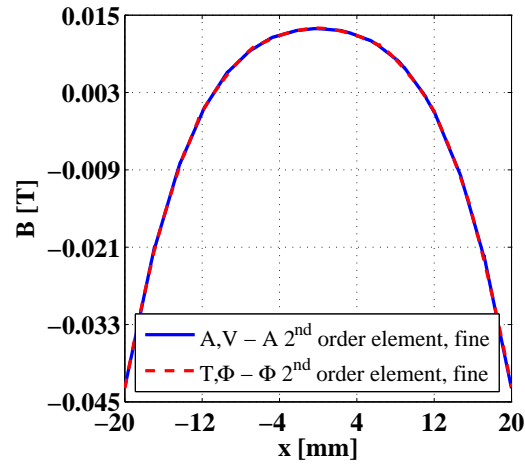


Fig. 5.11. Comparison between the potential formulations by the same order element and FEM mesh.

equations is linear, depending on the medium to be analyzed. Then this global system of equations must be solved by a solver. The computation may contain iteration. If the problem is solved in the time-domain, then the solution must be worked out at every discrete time instant.

If the problem is solved in the time-domain, the numerical computations were performed using computer programs developed under MATLAB environment using the COMSOL script language. Fig. 5.12 shows one part of the iteration script of the $\vec{T}, \Phi - \Phi$ - formulation in the time-domain.

A. Solvers

Generally, computation programs take into account the symmetry of the global matrix, and storing only the half of this matrix in the memory. However, in this case the whole matrix must be stored, because the global matrix is unsymmetric [10,32,35]. In practice, analysis with velocity terms normally needs a separate solver [10].

At the $\vec{A}, V - \vec{A}$ - potential formulation, the vector potential function \vec{A} has been approximated by nodal shape function, i.e. the problem based on nodal finite elements have been solved by the direct solver UMFPACK (Unsymmetric MultiFrontal PACKage) solver [39,40].

In the $\vec{T}, \Phi - \Phi$ - potential formulation, the current density \vec{J}_0 of winding has been represented by the impressed current vector potential \vec{T}_0 approximated by edge shape functions. The edge shape functions have been approximated by vector elements, and the iterative solver GMRES (Generalized Minimum Residual Method) solver [7,39] with SSOR (Symmetric Successive Over-Relaxation) preconditioner [39,41] has been applied. In Fig. 5.13 the real part of the impressed current vector potential can be seen. The current vector potential \vec{T} has been approximated by edge shape functions and the

```

7
8   rng_T1      = find(asseminit(fem,'Init',{'tTxTy10',1}), 'Out','U');
9   rng_T2      = find(asseminit(fem,'Init',{'tTxTy20',1}), 'Out','U');
10  rng_T3      = find(asseminit(fem,'Init',{'tTxTy21',1}), 'Out','U');
11  rng_T        = [rng_T1;rng_T2;rng_T3];
12  rng_Told     = find(asseminit(fem,'Init',{'tToldxToldy10',1}), 'Out','U');
13  rng_T2old    = find(asseminit(fem,'Init',{'tToldxToldy20',1}), 'Out','U');
14  rng_T3old    = find(asseminit(fem,'Init',{'tToldxToldy21',1}), 'Out','U');
15  rng_Told     = [rng_Told;rng_T2old;rng_T3old];
16  rng_FI      = find(asseminit(fem,'Init',{'FI',1}), 'Out','U');
17  rng_FIold    = find(asseminit(fem,'Init',{'FIold',1}), 'Out','U');
18
19 SOL = fem.sol.u;
20 SOL([rng_T;rng_FI;rng_Told;rng_FIold]) = 0;
21 fem.sol = femsol(SOL);
22
23 A      = xmeshinfo(fem);
24 rng_xyz = find(A.nameinds==3);
25 xyz_specimen = A.coords(:,rng_xyz);
26
27 tic;
28
29 for k=1:str2double(fem.const(26))*str2double(fem.const(28)),
30   disp(k);
31
32   fem.const(24) = num2str(k);
33   fem.xmesh=meshextend(fem, 'linshape', []);
34   step = 0;
35
36   % Solve problem
37   fem.sol=femstatic(fem, ...
38     'u',fem.sol, ...
39     'solcomp',{'tTxTy10','tTxTy21','tTxTy20','FI'}, ...
40     'outcomp',{'tToldxToldy21','FIold','tToldxToldy20','tT0xT0y20','tTxTy10','tTxTy21','tT0xT0y10','tTxTy20','FI','tT0xT0y21','tToldxT
41     'linsolver','spooles');

```

Fig. 5.12. One part of the script of the time-domain iteration.

reduced magnetic scalar potential Φ has been approximated by nodal elements, and this has been solved by the direct solver SPOOLES (SParse Object Oriented Linear Equations Solver) [39,42]. This solver used, because of the UMFPAK has been used much more memory than the SPOOLES, and as mentioned above, the number of unknowns at the $\vec{T}, \Phi - \Phi$ - potential formulation, is more than .

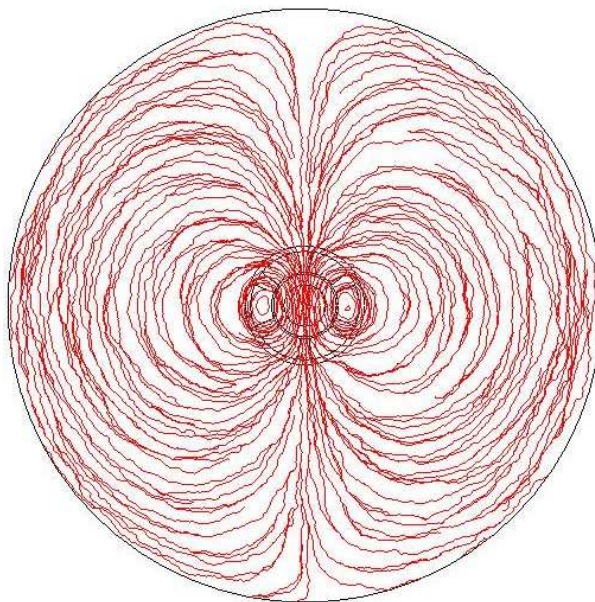


Fig. 5.13. Solution of impressed current vector potential.

5.1.4 Postprocessing

The result of computations is the approximated potential values in the FEM mesh. Any electromagnetic field quantity (e.g. magnetic field intensity, magnetic flux density, etc.) can be calculated by using the potentials at the postprocessing stage. Loss, inductance, energy, force and other quantities can also be calculated. The postprocessing gives a chance to modify the geometry, the material parameters or the FEM mesh to get more accurate result.

In the $\vec{A}, V - \vec{A}$ - formulation the magnetic flux density \vec{B} is the primer quantity. In the $\vec{T}, \Phi - \Phi$ - fomulation the magnetic field intensity \vec{H} is the primer quantity. The primer quantity coupled with e.g. constitutive relations gives the other quantities.

This section deals with the determination of the torque, the induced voltage, and the losses of the rotor, and of the rotor steel. In Fig. 5.14 the regions e.g. S , Ω_{RS} and Ω_{RAI} and the boundary Γ of the computed quantities can be seen.

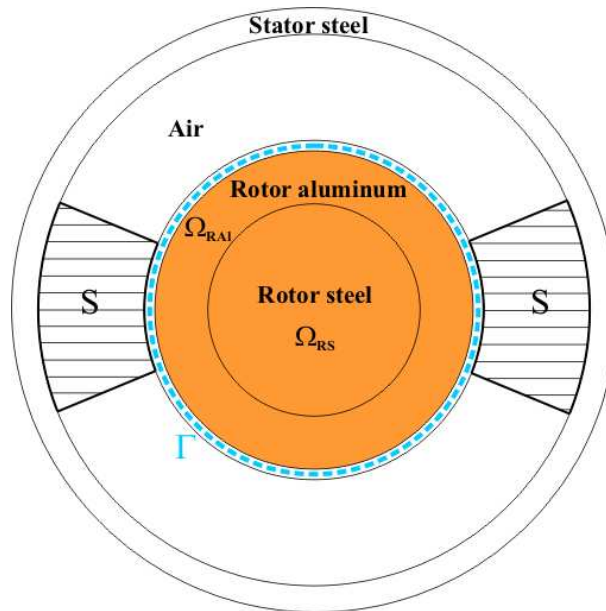


Fig. 5.14. Regions and surface of the computed quantities.

A. Torque

A precise analysis of an electrical rotating machine requires the study of the interaction between mechanical and electrical quantities. The electromagnetic torque plays a fundamental role in the corresponding energy conversation.

There are different methods, based in several formulations, to evaluate the torque.

The method of the Maxwell's stress tensor to calculate the torque [10, 13, 29, 43–49]. This is commonly used in the calculation of forces and torques in the numerical analysis of electrical devices.

The electromagnetic torque is obtained as a surface integral, but in two dimensional case the surface integral is reduced to a line integral along the air gap.

For the practical application of Maxwell's stress tensor, suppose that the magnetic field intensity \vec{H} is known on the surface Γ enclosing the rotor. It is also required that this body is located in air or within a material with permeability $\mu = \mu_0$. Fig. 5.15 shows such a body, where Γ is a line along the air gap, \vec{n} is a unit vector. Maxwell's stress tensor is given by

$$d\vec{F} = \mu_0(\vec{H} \cdot \vec{n})\vec{H} - \frac{\mu_0}{2}H^2\vec{n}, \quad (5.25)$$

where \vec{H} is the magnetic field intensity, and $H = |\vec{H}|$ is the absolute value of magnetic field intensity.

Substitute the $\vec{H} = 1/\mu_0 \vec{B}$ into the above equation gives the next equation

$$d\vec{F} = \frac{1}{\mu_0}(\vec{B} \cdot \vec{n})\vec{B} - \frac{1}{2\mu_0}B^2\vec{n}, \quad (5.26)$$

where \vec{B} is the magnetic flux density, and $B = |\vec{B}|$ is the absolute value of magnetic flux density.

The electromagnetic torque is obtained as a line integral [10, 13, 29, 43–49]

$$\vec{T}_e = L \int_{\Gamma} (\vec{r} \times d\vec{F}) d\Gamma = L \int_{\Gamma} \left(\vec{r} \times \left[\frac{1}{\mu_0}(\vec{B} \cdot \vec{n})\vec{B} - \frac{1}{2\mu_0}B^2\vec{n} \right] \right) d\Gamma, \quad (5.27)$$

where L is a depth of the domain (in the z -direction), and \vec{r} is the position vector linking the rotation axis to the element $d\Gamma$, and Γ is a surface, which places around the air gap.

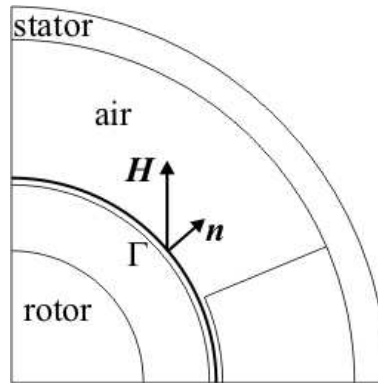


Fig. 5.15. Body under magnetic field surrounded by the surface Γ .

B. Induced voltage

Compute by the $\vec{A}, V - \vec{A}$ - formulation. In particular, the induced voltage [1, 13, 49–54] means the induced voltage per unit depth per turn. The winding is assumed to be comprised of N turns per unit cross-sectional area S (in Fig. 5.14 the lined regions). The

voltage/turn induced in a winding can be predicted by computing the average magnetic vector potential \vec{A} for the forward winding less that for the reverse winding. For the single turn winding having a cross-section S . Only in the phase coil A has been used in computing the induced voltage at the three-phase machine.

In the time domain, the equation is the following:

$$V_i = N \frac{L}{S} \int_S \frac{\partial \vec{A}}{\partial t} \cdot d\vec{S}, \quad (5.28)$$

where N is the number of turns in the winding, L is the length of the motor in the z -direction.

In this problem, the winding is a single turn winding, i.e. $N = 1$, and the length of the motor is 1m, i.e. $L = 1$ m, and the magnetic vector potential has only z -component. These are considering, gives the following equations:

$$V_i = \frac{1}{S} \int_S \frac{\partial A_z}{\partial t} \vec{e}_z \cdot d\vec{S}. \quad (5.29)$$

The induced voltage in the frequency domain only the derivation by time is transformed to a multiplicate by $j\omega$. It has been computed as the integral of the average magnetic vector potential \vec{A} in the total area of the winding cross-section, i.e. [51]

$$V_i = j\omega \frac{1}{S} \int_S A_z \vec{e}_z \cdot d\vec{S}. \quad (5.30)$$

Fig. 5.16 shows the induced voltage in the whole motor. In the phase coils, the induced voltage is much higher than the other parts, and it is the smallest in the stator and in the rotor steel.

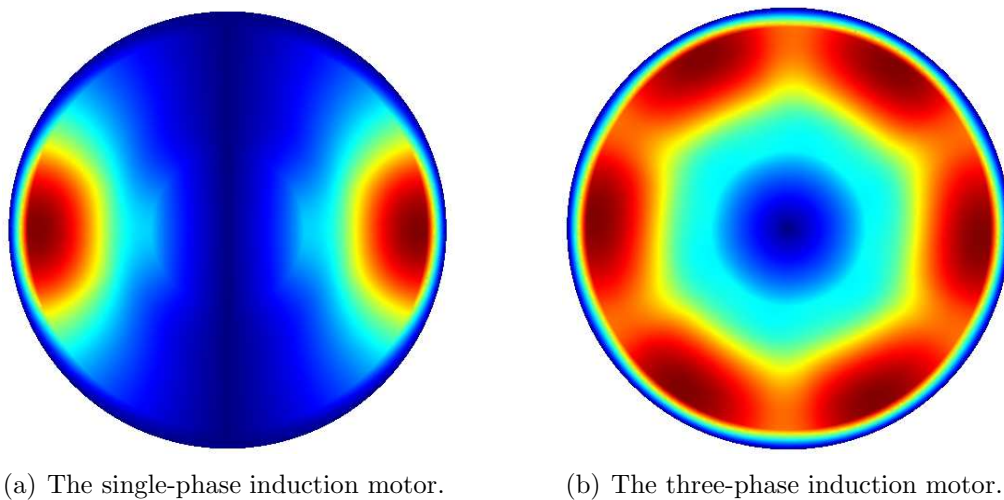


Fig. 5.16. The induced voltage in the induction motors.

Compute by the $\vec{T}, \Phi - \Phi$ - formulation. This potential formulation has not been used in the simulation of induction machines, because some quantities has not been common computed by the $\vec{T}, \Phi - \Phi$ - fomultaion, for example this induced voltage.

Firstly, transformed the (5.28) and gives the following

$$V_i = -N \frac{L}{S} \int_S \vec{E} \cdot d\vec{S}, \quad (5.31)$$

where \vec{E} is the electric field intensity.

The above equation is not usable in this formulation, because in the $\vec{T}, \Phi - \Phi$ - formulation, the $\vec{E} = \nabla \times \vec{T}$, and the current vector potential \vec{T} is presented only the eddy current region. Furthermore, the phase coil A, where computed the induced voltage is in the eddy current free region.

The other one chance has been used the (2.4) to denote the \vec{E} .

$$\nabla \times \vec{E} = -\frac{\partial \vec{B}}{\partial t} = -\frac{\partial}{\partial t} \mu \vec{H} = -\frac{\partial}{\partial t} \mu (\vec{T}_0 - \nabla \Phi), \quad (5.32)$$

but the curl is not vanished the equation, hence the electric field intensity is not denoted by this way.

Some papers in the literature can be found about the voltage computation by this formulation [55, 56]. From this papers, the voltage is the following

$$u = \int_{\Omega} \vec{E} \cdot \nabla \times \vec{T}_0 d\Omega, \quad (5.33)$$

where Ω the whole problem region. This equation seems to be the most usable way, but this voltage is not same the induced voltage from the TEAM problem.

The induced voltage is not computed by the $\vec{T}, \Phi - \Phi$ - potential formulation yet, because could not find, how is compute the induced voltage.

C. Losses

Losses means the rotor loss, and the steel loss as well. These two losses due the average power dissipation in the body of rotor, which due to the eddy current losses of the rotor and the rotor steel [10, 25, 38, 44, 49–51, 54]. The rotor loss is computed as a sum of the eddy current loss of rotor steel Ω_{RS} and rotor aluminum Ω_{RAI} . These regions shows in the Fig. 5.14. Furthermore, the rotor steel loss due to I^2R dissipation [50, 54].

The average power dissipation due to the eddy current losses of the rotor. The average power dissipation has been calculated by the following equation [10, 25, 38, 44, 49–51, 54]

$$P_d = \frac{1}{T} \int_0^T \int_{\Omega} \sigma |\vec{E}|^2 d\Omega dt, \quad (5.34)$$

where the power density loss, i.e. the integrand can be integrated over the surface of the rotor body Ω , and \vec{E} is the electric field intensity, moreover T is the period of time. The region $\Omega = \Omega_s$ when the steel loss is computed, and $\Omega = \Omega_{Al} \cup \Omega_s$ when the rotor loss is computed.

In the frequency domain the equation of eddy current losses are the following

$$P_d = \int_{\Omega} \Re \left\{ \frac{1}{2} \sigma \vec{E} \cdot \vec{E}^* \right\} d\Omega, \quad (5.35)$$

where \Re denotes the real part of the power density loss $\frac{1}{2} \sigma \vec{E} \cdot \vec{E}^*$, which can be integrated over the surface of the rotor Ω , and \vec{E} is the electric field intensity, and moreover \vec{E}^* conjugated of electric field intensity.

Fig. 5.17 shows the average power dissipation in the rotor. The power dissipation in the rotor aluminum is nearly hundred times bigger than the rotor steel, this is why the power dissipation in the rotor steel seems to be equal zero.

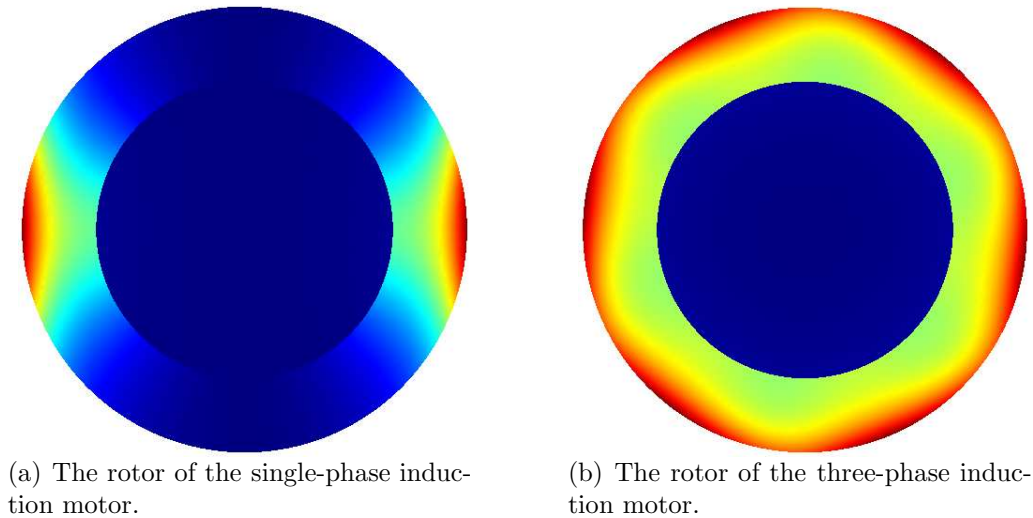


Fig. 5.17. The power dissipation in the rotor.

Chapter 6

Solution of the Problem

The Problem 30a of TEAM Workshops is a benchmark problem, and the different methods, formulations have been compared by this problem.

This problem has been solved by analyticaly [50], by the boundary element method [51], and by the time-harmonic finite element method [30, 31].

The above sections show the used potential formulations of the simulation, and the methods of secondary quantities (e.g. torque) in the time domain, and in the frequency domain.

The used potential formulations are the $\vec{A}, V - \vec{A}$ - potential formulation and the $\vec{T}, \Phi - \Phi$ - potential formulation with motion voltage term in the time domain, and in the frequency domain, too.

Furthermore, the results of the commercial finite element code, the COMSOL Multiphysics [49]. These results have been computed in the frequency domain, because of the moving part option of COMSOL is only in the frequency domain computation.

These results of formulations have been compared with the analytical solution, and to each others. The results of analytic analysis is presented in [4, 50].

The time-dependent numerical computations were performed using computer programs developed under MATLAB environment using COMSOL script language. The programs have been run on a Genuine Intel(R) processor with the clock frequency of the processor 1.6GHz with 4GByte RAM.

The time-harmonic numerical computations were performed using the computer programs developed by using functions of COMSOL Multiphysics. The procedures have been run on an Intel(R) Core(TM)2 Duo CPU T9300 with the clock frequency of the processor 2.50 GHz with 2Gbyte RAM.

6.1 Results of the single-phase induction motor

In this section the simulations results are presented, as well as the computed quantities of the single-phase motor by some field plots and tables with the exact values of

computation and figures to compare the different results.

In the $\vec{A}, V - \vec{A}$ -formulation, the used mesh consist of 43522 second-order triangular element, and the number of unknowns is 87405.

In the $\vec{T}, \Phi - \Phi$ -formulation the used mesh consists of firstly (when compute the \vec{T}_0) 223426 second-order triangular element, and the total number of unknowns are 404286. The computation time is 388s becasue the impressed current vector potential has been used and the iterative solver (GMRES with SSOR preconditioner), and the number of iterations are 1157. In Fig. 6.1, the error as function of the number of iterations can be seen. The computation of $\vec{T}, \Phi - \Phi$ the used mesh consist of 43522, and the number of unknowns are 147107.

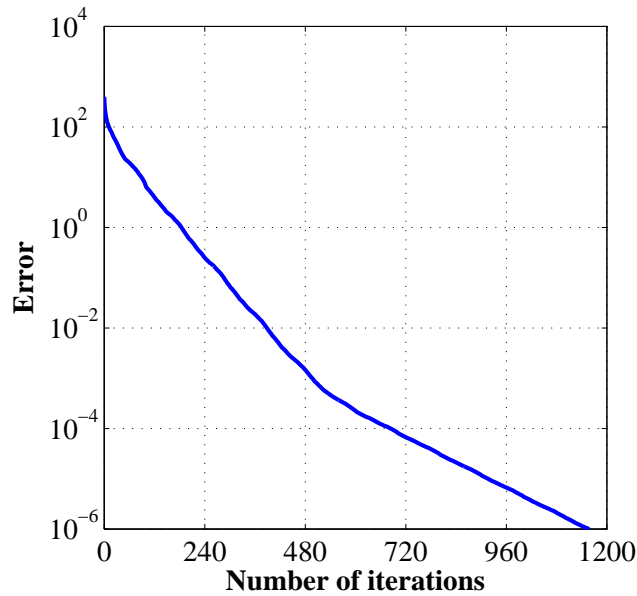


Fig. 6.1. The number of iteration of computation of \vec{T}_0 .

In the time domain, the stationary state of this eddy current field problem can be reached after the third period of the excitation, but six periods have been calculated. In this simulation, a period of the current excitation has been divided into 720 time steps. The error of the Euler formula $[x(n+1) - x(n)]/\Delta t$ is small, then Δt is small, e.g. the period of excitation current has been divided into small enough. All of quantities in the time domain have been computed in the sixth period.

Table 6.1 presents the computation time consumption of the different formulation. In the frequency domain, the $\vec{A}, V - \vec{A}$ -formulation is the fastest, because computation time of this formulation is ranging from 5.48s to 6.61s, whereas the CPU time of $\vec{T}, \Phi - \Phi$ -formulations is ranging from 13.62s to 23.05s. Furthermore, the impressed current vector potential \vec{T}_0 has been computed when the edge-element based $\vec{T}, \Phi - \Phi$ -formulation is applied, and this adds about 388s in every simulations. The computation time of $\vec{T}, \Phi - \Phi$ -formulation in the time domian is the total computation time, with the computation

Table 6.1. The computation time of single-phase motor.

Computation time				
[sec]				
Angular Velocity [rad/s]	$\vec{A}, V - \vec{A}$ Frequency domain	$\vec{T}, \Phi - \Phi$ Frequency domain	$\vec{A}, V - \vec{A}$ Time domain	$\vec{T}, \Phi - \Phi$ Time domain
0	5.86	13.62	21340.53	22639.86
39.79351	6.61	20.59	20777.19	23384.88
79.58701	6.18	20.41	20303.44	24483.06
119.3805	5.48	20.17	21227.74	22473.55
159.174	5.57	21.1	21287.39	23467.34
198.9675	6.1	20.84	20909.61	23956.02
238.761	5.48	20.96	21471.22	23948.47
278.5546	6.2	21.07	22034.45	23694.19
318.3481	5.8	20.93	22186.13	23734.68
358.1416	6.42	23.05	21915.94	23511.65

time of impressed current vector potential. The computation time of impressed current vector potential in time domain is same than the frequency domain, e.g. 388s. In the time domain the $\vec{A}, V - \vec{A}$ - formulation is the fastest, too, because the CPU time of this formulatin is about 21000s, whereas the computatin time of $\vec{T}, \Phi - \Phi$ - formulations is more than 23000s.

Firstly, the primer quantities are studied, e.g. magnetic flux density \vec{B} . Fig. 6.2 shows the peak value of real part of the magnetic flux density lines of the single-phase motor

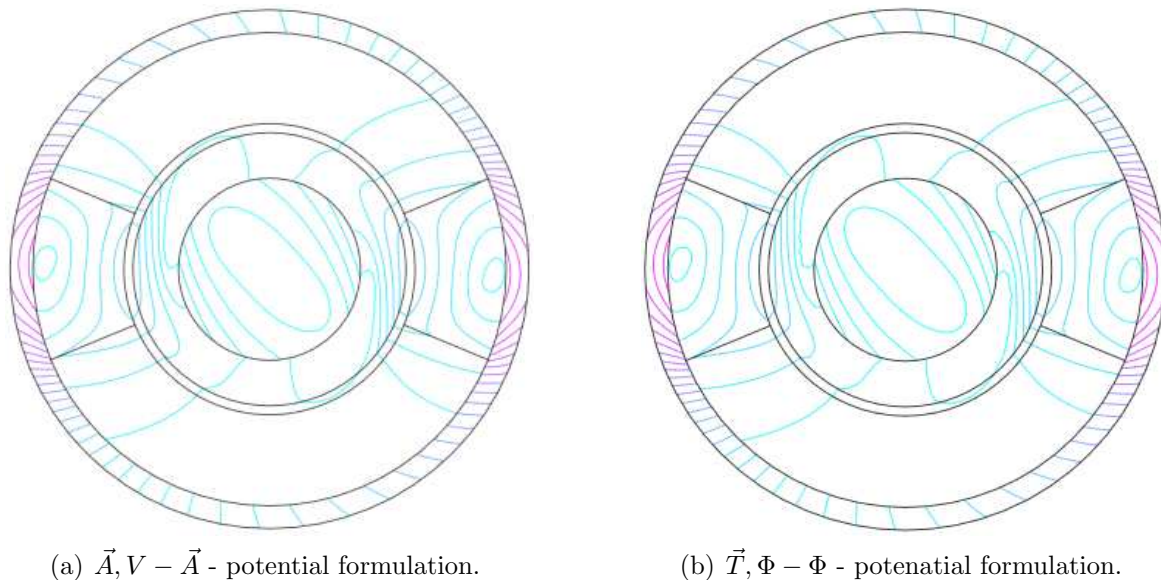


Fig. 6.2. The magnetix flux lines in the frequency domain at 278 rad/s angular velocity.

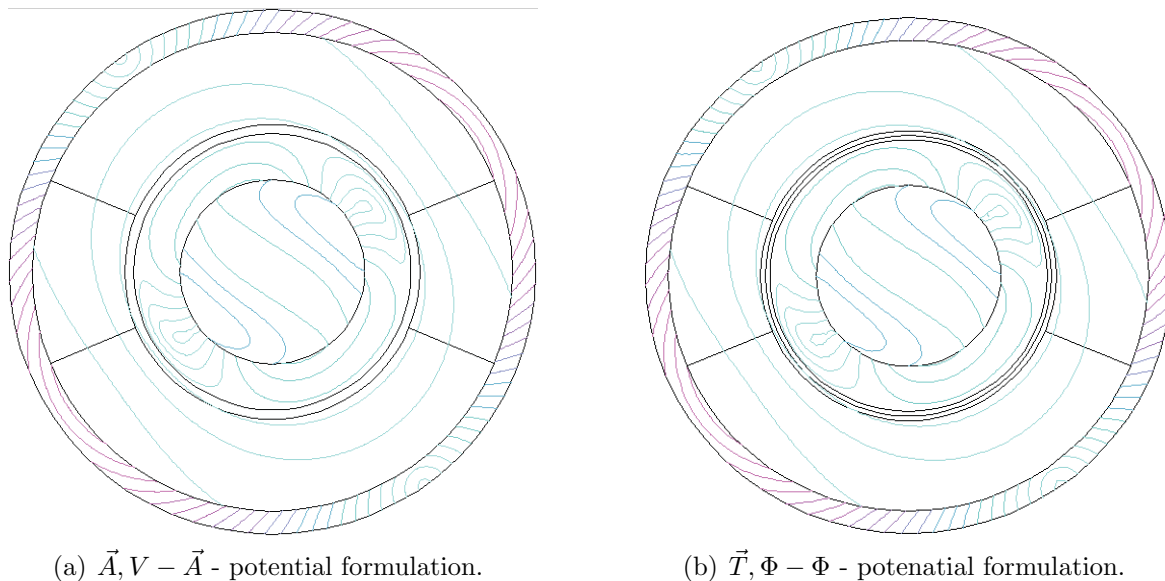


Fig. 6.3. The magnetix flux lines in the time domain at 278 rad/s angular velocity.

in the frequency domain at 278 rad/s angular velocity. Fig. 6.3 shows the magnetic flux lines of the single-phase motor computed in the time domain, in the last step of sixth period at 278 rad/s angular velocity. The magnetic flux lines seem to be equal in the figures in the time and in the frequency domain.

Fig. 6.4 shows the computed equipotential lines of the magnetic vector potential at 278 rad/s angular velocity. Fig. 6.4(a) shows the real part of the magnetic vector potential, and Fig. 6.4(b) presents the imaginary part of magnetic vector potential. These figures are almost the same as the presented figures in the papers [30, 31].

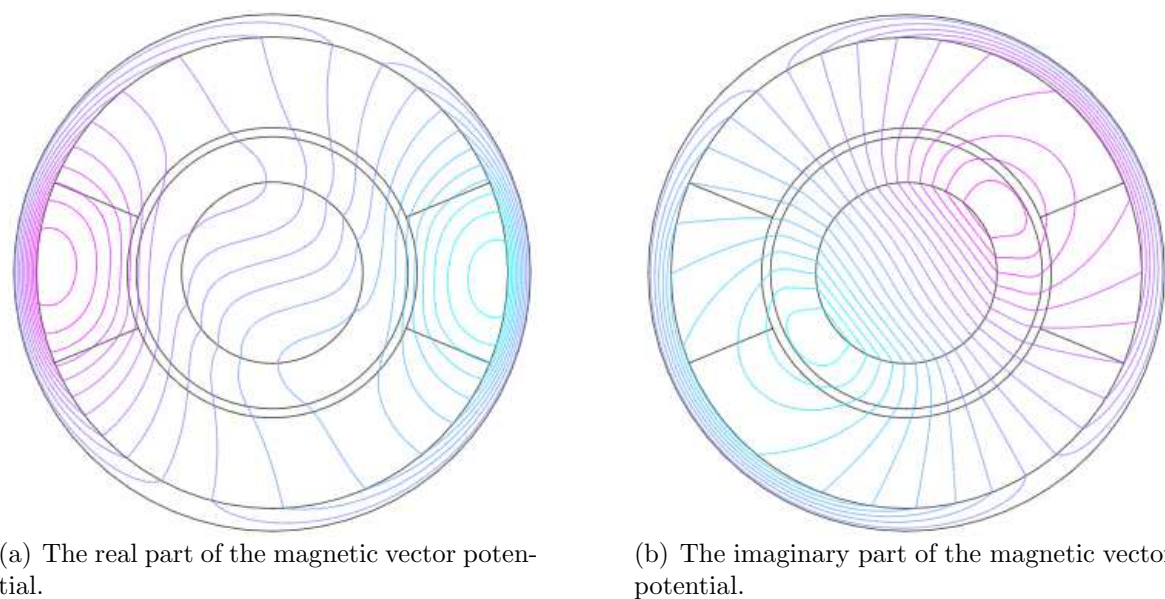


Fig. 6.4. Real and imaginary part of the magnetic vector potential at the maximum of the torque.

Table 6.2. Torque in the single-phase motor

TORQUE						
[Nm]						
Angular Velocity [rad/s]	Analytical Solution	COMSOL Multiphysics	$\vec{A}, V - \vec{A}$ Frequency domain	$\vec{T}, \Phi - \Phi$ Frequency domain	$\vec{A}, V - \vec{A}$ Time domain	$\vec{T}, \Phi - \Phi$ Time domain
0	0	5.468e-9	1.681e-5	1.566e-4	1.011e-5	6.125e-6
39.79351	0.052766	0.04422	0.04428	0.04434	0.0436	0.0436
79.58701	0.096143	0.08571	0.85808	0.08584	0.0851	0.0851
119.3805	0.14305	0.12569	0.12673	0.12677	0.1246	0.1245
159.174	0.19957	0.17555	0.17574	0.17575	0.1738	0.1738
198.9675	0.2754	0.24126	0.24149	0.24146	0.2363	0.2362
238.761	0.367972	0.31915	0.32021	0.32015	0.3135	0.3134
278.5546	0.442137	0.37683	0.37713	0.37702	0.3645	0.3633
318.3481	0.375496	0.30146	0.30182	0.30166	0.2857	0.2855
358.1416	-0.0707	-0.10068	-0.10024	-0.10046	-0.1113	-0.1115

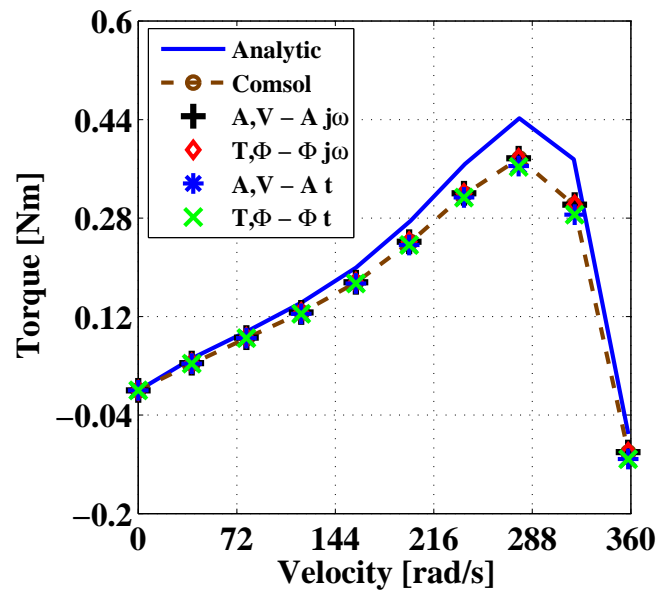


Fig. 6.5. Torque-speed characteristics of the single-phase motors.

Table 6.2 presents the analytic values and the computed electromagnetic torque values by the presented potential formulations, where the value of the angular velocity can be seen, as well. The quantity of torque can be seen in Fig. 6.5. In this figure the five different finite element approaches are practically the same. The difference between the analytic and the finite element results is increased with the increase of velocity, and the difference is the biggest at the maximum of torque or the point of breakdown torque. Furthermore the curves shows the typical torque-speed characteristic of single-phase

Table 6.3. Rotor loss in the single-phase motor

ROTOR LOSS						
[W/m]						
Angular Velocity [rad/s]	Analytical Solution	COMSOL Multiphysics	$\vec{A}, V - \vec{A}$ Frequency domain	$\vec{T}, \Phi - \Phi$ Frequency domain	$\vec{A}, V - \vec{A}$ Time domain	$\vec{T}, \Phi - \Phi$ Time domain
0	341.7676	321.8952	321.8952	321.8952	321.2812	321.2811
39.79351	341.2465	321.461	321.4612	321.4609	320.9589	320.9588
79.58701	340.4618	320.5624	320.5624	320.5623	319.9352	319.9531
119.3805	340.0396	320.0629	320.063	320.0625	319.4121	319.4118
159.174	340.225	320.1429	320.1429	320.1423	319.3881	319.3877
198.9675	339.2994	319.1407	319.1407	319.1406	318.0969	318.0964
238.761	333.6163	313.5793	313.5792	313.5784	312.5161	312.5154
278.5546	317.9933	298.7739	298.774	298.7728	297.4517	297.3147
318.3481	288.079	271.4886	271.4886	271.4873	270.6503	270.6492
358.1416	256.6437	244.3109	244.311	244.3093	244.1438	244.1427

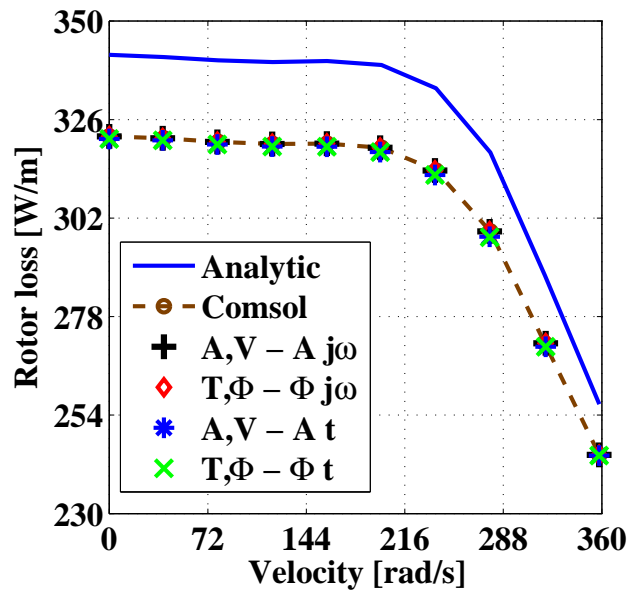


Fig. 6.6. The power dissipation of rotor of the single-phase motors.

induction motors, and the point of full load torque is nearly 350 rad/s.

The next table (Table 6.3) represents the total rotor loss in both the aluminum and the rotor steel. The solutions of both potential formulations and the commercial FEM code seem to be equal in frequency and time domain at all different angular velocities. The character of finite element results similar than of the analytic solution. The characteristics of solutions are represents the Fig. 6.6. The difference between the characteristics is decreased when de speed becomes higher. The difference is the biggest

Table 6.4. Steel loss in the single-phase motor

STEEL LOSS						
[W/m]						
Angular Velocity [rad/s]	Analytical Solution	COMSOL Multiphysics	$\vec{A}, V - \vec{A}$ Frequency domain	$\vec{T}, \Phi - \Phi$ Frequency domain	$\vec{A}, V - \vec{A}$ Time domain	$\vec{T}, \Phi - \Phi$ Time domain
0	3.944175	3.707725	3.707716	3.707715	3.683761	3.683762
39.79351	3.933111	3.696603	3.696601	3.696603	3.674073	3.674071
79.58701	3.900878	3.664197	3.664213	3.664209	3.639751	3.639753
119.3805	3.848117	3.611196	3.611191	3.611203	3.586207	3.586204
159.174	3.767681	3.530708	3.530713	3.53071	3.504074	3.504077
198.9675	3.635357	3.399406	3.400102	3.399497	3.368849	3.368851
238.761	3.404092	3.172887	3.172904	3.172902	3.142321	3.142326
278.5546	2.999715	2.784787	2.784802	2.784803	2.751628	2.749486
318.3481	2.355622	2.186231	2.186245	2.186238	2.163209	2.163214
358.1416	1.674353	1.577268	1.577313	1.577316	1.568528	1.568523

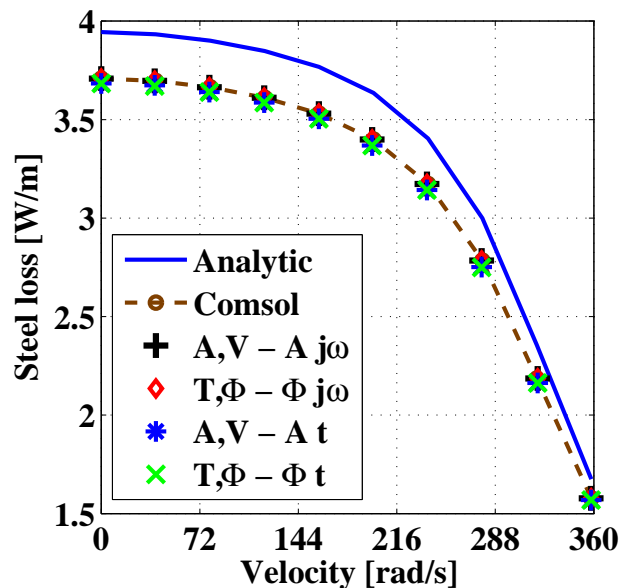


Fig. 6.7. The power dissipation of rotor steel of the single-phase motors.

when the motor is standstill.

Table 6.4 represents just the rotor steel loss, which is due to the I^2R dissipation. The curves of the steel loss similar to the curves of rotor loss, but the steel loss a good deal smaller. Furthermore, the differences of analytic and finite element analysis are the largest here as well, at the standstill motor. The difference between the curve of analytic results and of FEM results is decreased when the speed becomes higher. The steel loss versus angular velocity can be seen in Fig. 6.7.

Table 6.5. Induced voltage in the single-phase motor

INDUCED VOLTAGE				
[V/m/turn]				
Angular Velocity [rad/s]	Analytical Solution	COMSOL Multiphysics	$\vec{A}, V - \vec{A}$ Frequency domain	$\vec{A}, V - \vec{A}$ Time domain
0	0.536071	0.521899	0.521902	0.5187
39.79351	0.537466	0.523172	0.523201	0.5201
79.58701	0.541495	0.527026	0.527032	0.5239
119.3805	0.548603	0.533771	0.533784	0.5307
159.174	0.650074	0.544594	0.544612	0.5416
198.9675	0.578808	0.562153	0.562152	0.5587
238.761	0.609649	0.590768	0.590797	0.5853
278.5546	0.658967	0.635713	0.635708	0.6245
318.3481	0.728552	0.697472	0.697494	0.6728
358.1416	0.790068	0.750178	0.750188	0.7091

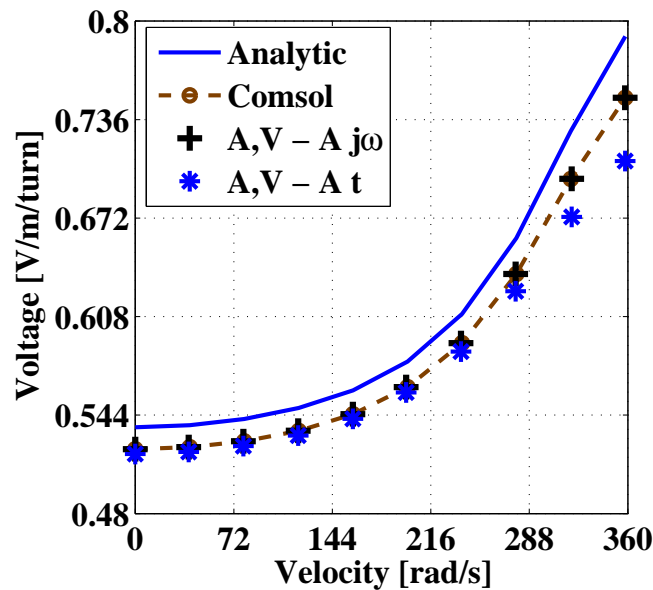


Fig. 6.8. The induced voltage of the single-phase motor.

The last quantity of single-phase machine, which presents, the induced voltage in the phase coil A. The induced voltage has been computed by the magnetic vector potential \vec{A} . Table 6.5 shows the computed values of the induced voltage by analytic and by finite element method. The two finite element solutions in the frequency domain are nearly same, and the difference between the analytic and the frequency domain solutions are unchanged all angular velocity. This can be shown in Fig. 6.8. The difference between the analytic and the finite element result in time domain, and between the solutions of

frequency domain and if time domain is increased with the increasing velocity, and the difference is the biggest at the maximum of velocity, at 358 rad/s angular velocity.

6.2 Results of the three-phase induction motor

In this section shows the simulations results, and the computed quantities of the three-phase motor by some field plots and tables with the exact values of computation and figures to compare the different results.

In the $\vec{A}, V - \vec{A}$ - formulation and in the $\vec{T}, \Phi - \Phi$ - formulation, the used meshes, the number of unknowns are same than the single-phase case. In the \vec{T}_0 computation the impressed current vector potential has been used and the same iterative solver, however the computation time of the impressed current vector potential is 1139s.

Furthermore, at the three-phase motor in the time domain eight period have been calculated, but the period of the current excitation is same, 720 time steps.

Table 6.6. The computation time of three-phase motor.

Computation time				
[sec]				
Angular Velocity [rad/s]	$\vec{A}, V - \vec{A}$ Frequency domain	$\vec{T}, \Phi - \Phi$ Frequency domain	$\vec{A}, V - \vec{A}$ Time domain	$\vec{T}, \Phi - \Phi$ Time domain
0	4.78	13.06	24411.51	24631.74
200	4.88	21.12	25146.18	30071.09
400	5.11	25.82	24134.82	29124.82
600	5.18	35.14	25885.04	28873.51
800	5.15	51.54	23415.82	29348.17
1000	5.21	70.21	25145.21	30178.72
1200	4.97	79.77	23543.02	31471.19

Table 6.6 presents the computation time consumption of the different formulation. In the frequency domain, the $\vec{A}, V - \vec{A}$ - formulation is the fastest, because computation time of this formulation is nearly 5s, whereas the CPU time of $\vec{T}, \Phi - \Phi$ - formulations is ranging from 13s to 79s. Furthermore, the impressed current vector potential \vec{T}_0 has been computed when the edge-element based $\vec{T}, \Phi - \Phi$ - formulation is applied, and this adds about 1139s in every simulations. The computation time of $\vec{T}, \Phi - \Phi$ - formulation in the time domain is the total computation time, with the computation time of impressed current vector potential. The computation time of impressed current vector potential in time domain is same than the frequency domain, e.g. 1139s. In the time domain the $\vec{A}, V - \vec{A}$ - formulation is the fastest, too, because the CPU time of this formulatin is

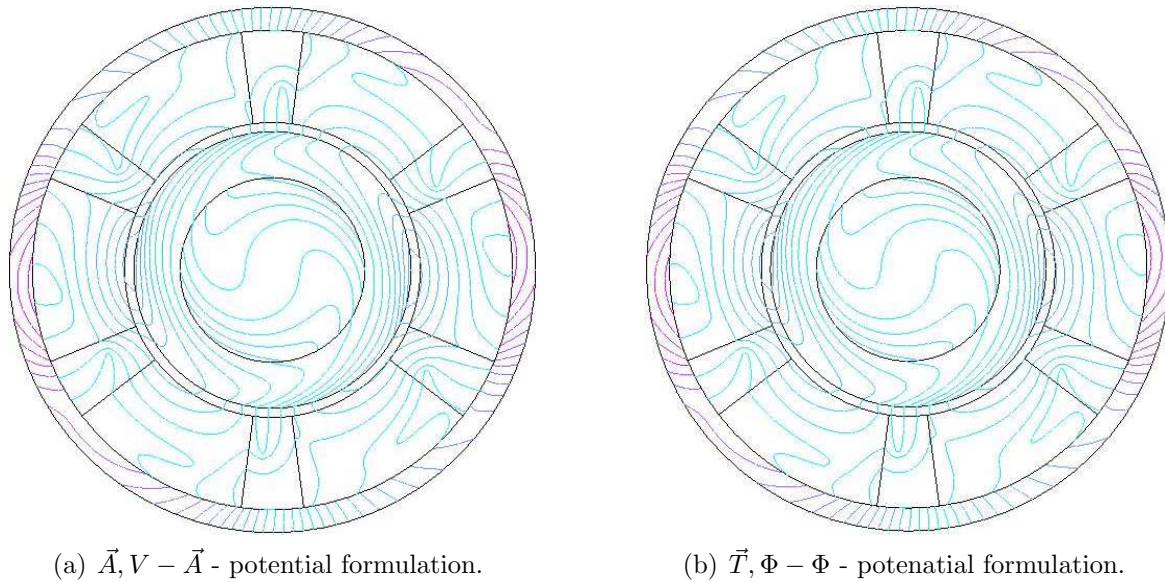


Fig. 6.9. The magnetix flux lines in the frequency domain at 1200 rad/s angular velocity.

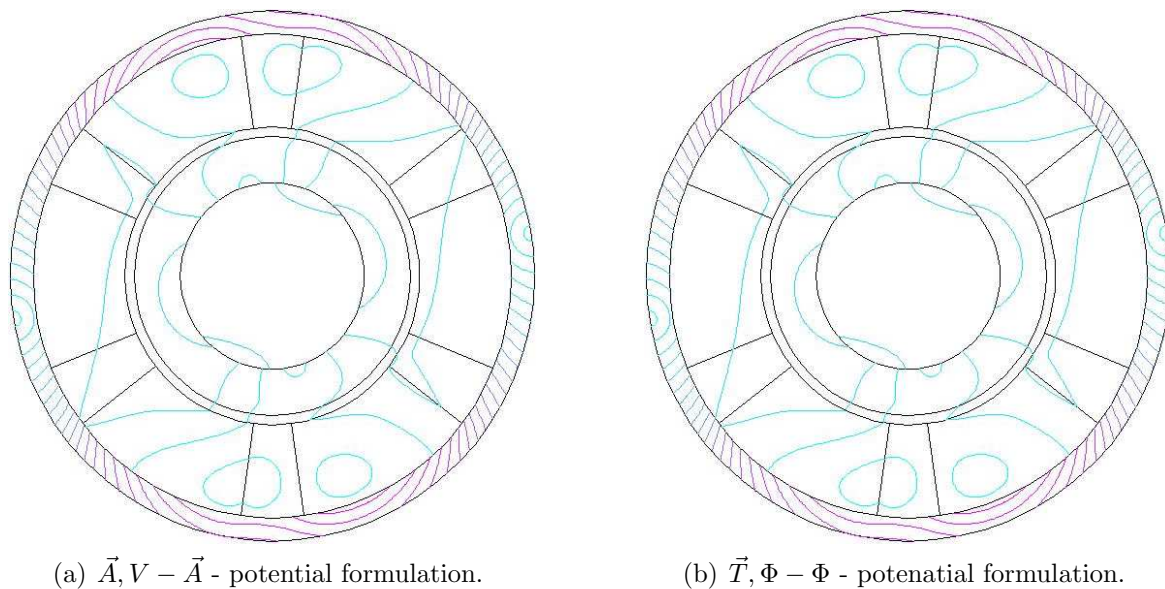


Fig. 6.10. The magnetix flux lines in the time domain at 1200 rad/s angular velocity.

ranging from 23415s to 25885s, whereas the computatin time of $\vec{T}, \Phi - \Phi$ - formulations is ranging from 24631s to 31471s.

Firstly in the three-phase motor, the primer quantities are studied, e.g. magnetic flux density \vec{B} . Fig. 6.9 shows the peak value of real part of the magnetic flux density lines of the three-phase motor in the frequency domain at 1200 rad/s angular velocity. Fig. 6.10 shows the magnetic flux lines of the single-phase motor computed in the time domain, in the last step of eighth period at 1200 rad/s angular velocity. The magnetic flux lines are practically the same in the figures in the time and in the frequency domain. The magnetic field lines are equal in both domain as well, because in this problem has

Table 6.7. Torque in the three-phase motor

TORQUE						
[Nm]						
Angular Velocity [rad/s]	Analytical Solution	COMSOL Multiphysics	$\vec{A}, V - \vec{A}$ Frequency domain	$\vec{T}, \Phi - \Phi$ Frequency domain	$\vec{A}, V - \vec{A}$ Time domain	$\vec{T}, \Phi - \Phi$ Time domain
0	3.825857	3.59153	3.5912	3.5919	3.5884	3.6113
200	6.505013	6.02069	6.0209	6.0215	5.9835	6.0117
400	-3.89264	-3.39807	-3.3979	-3.3976	-3.2941	-3.3138
600	-5.75939	-5.63975	-5.3697	-5.3694	-5.3482	-5.3676
800	-3.59076	-3.37833	-3.3778	-3.3779	-3.3763	-3.3771
1000	-2.70051	-2.54736	-2.5465	-2.5469	-2.5472	-2.5469
1200	-2.24996	-2.12514	-2.1241	-2.1247	-2.1249	-2.1251

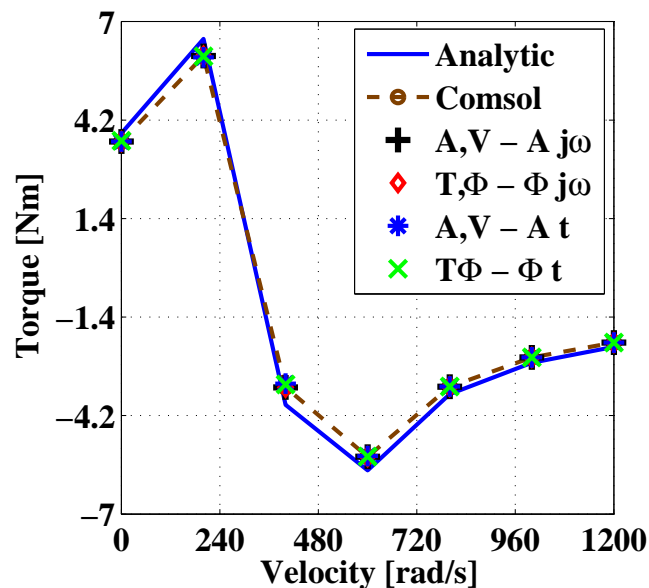


Fig. 6.11. Torque-speed characteristics of the three-phase motors.

been linear relation between \vec{H} and \vec{B} .

Table 6.7 presents the analytic values and the computed electromagnetic torque values by the presented potential formulations, where the value of the angular velocity of the three-phase motor analysis can be seen, as well. The quantity of torque can be seen in Fig. 6.11. In this figure the five different finite element approaches seem to be nearly equal, and the solutions of the frequency domain are closed each others. The difference between the analytic and the finite element results is varying, but the maximum of the difference is less than 10%. The curves of FEM analysis are behave similar than the reference analytic curve. Additionally the curves shows the typical torque-speed characteristic of three-phase induction motor. Fig. 6.11 shows when the motor is operated

Table 6.8. Rotor loss in the three-phase motor

ROTOR LOSS						
[W/m]						
Angular Velocity [rad/s]	Analytical Solution	COMSOL Multiphysics	$\vec{A}, V - \vec{A}$ Frequency domain	$\vec{T}, \Phi - \Phi$ Frequency domain	$\vec{A}, V - \vec{A}$ Time domain	$\vec{T}, \Phi - \Phi$ Time domain
0	1455.644	1366.922	1366.922	1366.921	1366.104	1366.002
200	1179.541	1093.952	1093.952	1093.951	1087.317	1087.552
400	120.0092	108.5928	108.5922	108.5903	106.5816	107.0713
600	1314.613	1227.914	1227.912	1227.905	1223.403	1223.706
800	1548.24	1458.668	1458.666	1458.654	1458.401	1458.529
1000	1710.686	1615.641	1615.636	1615.621	1616.509	1616.233
1200	1878.926	1776.372	1776.637	1776.623	1778.113	1777.846

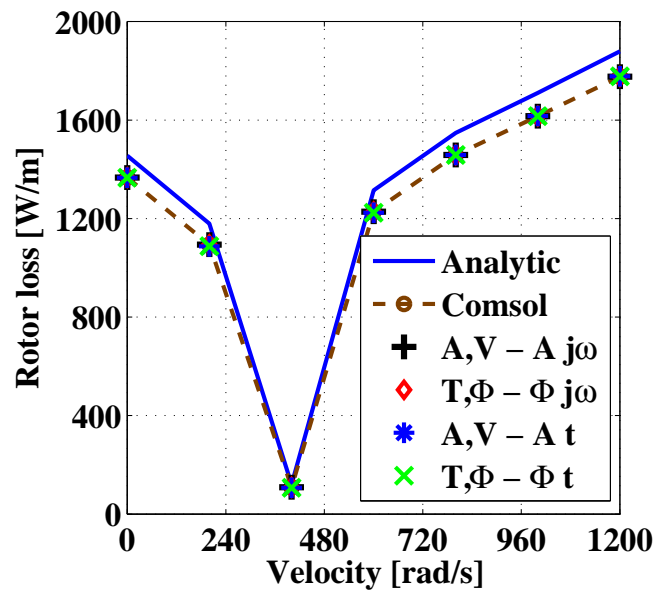


Fig. 6.12. The power dissipation of rotor of the three-phase motors.

than a motor and after about 300 rad/s than a generator.

The next table (Table 6.8) represents the total rotor loss of three-phase induction motor in both the aluminum and the rotor steel. The solutions by both potential formulations and by the COMSOL are practically the same in frequency and time domain at all different angular velocities. The character of finite element results similar than of the analytic solution. The characteristics of solutions are represents the Fig. 6.12. The difference between the characteristics is decreased to 400 rad/s, and after the difference is increased when de speed becomes high. The rotor loss is the smallest at 400 rad/s angular velocity. The difference is the biggest when the angular velocity is 1200 rad/s, in this point it is 5.4%.

Table 6.9. Steel loss in the three-phase motor

STEEL LOSS						
[W/m]						
Angular Velocity [rad/s]	Analytical Solution	COMSOL Multiphysics	$\vec{A}, V - \vec{A}$ Frequency domain	$\vec{T}, \Phi - \Phi$ Frequency domain	$\vec{A}, V - \vec{A}$ Time domain	$\vec{T}, \Phi - \Phi$ Time domain
0	17.40541	16.34462	16.34461	16.34462	16.25782	16.25661
200	16.98615	15.7367	15.7367	15.73672	15.55293	15.55238
400	1.383889	1.20661	1.20662	1.206611	1.167651	1.163473
600	17.87566	16.65631	16.6563	16.65631	16.50407	16.50374
800	16.88702	15.87404	15.87402	15.87404	15.79943	15.82615
1000	14.32059	13.49334	13.49335	13.49335	13.45032	13.45703
1200	12.01166	11.33068	11.3307	11.33066	11.30354	11.31948

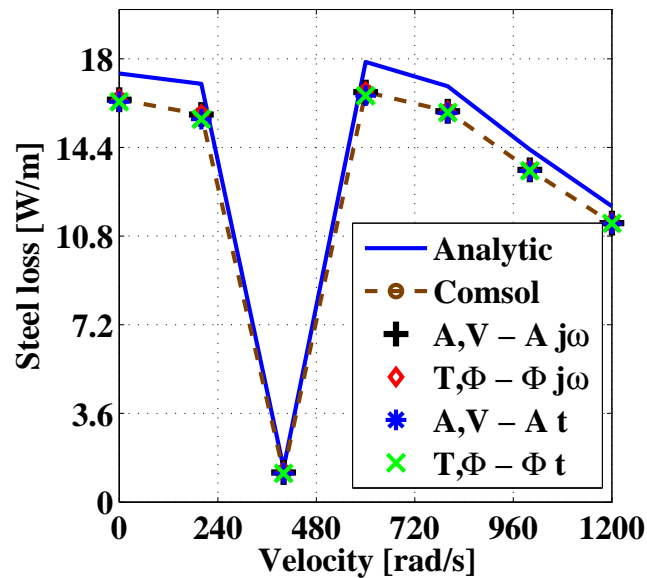


Fig. 6.13. The power dissipation of rotor steel of the three-phase motors.

Table 6.9 represents just the rotor steel loss, which is due to the I^2R dissipation. The results of potential formulations and of the commercial finite element code seem to be equal in frequency and time domain at all different angular velocities. The curves of the steel loss similar to the curves of rotor loss from 0 rad/s to 600 rad/s, because after the steel loss is decreased. Furthermore, the difference of analytic and finite element analysis are the largest at 200 rad/s angular velocity, in this point it is 7.4%, and the smallest at 400 rad/s angular velocity, than the case of rotor loss. The steel loss of three-phase motor versus angular velocity can be seen in Fig. 6.13.

Table 6.10 shows the exact value of induced voltage. The results of numerical analysis in the frequency domain are close same, too. The results are same from 0 rad/s to

Table 6.10. Induced voltage in the three-phase motor

INDUCED VOLATGE				
[V/m/turn]				
Angular Velocity [rad/s]	Analytical Solution	COMSOL Multiphysics	$\vec{A}, V - \vec{A}$ Frequency domain	$\vec{A}, V - \vec{A}$ Time domain
0	0.637157	0.625034	0.625058	0.6255
200	0.845368	0.825837	0.825844	0.8154
400	1.477981	1.399524	1.399531	1.3064
600	0.76176	0.746331	0.746335	0.7686
800	0.617891	0.606367	0.606386	0.6271
1000	0.575699	0.564498	0.564507	0.5829
1200	0.556196	0.545063	0.545083	0.5623

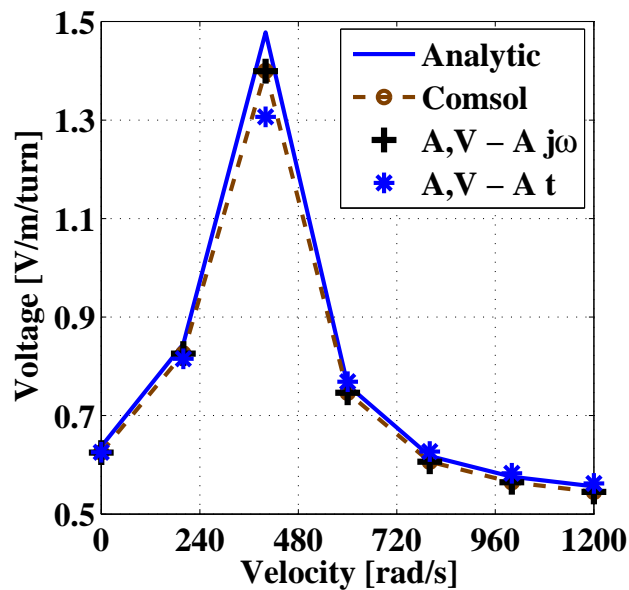


Fig. 6.14. The induced voltage of the three-phase motor.

400 rad/s, than at the single-phase machine, i.e. the difference between the analytic solution and the finite element solutions is increasing to 400 rad/s, and after this angular velocity is decreasing. This shown in the Fig. 6.14. The results of the time domain computation are only one angular velocity differ too, at the maximum of induced voltage.

The next quantities, i.e. the radial B field (B_r) and θ -directed H field (H_θ) computed only in the case of the three-phase exposed winding motor. These quantities are to be determined in the phase coil A, in ten different point along the x -axis. The radial magnetic flux density and the θ -directied magnetic field density at 200 rad/s angular velocity have also been simulated.

These quantities computed only in the frequency domian, because of the B_r and the

Table 6.11. Real Part of the Radial B field for the three-phase motor

$\Re \{B_r\}$				
[T]				
x	Analytical	COMSOL	$\vec{A}, V - \vec{A}$	$\vec{T}, \Phi - \Phi$
[m]	Solution	Multiphysics	Frequency	Frequency
			domain	domain
0.032	0.018854	0.01774	0.01777	0.01781
0.034222	0.017122	0.01612	0.01614	0.01616
0.036444	0.015643	0.01463	0.01468	0.01463
0.038667	0.014375	0.01341	0.01344	0.01338
0.040889	0.013284	0.01232	0.01235	0.01233
0.043111	0.012341	0.01143	0.01143	0.01141
0.045333	0.011522	0.01089	0.01063	0.01061
0.047556	0.010807	0.00997	0.00992	0.00991
0.049778	0.010179	0.00931	0.00929	0.00929
0.052	0.009625	0.00876	0.00876	0.00875

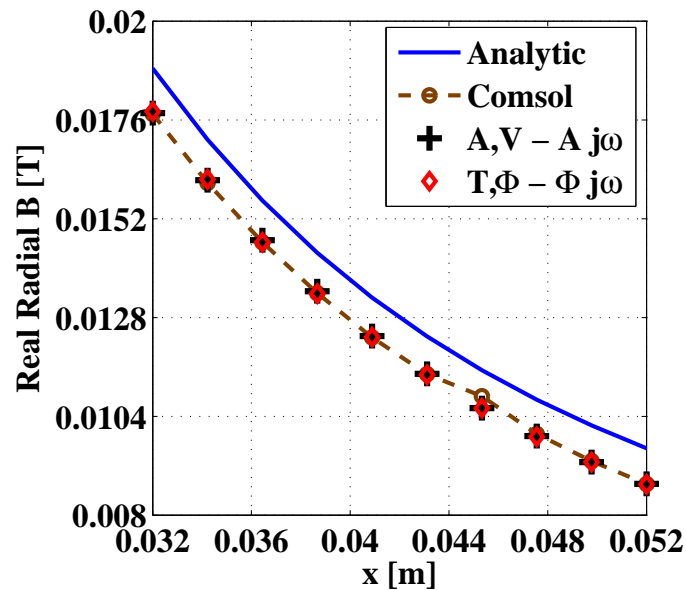


Fig. 6.15. The real part of radial magnetic flux density.

H_{Θ} have been divided into two part. These parts are the real and the imaginary part, and these are only in time-harmonic case.

The first is the real part of radial B field. The ten different points of computation in phase coil A are shown in Table 6.11, where the analytic results and the exact values of numerical computations can be seen, as well. The real part of B_r is the biggest the inner side of phase coil A, and continuous decreased from the inner side to the outter side of winding. This shows the Fig. 6.15. The three different finite element solution seems

Table 6.12. Imaginary Part of the Radial B field for the three-phase motor

x [m]	$\Im \{B_r\}$ [T]			
	Analytical Solution	COMSOL Multiphysics	$\vec{A}, V - \vec{A}$ Frequency domain	$\vec{T}, \Phi - \Phi$ Frequency domain
0.032	0.016392	0.01596	0.01596	0.01598
0.034222	0.017079	0.01654	0.01654	0.01654
0.036444	0.017412	0.01665	0.01665	0.01678
0.038667	0.017455	0.01676	0.01676	0.01675
0.040889	0.017266	0.01655	0.01655	0.01651
0.043111	0.016895	0.01611	0.01611	0.01609
0.045333	0.016385	0.01527	0.01527	0.01553
0.047556	0.015772	0.01488	0.01488	0.11488
0.049778	0.015085	0.01416	0.01416	0.01416
0.052	0.014347	0.01342	0.01343	0.01343

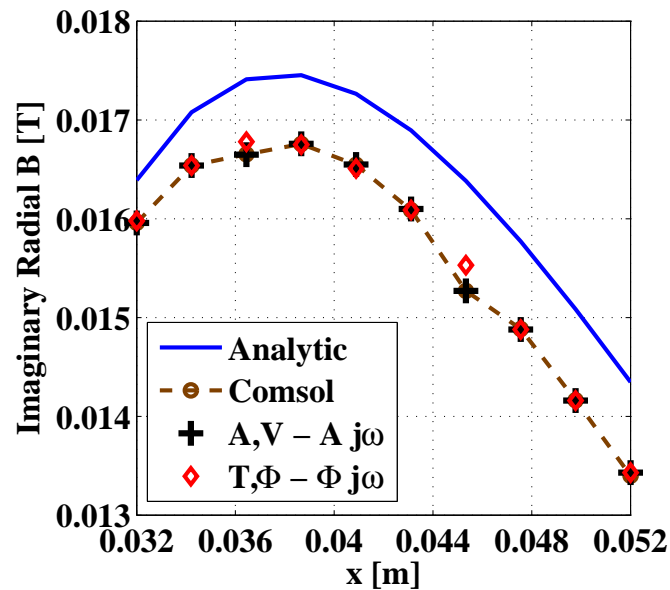


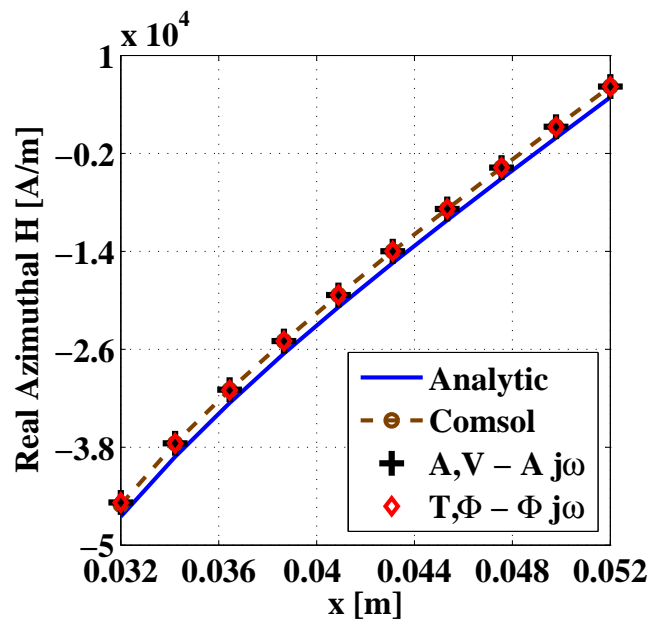
Fig. 6.16. The imaginary part of radial magnetic flux density.

to be equal all of points, only in the $x=0.45333$ has been a little difference between the results of the commercial FEM code and of the two potential formulations. The difference between the analytical and FEM analysis nearly same every points.

The next is the other part of the radial B field, the imaginary part. The values of different analysis presented the Table 6.12. The maximum of imaginary part is not the inner side of phase, than the real part. The maximum is inside the phase, it is in the $x=0.038667$ point. In Fig. 6.16 the curves of the results can be seen. The imaginary

Table 6.13. Real Part of the Azimuthal H field for the three-phase motor

x [m]	$\Re \{H_\theta\}$ [T]			
	Analytical Solution	COMSOL Multiphysics	$\vec{A}, V - \vec{A}$ Frequency domain	$\vec{T}, \Phi - \Phi$ Frequency domain
0.032	-46504.9	-45042.7	-44778.4	-44794.7
0.034222	-39165.7	-37526.1	-37523.3	-37526.9
0.036444	-32564.6	-30997.4	-30944.6	-31015.2
0.038667	-26449.5	-24985.6	-24983.9	-24987.4
0.040889	-20817.4	-19353.5	-19352.4	-19351.1
0.043111	-15405.7	-13979.5	-13980.8	-13976.1
0.045333	-10181.6	-8789.34	-8789.38	-8788.15
0.047556	-5084.64	-3718.38	-3717.22	-3720.01
0.049778	-71.2009	1271.767	1271.575	1271.508
0.052	4888.668	6212.994	6213.853	6215.281

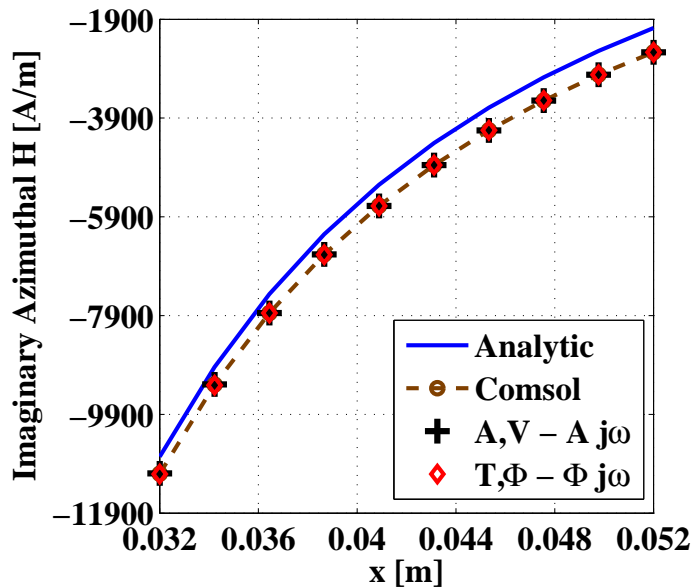
Fig. 6.17. The real part of θ -directed magnetic field intensity.

part of the radial magnetic flux density opposite the curve of real part, is growing the $x=0.038667$, and after this point is decreasing. The difference between the curve of the finite element analysis and of the analytic analysis is unchanged all along.

The next quantities is the θ -directed magnetic field. First of all, the real part of this quantity. Table 6.13 shows the exact results of θ -directed H field. This is the only one, where is the computed values are bigger than the analytic analysis results. Fig. 6.17 shows the comparison of analytic and computed H_θ . The difference between the two

Table 6.14. Imaginary Part of the Azimuthal H field for the three-phase motor

x [m]	$\Im \{H_\theta\}$ [T]			
	Analytical Solution	COMSOL Multiphysics	$\vec{A}, V - \vec{A}$ Frequency domain	$\vec{T}, \Phi - \Phi$ Frequency domain
0.032	-10757.6	-11101.6	-11096.6	-11107.5
0.034222	-8939.18	-9296.83	-9293.24	-9310.26
0.036444	-7462.55	-7846.27	-7847.01	-7848.92
0.038667	-6253.55	-6660.39	-6660.59	-6667.57
0.040889	-5250.13	-5677.03	-5679.32	-5677.96
0.043111	-4406.77	-4850.71	-4851.54	-4850.75
0.045333	-3690.02	-4148.36	-4149.02	-4147.22
0.047556	-3074.86	-3545.74	-3546.24	-3543.66
0.049778	-2542.22	-3024.09	-3024.16	-3023.87
0.052	-2077.37	-2568.85	-2568.87	-2567.37

Fig. 6.18. The imaginary part of θ -directed magnetic field intensity.

types of analysis is same every points, and the results of FEM analysis are nearly equal each points.

The last is the imaginary part of θ -directed H field. Table 6.14 presents the precise values of this quantity. Here as well the computed values are about equal each other. The curves of analytic and FEM analysis are shown in Fig, 6.18. The difference between the curve of analytic results and of FEM results is decreased from $x=0.32$ to $x=0.052$. At this quantity the character of curves of real and imaginary part is similar.

Chapter 7

Conclusions and future works

The analysis of induction motors is based on the numerical solution of the different potentials. The $\vec{A}, V - \vec{A}$ - potential formulation coupled with moving velocity seems to be the most widely used formulation of electrical machines. This formulation has been worked out with motional voltage term in numberless articles and papers, and quantities of machines e.g. torque, losses have been realized by this formulation. The $\vec{T}, \Phi - \Phi$ - potential formulation coupled with moving velocity has not been used in the simulation of induction machines, but few papers in the literature can be found from the other part of FEM analysis. This is why has been applied the $\vec{T}, \Phi - \Phi$ - formulation coupled with motion to solved this induction motor problem.

The used numerical procedure of eddy current field calculation results in the expected data. The two different potential formulations, and the time domain and frequency domain solutions have been compared and the results seem to be close to each other. The numerical results have been compared to analytical results and the used potential formulation is allowing fine approximation. The computed and analytic results agree within 10 %.

In the two dimensional case, the $\vec{A}, V - \vec{A}$ - potential formulation seems to be better solver with motion voltage term. The $\vec{A}, V - \vec{A}$ - potential formulation with motion voltage term faster, the number of elements and unknowns are less than the $\vec{T}, \Phi - \Phi$ - potential formulation with motion voltage term.

The one of further research is the nonlinear analysis of induction motors by means of the $\vec{A}, V - \vec{A}$, and the $\vec{T}, \Phi - \Phi$ - potential formulation taking the ferromagnetic hysteresis into account. The hysteresis is considered through a vector Preisach model [9, 52, 57–60]. The 2D finite element analysis taking the hysteresis into account by combining a Preisach model and the Fixed-Point iterative technique [9, 28, 60–63].

The other further investigation, continue this work, and will be computed the induced voltage by the $\vec{T}, \Phi - \Phi$ - potential formulation, and will be solved another TEAM problems.

Chapter 8

Acknowledgement

This work was carried out in the Laboratory of Electromagnetic Fields at Széchenyi Istvan University.

I would like to express my gratitude to Dr. Miklós Kuczmann, Ph.D., associate professor, Head of the Laboratory of Electromagnetic Fields, for the guidance, advice and encouragement during the course of this work.

Special thanks to Professor Herbert De Gersem, Professor Oszkár Biró and Professor Kent R. Davey for the guidance and advice of this work and Professor Herbert De Gersem for lectorate of my diploma.

I wish to thanks the Department of Telecommunication for the place of the laboratory.

I thank my family, my parents and my sister for constant understanding, encouragement and support.

The financial support of the János Bolyai Research Scholarship of the Hungarian Academy of Science (BO/00064/06), the Széchenyi Istvan University (12-3210-02) and the Hungarian Scientific Research Fund, OTKA PD73242.

Dániel Marcsa
Győr, 30th November 2008

Bibliography

- [1] B. I. Bleaney, B. Bleaney. Electricity and Magnetism. Oxford University Press, Oxford, 1963.
- [2] A. Frigyes, L. Schnell, I. Szita, R. Tuschák. Electrotechnics (in Hungarian). Tankönyvkiadó, Budapest, 1961.
- [3] Á. G. Pattantyús. Theory of the Machines Operation (in Hungarian). Műszaki Könyvkiadó, Budapest, 1983.
- [4] TEAM Benchmark Problems, Problem No. 30a - Induction Motor Analyses, <http://www.compumag.co.uk/>.
- [5] M. Koltai and L. Zombory. Computer Aided Electromagnetic Field Calculation (in Hungarian). Műszaki Könyvkiadó, Budapest, 1979.
- [6] A. Iványi. Continuous and Discrete Simulations in Electrodynamics (in Hungarian). Akadémiai Kiadó, Budapest, 2003.
- [7] <http://mathworld.wolfram.com/>
- [8] C. A. Brebbia. The Boundary Element Method for Engineers. Pentech Press, London, 1980.
- [9] M. Kuczmann, A. Iványi. The Finite Element Method in Magnetics. Akadémiai Kiadó, Budapest, 2008.
- [10] J. P. A. Bastos, N. Sadowski. Electromagnetic Modeling by Finite Element Methods. Marcel Dekker Inc., New York, 2003.
- [11] O. Bíró, K. R. Richter. CAD in electromagnetism. In Series Advances in Electronics and Electron Physics, Academic Press, New York, 1991, pp. 82.
- [12] J. Jin. The Finite Element Method in Electromagnetics. JohnWiley and Sons, New York, 2002.

- [13] J. Luomi. Finite Element Methods for Electrical Machines (lecture Notes for postgraduate course in electrical machines). Chalmers University of Technology, Göteborg, 1993.
- [14] P. P. Silvester and R. L. Ferrari. Finite Elements for Electrical Engineers. Cambridge University Press, Cambridge, 1983.
- [15] O. C. Zienkiewicz and R. Taylor. The Finite Element Method. McGraw-Hill, Maidenhead, 1991.
- [16] J. D. Jackson. Classical Electrodynamics. 3rd Edition, John Wiley, 1999.
- [17] J. A. Stratton. Electromagnetic Theory. McGraw Hill, London, 1941.
- [18] K. Simonyi and L. Zombory. Theoretical Electromagnetics (in Hungarian). Műszaki Könyvkiadó, Budapest, 2000.
- [19] Gy. Fodor. Theory of Electromagnetism I (in Hungarian). Tankönyvkiadó, Budapest, 1987.
- [20] I. Standeisky. Electrodynamics (in Hungarian). Universitas-Győr Kht., Győr, 2006.
- [21] O. Bíró. Edge element formulations of eddy current problems. *Comput. Meth. Appl. Mech. Engrg.*, 169:391405, 1999.
- [22] O. Bíró. Potential Functions in Eddy Current Field Analysis by the Finite Element Method (in Hungarian). Hungarian Academy of Sciences, 2003.
- [23] O. Bíró, K. Preis, K. R. Richter. On the use of the magnetic vector potential in the nodal and edge finite element analysis of 3D magnetostatic problems. *IEEE Trans. on Magn.*, 32:651654, 1996.
- [24] O. Bíró, K. Preis, G. Vrisk, K. R. Richter, I. Tícar. Computation of 3-D magnetostatic fields using a reduced scalar potential. *IEEE Trans. on Magn.*, 29:13291332, 1993.
- [25] A. Iványi. Magnetic Field Computation with R-functions. Akadémiai Kiadó, Budapest, 1998.
- [26] T. Nakata, N. Takahashi, K. Fujiwara, and T. Imai. Effects of permeability of magnetic materials on errors of the $\vec{T} - \Phi$ method. *IEEE Trans. on Magn.*, 26:698701, 1990.
- [27] T. Nakata, N. Takahashi, K. Fujiwara, and Y. Okada. Improvements of the $\vec{T} - \Phi$ method for 3-D eddy current analysis. *IEEE Trans. on Magn.*, 24:9497, 1988.

- [28] D. Marcsa, M. Kuczmann. Eddy current analysis with nonlinearity. *Pollack Periodica*, Vol. 3, No. 2, 2008, pp. 97-109.
- [29] A. Arkkio. Analysis of induction motors based on the numerical solution of the magnetic field and circuit equations. Ph.D. thesis, Helsinki University of Technology, Espoo, 1987.
- [30] H. De Gersem, K. Hameyer. Comparison of motional and nonmotional time-harmonic finite element simulation of solid rotor single-phase induction machines. In *9th Biennial IEEE conference on electromagnetic field computation - CEFC 2000 (abstract)*, pp. 108 pages, June 2000.
- [31] H. De Gersem, K. Hameyer. Motional finite element simulation of magnetic brakes and solid rotor induction machines. *Journal of Technical Physics*, ISSN 0324-8313, vol. 43, no. 4, pp. 389-397, 2002.
- [32] B. Davat, Z. Ren, M. Lajoie-Mazenc. The movement in field modeling. *IEEE Trans. on Magn.*, Vol. MAG-21, No. 6, November 1985, pp. 2296-2298.
- [33] N. Burais, A. Foggia, A. Nicolas, J. P. Pascal, J. C. Sabonnadiere. Numerical Solution of Eddy Currents Problems Including Moving Conducting Parts. *IEEE Trans. on Magn.*, Vol. MAG-20, No. 5, 1984, pp. 1995-1997.
- [34] A. Slama, V. Mazauric, Y. Maréchal, G. Meunier. Electric railgun 3D modeling: Computation of eddy currents and Lorenz force. *IEEE Trans. on Magn.*, Vol. 37, No. 1, 2001, pp. 139-142.
- [35] K. Muramatsu, N. Takahashi, T. Hashio, C. Yamada, M. Ogawa, S. Kobayashi, T. Kuwahara. 3-D eddy current analysis in moving conductor of permanent magnet type of retarder using moving coordinate system. *IEEE Trans. on Magn.*, Vol. 14, No. 4, 1999, pp. 1312-1317.
- [36] O. Chadebec, G. Meunier, V. G. Mazauric, Y. Le Floch, P. Labie. Eddy-current effect in circuit breakers during arc displacement phase. *IEEE Trans. on Magn.*, Vol. 40, No. 2, 2004, pp. 1358-1361.
- [37] D. Marcsa, M. Kuczmann. Nonlinear two-dimensional finite element modeling of a single-phase induction motor. *Proceedings of the 13th International IGTE Symposium on Numerical Field Calculation in Electrical Engineering and European TEAM Workshop*, Graz, Austria, September 21-24, 2008, CD Proceedings.
- [38] D. Marcsa, M. Kuczmann. Finite element analysis of single-phase induction motors. *COMSOL Conference Budapest 2008 - Proceedings on CD ROM*, Budapest, Hungary, 2008.

- [39] www.comsol.com
- [40] <http://www.cise.ufl.edu/research/sparse/umfpack/>
- [41] A. Neumaier, R. S. Varga. Exact convergence and divergence domains for the symmetric successive overrelaxation iterative (SSOR) method applied to H-matrices. *Linear Algebra Appl.* 58:261-272, 1984.
- [42] C. Ashcraft, R. Grimes. SPOOLES: An object-oriented sparse matrix library. *In Proceedings of the 9th SIAM Conference on Parallel Processing for Scientific Computing*, 1999.
- [43] N. Sadowski, Y. Lefèvre, M. Lajoie-Mazenc, J Cros. Finite element torque calculation in electrical machines while considering the mouvement. *IEEE Trans. on Magn.*, Vol. 28, No. 2, March 1992, pp. 1410-1413.
- [44] K. Davey, G. Vachtsevanos, R. Powers. The analysis of fields and torque in spherical induction motors. *IEEE Trans. on Magn.*, Vol. MAG-23, No. 1, January 1987, pp. 273-282.
- [45] A. A. Abdel-Razek, J. L. Coulomb, M. Felicahi, J. C. Sabonnadiere. The calculation of electromagnetic torque in saturated electrical machines within combined numerical and analytical solutions of the field equations. *IEEE Trans. on Magn.*, Vol. MAG-17, No. 6, November 1981, pp. 3250-3252.
- [46] T. Kabashima, A. Kawahara, T. Goto. Force calculation using magnetizing currents. *IEEE Trans. on Magn.*, Vol. 35, No. 3, May 1999, pp. 1402-1405.
- [47] G. Henneberger, Ph. K. Sattler, D. Shen. Force calculation with analytical accuracy in the finite element based computational magnetostatics. *IEEE Trans. on Magn.*, Vol. 27, No. 5, September 1991 pp. 4254-4257.
- [48] O. J. Antunes, J. P. A. Baston, N. Sadowski, A. Razek, L. Santandrea, F. Bouillault, F. Rapetti. Torque calculation with conforming and nonconforming movement. *IEEE Trans. on Magn.*, Vol. 42, No. 4, April 2006, pp. 983-986.
- [49] D. Marcsa, M. Kuczmann. Numerical analysis of single- and three-phase induction motors. Will be published in *Przegląd Elektrotechniczny*.
- [50] K. R. Davey. Analytic analysis of single- and three-phase induction motors. *IEEE Trans. on Magn.*, vol. 34, no. 5, September 1998, pp. 3721-3727.
- [51] K. R. Davey. Rotating field analysis using boundary element methods. *IEEE Trans. on Magn.*, Vol. 35, No. 3, May 1999, pp. 1402-1405.

- [52] D. Jiles. Introduction to Magnetism and Magnetic Materials. Chapman & Hall, London, 1998.
- [53] D. D. Micu, E. Simion, D. Micu, A. Ceclan. Numerical methods for induced voltage evaluation in electromagnetic interference problems. *9th issue of EPQU Conference*, October 2007.
- [54] F. W. Sears. Principles of Physics Series - Electricity and Magnetism. Addison-Wesley, Cambridge Mass., 1964.
- [55] P. J. Leonard, D. Rodger. Modelling voltage forced coils using the reduced scalar potential method. *IEEE Trans. on Magn.*, Vol. 28, No. 2, March 1992, pp. 1615-1618.
- [56] O. Biró, K. Preis, G. Buchgraber, I. Tičar. Voltage Driven coils in finite element formulations using a current vector and a magnetic scalar potential. *IEEE Trans. on Magn.*, Vol. 40, No. 2, March 2004, pp. 1402-1405.
- [57] I. D. Mayergoyz. Eddy current hysteresis and the Preisach model. *IEEE Trans. on Magn.*, Vol. 34, No. 4, July 1998, pp. 1261-1263.
- [58] A. Iványi. Hysteresis Models in Electromagnetic Computation. Akadémiai Kiadó, Budapest, 1997.
- [59] A. Stancu. Magnetization Process in Particulate Ferromagnetic Media. Certeza Universitara, Iasi, 2006.
- [60] J. Saitz. Newton-Raphson method and Fixed-Point technique in finite element computation of magnetic field problem in media with hysteresis. *IEEE Trans. on Magn.*, Vol. 35, No. 3, 1999, pp. 1398-1401.
- [61] E. A. Dlala. Magnetodynamic Vector Hysteresis Models for Steel Laminations of Rotating Electrical Machines. Helsinki University of Technology, Laboratory of Electromechanics, TKK Dissertations 111, Espoo 2008, 165 p., Doctoral Thesis.
- [62] O. Bottauscio, M. Chiampi, C. Ragusa. Polarization method for Static Field. *IEEE Trans. on Magn.*, Vol. 36, No. 4, 2000, pp. 672-675.
- [63] F. I. Hantila, G. Preda, M. Vasiliu. Transient Analysis of Hysteretic Field Problems Using Fixed Point Technique. *IEEE Trans. on Magn.*, Vol. 39, No. 3, 2003, pp. 1179-1182.